HYDROGEOPHYSICAL EVALUATION OF VEGETATION INFLUENCE ON ECOHYDROLOGICAL PROCESSES

By

BHARAT SHARMA ACHARYA

Bachelor of Science in Agriculture
Tribhuvan University
Chitwan, Nepal
2008

Master of Science in Agro-environmental Management
Aarhus University
Aarhus, Denmark
2011

Submitted to the Faculty of the
Graduate College of the
Oklahoma State University
in partial fulfillment of
the requirements for
the Degree of
DOCTOR OF PHILOSOPHY
May, 2016

HYDROGEOPHYSICAL EVALUATION OF

VEGETATION INFLUENCE ON

ECOHYDROLOGICAL PROCESSES

Dissertation Approved:

Dr. Chris B. Zou

Dissertation Adviser

Dr. Rodney E. Will

Dr. Todd Halihan

Dr. Garey Fox

ACKNOWLEDGEMENTS

This research was supported by the Oklahoma Agricultural Experimental Station, Boone Pickens School of Geology at Oklahoma State University (OSU), United States Geological Survey (USGS) (104G), Oklahoma Water Resources Research Institute (OWRRI), United States Department of Agriculture (USDA) National Institute of Food and Agriculture (NIFA) award (2014-67010-216530), National Science Foundation (NSF) Experimental Program to Stimulate Competitive Research (EPSCoR) (OIA-1301789) and NSF Dynamics of Coupled Natural and Human Systems (CNH) Program (DEB-1413900).

Many people have contributed to the completion of this study. I am highly indebted to my advisor Dr. Chris Zou for his incredible support, time, and guidance during my PhD study. His direction and encouragement have helped me grow both personally and professionally. I would like to express my sincere thanks to Dr. Todd Halihan for his cordial support and assistance with electrical resistivity imaging, as well as the subsequent data processing and interpretation. The many weekends he sacrificed in the field collecting data well into the night plus his help in drilling groundwater wells, even during inclement weather, is appreciated beyond measure. I extend many thanks to both Dr. Zou and Dr. Halihan for being my confidantes, and mentors. Additionally, I would like to acknowledge Dr. Rod Will and Dr. Garey Fox for all our thought-

provoking discussions, and for offering equipment and their expertise while I was developing my proposal and conducting this research. I am grateful to Dr. Tyson Ochsner, Briana Sallee, and Sonisha Sharma for their technical assistance with HYDRUS-1D.

I am thankful to Elaine Stebler and Chris Stansberry for both the field and lab assistance, and for logistical support. Elaine, you have been a great friend and guardian to me over these past four years. I would like to thank my dear friend and roommate Nabin Paudel, who has shared my longest days, joys, and sorrows. Thank you to Sulav Poudel, Binu Shrestha, Nirajan Bhattrai, Manita Guragain, Khagendra Timilsina, and Roshani Timilsina for your love that I will cherish throughout my life. Joseph Dale and Amanda West, you have been a great friends and I thank you for all of your love, encouragement and help in field. I am immensely grateful to Dipesh KC, Pradip Saud, Lei Qiao, Renato Rahal, Vanessa Biral, Qi Daihawa, and Ren Jian for their assistance in data collection. Thanks to Anup KC for his assistance in data analysis. I am thankful to Sulochana Dhital, Sun Xiangmin, Arjun Pandey, Jhapendra Sapkota, Laxman Adhikari, Anish Khanal, Safu Acharya, Saroj Kandel, Roman Poudel, Shishir Paudel, Jacob Dyer and Gehendra Kharel for their help, support and love.

Finally, I would like to express deepest thanks to my family for their immense love over years and for being with me through thick and thin.

Name: BHARAT SHARMA ACHARYA

Date of Degree: MAY, 2016

Title of Study: HYDROGEOPHYSICAL EVALUATION OF VEGETATION INFLUENCE ON ECOHYDROLOGICAL PROCESSES

Major Field: NATURAL RESOURCE ECOLOGY AND MANAGEMENT

Abstract: Understanding the spatio-temporal heterogeneity of ecohydrological processes at the soil-plant interface and through the vadose zone is necessary to understand soil, vegetation and climate relations for land use and water resource management and planning in the south-central Great Plains, USA. We calibrated and validated a frequency domain dielectric sensor to quantify litter water content to estimate litter interception of precipitation *in situ*. Results from 6-months in situ measurement showed that the litter interception of a closed canopy redcedar woodland accounted for about 10% of gross rainfall, constituting a substantial component of the water budget in a sub-humid environment. Time-lapse electrical resistivity imaging was used to track deep moisture dynamics in a tallgrass prairie, prairie encroached by redcedar, closed-canopy redcedar woodland, and oak forest, and to evaluate subsurface flow in the tallgrass prairie with a thin soil over porous bedrock. Results indicated vegetation induced changes in the vertical soil moisture profile, increased spatial-temporal variability in root zone hydraulic conductivity under redcedar encroachment, two-layered moisture migration profiles, and subsurface lateral flow in the tallgrass prairie. Lateral flow was confirmed by short term temporal ERI that tracked movement of water from a berm infiltrometer. Water level from shallow monitoring wells showed higher water levels in the tallgrass prairie than in the redcedar woodland, which suggests that woody plants can decrease the water table in a perched aquifer by a significant amount. Mean soil chloride content varied between 5 to 162 mg L^{-1} in the tallgrass prairie and 88 to 612 mg L^{-1} in the prairie encroached by redcedar. Higher soil chloride concentrations under redcedar encroachment indicate reduced percolation and groundwater recharge potential associated with woody plant encroachment. The estimated deep drainage rate was 9.0 mm and 0.30 mm in the tallgrass prairie and redcedar woodland respectively. This study demonstrates that vegetation controls soil water dynamics, and hydrogeophysical methods have the potential to be used for broader understanding of ecology and hydrology in ecosystem studies.

TABLE OF CONTENTS

Chapter Page

LIST OF TABLES

Chapter III

Chapter V

LIST OF FIGURES

Chapter II

Figure Page

Chapter III

Chapter IV

Chapter V

CHAPTER I

INTRODUCTION

A large portion of the Great Plains of the United States is located at the transition zone between grassland and forest. The ecotone exhibits a semi-arid to sub-humid climate and encompasses a mosaic of vegetation and diverse land use. The rangeland of the south and south-central Great Plains in particular is a heterogeneous landscape with patches of grassland, woodland and forest. A declining trend in cropland area was evident in this region from the beginning of the 20th century. This resulted in an increase in rangeland which is under rapid physiognomy transition as a result of woody plant encroachment [*Briggs et al.*, 2005; *Engle et al.*, 2008]. The process of woody plant encroachment follows two major trajectories: (a) expansion of riparian gallery forest [*Wine and Zou*, 2012] and (b) encroachment of woody species into the upland, primarily by a juniper species (*Juniperus virginiana*, eastern redcedar) [*Engle et al.*, 2008].

Vegetation, a key component in an ecohydrological system, influences different components of the water balance but its role varies with climate [*Huxman et al.*, 2005]. The coupling of vegetation and water flux is strong in semi-arid and sub-humid environments [*Huxman et al.*, 2005; *Zhang et al.*, 2001], and the conversion of vegetation from herbaceous to woody life forms is associated with a substantial increase in

evapotranspiration [*Liu et al.*, 2010]. In addition, an increase in woody components increases evaporation from canopy interception and reduces the amount of rainfall reaching the ground [*Everson et al.*, 2011]. Assuming no change in soil water storage for a given water year, the increase in evapotranspiration under a land surface transformation, such as woody plant encroachment, has to be balanced by reduction in either groundwater recharge or streamflow or both [*Zhang et al.*, 2001].

A recent experimental study showed that the streamflow from a woody plant encroached experimental watershed is substantially less than that from an adjacent grassland watershed [*Zou et al.*, 2014]. The connection of improved infiltration capacity and forest development has been well-established [*van Dijk and Keenan*, 2007]. A fundamental paradigm under which forest hydrology and water resource management operate is that afforestation reduces overland flow and facilitates subsurface flow and deep drainage into groundwater through trees' deeper rooting systems; dead or live. Reduction of overland flow with woody plant encroachment is plausible from this conventional forest hydrology paradigm [*Zou et al*., 2014]. However, the reduction of subsurface flow from woody plant encroached watersheds was also observed at the same time [*Zou et al.*, 2014]. These observations challenge the assumption that trees always facilitate subsurface flow and deep recharge in semi-arid and sub-humid climate.

An independent study using chloride accumulation showed that groundwater recharge is lower under woodland compared with grassland environments under the same climate [*Kim and Jackson*, 2012]. As a result, a further study focusing on the water movement into soil and through the vadose zone is critical for understanding the

compensation and tradeoff between runoff and deep recharge process in semi-arid and sub-humid ecosystem such as the ecotone of the Great Plains.

Soil moisture is the key parameter to link ecological processes and the hydrological cycle. Vegetation canopy and litter interception unavoidably affect soil moisture by reducing net rainfall input. Vegetation may also impact soil hydraulic properties. The water that passes through the canopy and litter and infiltrate into soil is critical for transpiration and deep recharge. Despite having a good understanding of incoming water loss to canopy interception, there is a lack of information of rainfall interception by litter, therefore net rainfall input to soil in the ecotone.

In addition to net rainfall input to soil, the spatial and temporal dynamics of soil water content interacts with precipitation to control the runoff and recharge processes [*Qiao et al.*, 2015]. Sensor based approaches were effective in studying surface and subsurface water content to improve hydrological models [*Qiao et al.*, 2015; *Zou et al.*, 2014]. However, soil moisture sensors are designed to work primarily in soil media and the depth of sensors being practically installed is usually limited. As a result, there is a paucity of information on soil water content dynamics at depths critical for understanding deep recharge.

Hydrogeophysical methods such as electrical resistivity imaging are recently being tested to study spatial and temporal variation in soil water content [*Jayawickreme et al.*, 2010; *Jayawickreme et al.*, 2014]. These methods provide an alternative approach to traditional methods to monitor deep moisture and water flow pathways. Similarly, monitoring wells can be used to understand temporal variability in water levels, which

will further assist to evaluate deep drainage and recharge potential in experimental catchments.

Objectives

The overarching goal of this dissertation was to improve our understanding of vegetation-induced changes in ecohydrological processes and subsurface water movement. The research looked into closely interrelated ecohydrological processes on soil-plant interface such as litter interception of rainfall, and subsurface water movement such as deep moisture dynamics, subsurface lateral flow, and deep drainage in the south-central Great Plains, USA. The influence of different vegetation types including grassland, eastern redcedar woodland and oak forest were investigated using different ecohydrological and hydrogeophysical methods. The specific objectives of this dissertation research include:

- Objective 1. To quantify rainfall interception by eastern redcedar litter under controlled and field conditions using leaf wetness sensor;

- Objective 2. To evaluate how grassland, eastern redcedar, and oak forest control downward water movement through vadose zone using electrical resistivity imaging;

- Objective 3. To demonstrate subsurface lateral flow using temporal electrical resistivity imaging; and

- Objective 4. To quantify and contrast drainage rates in dry sub-humid grassland and eastern redcedar encroached site using a chloride mass balance and HYDRUS-1D modeling.

REFERENCES

Briggs JM, Knapp AK, Blair JM, Heisler JL, Hoch GA, Lett MS, McCarron JK. 2005. An ecosystem in transition: causes and consequences of the conversion of mesic grassland to shrubland. Bioscience, **55**: 243-254.

Engle DM, Coppedge BR, Fuhlendorf SD. 2008. From the dust bowl to the green glacier: human activity and environmental change in Great Plains grasslands. In: Western North American Juniperus Communities, Springer, pp: 253-271.

Everson C, Dye P, Gush M, Everson T. 2011. Water use of grasslands, agroforestry systems and indigenous forests. Water SA, **37**: 781-788.

Huxman TE, Wilcox BP, Breshears DD, Scott RL, Snyder KA, Small EE, Hultine K, Pockman WT, Jackson RB. 2005. Ecohydrological implications of woody plant encroachment. Ecology, **86**: 308-319.

Jayawickreme DH, Jobbágy EG, Jackson RB. 2014. Geophysical subsurface imaging for ecological applications. New Phytologist, **201**: 1170-1175.

Jayawickreme DH, Van Dam RL, Hyndman DW. 2010. Hydrological consequences of land-cover change: Quantifying the influence of plants on soil moisture with time-lapse electrical resistivity. Geop., **75**: WA43-WA50.

Kim JH, Jackson RB. 2012. A global analysis of groundwater recharge for vegetation, climate, and soils. Vadose Zone Journal, **11**: 0-0.

Liu W, Hong Y, Khan SI, Huang M, Vieux B, Caliskan S, Grout T. 2010. Actual evapotranspiration estimation for different land use and land cover in urban regions using Landsat 5 data. Journal of Applied Remote Sensing, **4**: 041873-041873-041814.

Qiao L, Zou CB, Will RE, Stebler E. 2015. Calibration of SWAT model for woody plant encroachment using paired experimental watershed data. Journal of Hydrology, **523**: 231-239.

van Dijk AI, Keenan RJ. 2007. Planted forests and water in perspective. Forest Ecology and Management, **251**: 1-9.

Wine ML, Zou CB. 2012. Long-term streamflow relations with riparian gallery forest expansion into tallgrass prairie in the Southern Great Plains, USA. Forest Ecology and Management, **266**: 170-179.

Zhang L, Dawes W, Walker G. 2001. Response of mean annual evapotranspiration to vegetation changes at catchment scale. Water Resources Research, **37**: 701-708.

Zou CB, Turton DJ, Will RE, Engle DM, Fuhlendorf SD. 2014. Alteration of hydrological processes and streamflow with juniper (Juniperus virginiana) encroachment in a mesic grassland catchment. Hydrological Processes, **28**: 6173-6182. DOI: 10.1002/hyp.10102.

CHAPTER II

MONITORING LITTER INTERCEPTION OF RAINFALL USING LEAF WETNESS SENSOR UNDER CONTROLLED AND FIELD CONDITIONS

ABSTRACT

Litter interception of water is an integral component of the water budget for vegetated ecosystems. However, loss of rainfall to litter receives considerably less attention than canopy interception of water due to lack of suitable sensors to measure changes in litter water content. In this study, we calibrated a commercially available leaf wetness sensor to the gravimetric water content of redcedar (*Juniperus virginiana*) litter and used this sensor-based measurement method to estimate litter interception of water in a redcedar woodland. Under controlled laboratory conditions, we found a strong linear correlation between leaf wetness sensor counts (C_{LWS}) and measured gravimetric litter water content (*m*WC): *m*WC = 0.606 x C_{LWS} – 252.62 (R^2 = 0.93, P <0.001). The laboratory relationship was validated with field sampling and C_{LWS} accounted for 48% of the observed variance in the measured litter water content (*m*WC). Our continuous field measurements showed that redcedar litter intercepted approximately 10% of the gross

rainfall that fell between 16 December, 2014 and 31 May, 2015. Therefore, rainfall loss to litter can constitute a substantial component of the annual water budget in sub-humid environments. The leaf wetness sensor can be calibrated to assist with long-term *in situ* measurement of litter interception loss to gain a better estimate of the litter layer contribution to the site water budget.

KEY WORDS: leaf wetness sensor; gravimetric litter water content; litter interception; *Juniperus virginiana;* water budget; interception storage capacity

INTRODUCTION

Dead plant debris forms a thin litter layer in some vegetated ecosystems. The litter layer can serve as a direct barrier to precipitation infiltrating the soil. A large amount of water falling through the canopy to the ground below may be retained in the litter layer and is likely to evaporate without ever reaching the bulk soil beneath. Consequently, the dynamic interception of rainfall by both the canopy and the litter affects soil moisture conditions, catchment water budget, and ecosystem productivity [*Helvey and Patric*, 1965; *Owens et al.*, 2004; *Thurow et al.*, 1987]. However, there has been much less research on litter interception compared with canopy interception of rainfall [*Bulcock and Jewitt*, 2012a]. Lack of interest in litter interception may be the result of two misperceptions – the insignificance of the issue and the difficulty of addressing the issue. For the former, it is apparent that the litter layer is far smaller in mass compared to canopy crown in many water-limited ecosystems and therefore the litter layer's ability to intercept rainfall is smaller in the overall interception estimation [*Gerrits et al.*, 2007b; *Li et al.*, 2013; *Sharafatmandrad et al.*, 2010]. For the latter, the depth, composition, and mass of litter layer exhibit complicated spatio-temporal variations that are determined primarily by vegetation types, species composition, season, and management practices [*Putuhena and Cordery*, 1996; *Sayer*, 2006; *Sharafatmandrad et al.*, 2010]. The evaporation of retained water in litter is controlled by below canopy climatic drivers [*Helvey and Patric*, 1965; *Llorens et al.*, 1997] and therefore interception loss may vary for similar litter mass under different climate. The complex spatio-temporal and climate variations make limited spot-checks of gravimetric measurements of litter water content

impractical and most likely highly unrepresentative of an entire area or even a small time period. Perhaps the most important reason for lack of *in situ* litter interception studies is that there are no straightforward easy methods or readily available equipment to measure the interception capacity of litter [*Putuhena and Cordery*, 1996]. Therefore, finding a suitable commercially available sensor would greatly simplify and improve the challenging and tedious task of manually tracking changes of litter water content in order to obtain good estimations of litter interception.

Worldwide studies have shown that litter interception ranges from as low as 0.2% to as high as 40% of gross precipitation depending on the mean annual precipitation, litter mass, and shape of leaves [*Gerrits et al.*, 2007a; *Naeth et al.*, 1991; *Walsh and Voigt*, 1977]. Litter interception is either relatively negligible (less than 1% of precipitation) in water-limited region due to small litter mass [*Sharafatmandrad et al.*, 2010] compared to canopy interception [*Zou et al.*, 2015] or ineffectiveness in retaining water such as in eucalyptus leaves [*Neto et al.*, 2012]. However, litter interception can be substantial if a deep layer of litter builds up under the canopy, especially in semi-arid regions where below canopy evaporative demand is high. For instance, approximately 5% of rainfall was estimated to be lost to litter layer of juniper communities in Texas, USA [*Owens et al.*, 2004]. Interception loss to dense canopy, especially evergreen species, in semi-arid and sub-humid regions is high [*Zou et al.*, 2015] to a degree that water budgets are meaningfully altered with vegetation transition such as woody plant encroachment into grassland [*Zou et al.*, 2014]. Thus, an improved understanding of litter interception is critical to understand surface soil moisture heterogeneity, catchment water balance

[*Owens et al.*, 2006] and potential impact of vegetation cover change on the provisional services of rangeland catchments [*Zou et al.*, 2014].

Other studies have suggested strong relationships between surface moisture and near-surface relative humidity in dryland ecosystems exhibiting a thin litter layer [*Wang et al.*, 2015] and between relative humidity and eucalyptus litter water content [*Viney*, 1991]. Recently, iButton relative humidity sensors (model DS1923-F5#, Maxim, Sunnyvale, CA, USA) were tested to continuously measure gravimetric water content of litter in a microcosm study [*Wang et al.*, 2015] highlighting the potential use of commercially available sensors for continuously quantifying litter interception. The Decagon leaf wetness sensor (LWS) (Decagon Devices Inc, Utah, USA) is a frequency domain dielectric sensor that is increasingly being used in agriculture and forestry. It produces an output voltage that depends on the dielectric constant of the medium surrounding the probe, therefore the wetness of the medium. It has been used to monitor leaf wetness or dew presence for disease risk forecasting and pest control in agriculture [*Junk et al.*, 2008], fire risks in a semi-arid North American pine forest (*Huffman et al.* [2013], frost occurrence and duration in a short-grass surface in South Africa [*Savage*, 2012], and to evaluate micro-climate condition for habitat suitability of at-risk plant species in Hawaii, USA [*Questad et al.*, 2013]. However, few efforts have yet been made to use the leaf wetness sensor in a media other than air, such as forest litter, to determine the moisture content of the media.

The overall objective of this study was to calibrate and validate a frequency domain dielectric sensor to quantify litter interception of eastern redcedar woodland. The

specific objectives were to (1) determine if a relationship can be defined between LWS counts obtained from a Decagon leaf wetness sensor and gravimetrically measured litter water content in the laboratory, (2) determine whether we can validate the laboratory relationship by grab sampling in the field, and (3) determine litter interception for redcedar woodland by continuously monitoring litter water content *in situ*.

MATERIALS AND METHODS

Field site

The field portion of this study was conducted on lands managed by Oklahoma State University and located about 11 km southwest of Stillwater in Payne County, Oklahoma, USA (36^{o} 03' N, 97^{o}11' W, elevation 331 m above sea level). Based on long-term climate data (from 1971 to 2000) for Payne County, the site has a continental climate with mean annual temperature of 15.5 ^{o}C, mean annual precipitation of 948 mm, and average relative humidity of 69% [*McPherson et al.*, 2007; *Oklahoma Climatological Survey*, 2012]. The study site was historically a mosaic landscape with both tallgrass prairie and oak forest delineated primarily by soil texture. During the last 50 to 100 years some of the prairie has been heavily encroached by a juniper species, eastern redcedar and transformed into redcedar woodland. Meanwhile the number of redcedar trees occurring in oak forest has increased as well. The oak forest is thus also threatened by eastern redcedar encroachment and could physiognomically transform into redcedar woodland [*Engle et al.*, 2008; *Wine and Zou*, 2012; *Wine et al.*, 2012; *Zou et al.*, 2014].

During the study, precipitation was measured at 5-minute intervals using a TB3 siphoning tipping bucket rain gage with 0.254 mm per tip (Hydrological Services America, Lake Worth, FL, USA). Other meteorological data were collected as described in *Zou et al.* [2015]. A 4-hour period of no-rainfall was selected to separate rainfall events.

Laboratory calibration

Litter layer is an organic (O) horizon of soil profile, which is further classified into sapric (Oa), hemic (Oe) and fibric (Oi) horizons. Soil organic materials in these horizons are highly decomposed, intermediately decomposed and slightly decomposed, respectively [*Schaetzl and Thompson*, 2015]. Therefore, litter layer is composed of organic materials or dead plant residues which are at different stages of decomposition. In this study, litter was defined as "all dead organic material made of both decomposed and undecomposed plant products which are not incorporated into the mineral soil beneath" [*Naeth et al.*, 1991]. Litter samples from the study site's redcedar woodland were collected and brought to the laboratory to determine the relationship between the output from a Leaf Wetness Sensor (LWS) (Decagon Devices Inc, Utah, USA) inserted into litter and the gravimetrically measured water content of juniper litter. Fifty grams of oven-dried redcedar liter were distributed to each of 18 resealable plastic bags. Known volumes of water were sprayed on the litter in the bags to form a gradient of percent water content (by weight) ranging from 10% to 500%. The bags were then sealed, shaken, and set aside overnight in the laboratory for the water content to become evenly distributed throughout the litter. The following day, the dielectric constant of the

equilibrated litter was measured by inserting a LWS into the liter in the bag. The sensor was connected to an EM50 data logger (Decagon Devices Inc, Utah, USA) and the measurement was read as LWS counts (C_{LWS}) after a minimum of 15 minutes was allowed for sensor equilibrium. The percent gravimetric litter water content (*m*WC) was calculated using the following equation:

*m*WC = [(wet weight-dry weight)/dry weight] x 100 (1).

Linear regression correlation was applied to the data (C_{LWS} and *m*WC) and then used in the remainder of the study to obtain the predicted litter water content (*p*WC).

Verification with field data

Field verification was performed by recording LWS counts in undisturbed redcedar woodland for several wetting and drying conditions associated with rainfall events. The LWS was inserted into the litter at an angle of 45° to the litter surface (Figure 2.1) and a minimum of 15 minutes was allowed for sensor equilibrium before recording $C_{LWS.}$ Litter samples were collected from the spot where the sensor readings were taken using a 0.04 m^2 quadrat so that litter biomass could be calculated. The samples were brought to the laboratory, weighed immediately, and then oven dried at 60^{o} C for 48 hours to obtain the measured water content using equation 1. LWS counts were converted into predicted water content (*p*WC) using the relationship established from the laboratory calibration procedure.

Maximum water storage capacity (S)

Litter samples were oven dried at 60^{o} C for 24 hours and litter masses of 0.56, 0.96, 1.97, 2.93, 3.91, and 4.86 kg m^{-2} were tested for maximum water storage capacity. Samples were placed in collars made from polyvinyl chloride (PVC) pipe sections. The bottom of the collar was covered with fine wire screen and tightly secured with metal hose clamp. Samples were soaked in water for 24 hours for complete saturation. Evaporation was prevented by covering the collars with a clear plastic box and samples were lifted out of water after 24 hours and allowed to drain until drainage ceased before weighing. Maximum water storage capacity (*S*) for this study was the maximum amount of water that would be potentially retained by the litter and was equivalent to the difference between oven dried mass and saturated litter mass after drainage has ceased [*Li et al.,* 2013; *Putuhena & Cordery,* 1996].

In situ litter water content

On 16 December 2014 we added one LWS to each of six EM50 data loggers which were part of a larger study measuring volumetric soil moisture. The LWS allowed us to continuously measure dielectric constant of the redcedar litter *in situ*. The LWSs were inserted all the way into litter at an angle of 45^{o} to the litter surface (Figure 2.1) and attached to short pieces of PVC to hold them in place. LWS counts were recorded every 15 minutes. Six LWSs were initially deployed for *in situ* measurements but by two months into the study, the wiring on one of the sensors was damaged by rodents and it became non-functional. By the end of four months, three more sensors were destroyed by rodents. Measurements were concluded on 31 May 2015.

The maximum water content (% by weight) in this study was computed by converting the maximum C_{LWS} during a rainfall event (Figure 2.2) to *p*WC using the linear model generated from the laboratory calibration (equation 3). Similarly, we derived the predicted % water content after allowing for drainage; we used one hour after the cessation of rain event. A previous survey on litter mass based on five 0.04 m^2 plots combined into one sample from 60 different random points in redcedar-encroached catchments (total area of about 8 hectares) at our study site showed that the litter biomass ranged from 84 to 7,049 g/ m^2 with mean litter biomass of 2,931 g/ m^2 (unpublished data). We used this average value to convert the predicted percent water content of litter to mm of water depth. Maximum interception storage capacity (C_{max}) is the maximum water content during a rainfall event and it includes gravitational water. Water retained in litter layer after the drainage ceased is called minimum interception storage capacity (C_{min}). The C_{min} does not include gravitational water, and is removed by evaporation only [*Putuhena and Cordery*, 1996]. Litter interception loss in this study was computed by subtracting litter water depth (mm) immediately prior to the start of the rain event ($LWD_{prior\ rain}$) from the C_{min} water depth one hour after the rain ceased ($LWD_{1\ hour\ after\ rain\ ceased}$) The sum of the litter water depths was divided by the sum of the event rainfall depths (RD_{event}) to calculate the percent litter interception loss (I_{loss}) for a given time period.

$$I_{loss} = \frac{\sum(LWD_{1\ hour\ after\ rain\ cease} - LWD_{prior\ rain})}{\sum RD_{event}} \quad (2).$$

For the *in situ* data, the maximum 15-minute rainfall rate was used to obtain a relationship between rainfall intensity, and C_{max}, C_{min}, and I_{loss}.

Data Analysis

For both laboratory calibration and field evaluation, the relationship between *m*WC and LWS counts was analyzed using regression analyses at a significance level of $\alpha = 0.05$ in SigmaPlot (SigmaPlot 11.0, Systat Software, Inc). Data were tested for normality and constant variance, and if the correlation passed these tests, we accepted the regression equation. Data quality was evaluated through R^2, R, and root mean square error (RMSE) when necessary.

RESULTS

Maximum water storage capacity (S)

Litter masses ranged from 0.56 to 4.86 kg m^{-2} and retained 3.07 to 12.87 mm of water. Maximum water storage capacity (*S*) was strongly correlated to the mass of litter (M) ($R^2 = 0.99$, $P < 0.001$) and *S* increased linearly as the M increased (Figure 2.3).

Laboratory Calibration

Changes in LWS counts (C_{LWS}) were strongly correlated to the gravimetrically measured percent water content of the wetted litter (*m*WC) ($R^2 = 0.93$, $P < 0.001$).

Laboratory $m\text{WC} = (0.606 \times C_{LWS}) - 252.62$ (3).

LWS counts increased linearly as the measured water content increased from 10% to 500% (Figure 2.4A).

Field validation

C_{LWS} was significantly correlated with *m*WC under field conditions ($P < 0.001$) (Figure 2.4 B). C_{LWS} accounted for about 48% of variation of *m*WC with a linear regression of

$$\text{Field } m\text{WC} = (0.39 \times C_{LWS}) - 134.34 \quad (4).$$

The gravimetrically measured water content of the field samples and their predicted water content values generated from the laboratory calibration equation (eq. 3) were compared with respect to the 1:1 line (Figure 2.4C). The data were close to the potential 1:1 line and the RMSE was 22%.

In situ litter water content

From16 December 2014 through May 2015, there were 66 rain events ranging from 0.25 to 63.75 mm with the peak 15-minute rain intensity ranging from 1.02 to 70.10 mm h^{-1}. Litter interception loss was calculated for each of those events. From the two sensors that were operational during the entire 5.5 month period, the total water loss to litter interception was estimated to be 46 mm, equivalent to 10% of the gross rainfall (473 mm). The interception loss (I_{loss}) was also computed using five sensors for the shortened time period from 16 December 2014 through April 2015. The average interception loss was 20 mm, 10% of the 202 mm of rainfall for the period.

The maximum interception storage capacity (C_{max}) ranged between 0.43 and 10.77 mm and the minimum interception storage capacity (C_{min}) ranged between 0.36 and 9.11 mm. The C_{max} of 10.77 mm equates to a predicted maximum of 367% water content of the litter by weight. There was no clear relationship between C_{min} and rainfall intensity.

The mm of rain that was intercepted was linearly correlated to the rainfall amount; pseudo $R^2 = 0.66$ for the maximum amount retained by litter and pseudo $R^2 = 0.51$ for the amount retained after allowing for drainage.

DISCUSSION

LWS counts and litter water content

The leaf wetness sensor detects moisture on its upper surface and measures the duration of leaf wetness. The sensor is designed in a way to serve as a surrogate for leaf wetness through radiation balance and thermodynamic properties close to real leaves [*Decagon Devices*, 2014; *Savage*, 2012]. The sensor can represent atmospheric conditions at 10 mm above the sensor and therefore can detect moisture in air. According to the manufacturer, a dry sensor yields 450 raw counts (wetness threshold) but when the sensor is wet, the value can go up to 1400 raw counts. In the laboratory, we sequentially increased the water content of litter to represent minimum (dry) to maximum water holding capacity during the establishment and calibration of the relationship between C_{LWS} and *m*WC. We were able to create litter wetness conditions to produce sensor counts ranging from 440 to 1100 (at 500% *m*WC). Our maximum C_{LWS} did not go as

high as the maximum specified in the sensor product literature. However, the highest C_{LWS} value recorded in the field was 1023, equivalent to ~367% in gravimetric water content, by weight, in litter. The range of litter water content that we used in the laboratory calibration and the field verification was adequate for continuous *in situ* litter wetness monitoring during the 5 months of this study.

The position and angle of various sensors and their contact with the litter are critical parameters for interception measurement and vertical insertion of probes may result in higher dielectric constants compared to horizontal [*Ataka et al.*, 2014; *Wilson et al.*, 2014; *Yoshikawa et al.*, 2004]. We inserted the Decagon leaf wetness sensor all the way into the litter at an angle of 45° from the soil surface based on other studies [*Savage*, 2012]. While the angle of insertion is important in getting the best values, it is also critically important that the angle and method of insertion remains consistent for all of the calibration work and the use of the sensor in the field. The insertion of the sensor at the 45° angle into the litter was somehow influenced by the dimension of the sensor and depth of litter. We intended to use multiple sensors to capture the variance of throughfall input to better estimate interception loss. However, due to the rodent damage to sensors, we were unable to obtain the replication and length of study that was intended.

LWS method vs other litter interception estimation approaches

Litter interception approaches include drainage experiments [*Helvey*, 1964; *Neto et al.*, 2012], weighing trays and cylinders [*Kittredge*, 1955; *Naeth et al.*, 1991; *Pathak et al.*, 1985; *Reynolds and Knight*, 1973], forest floor mapping [*Putuhena and Cordery*, 1996], interception devices [*Li et al.*, 2013], interception basins [*Bulcock and Jewitt*,

2012b; *Gerrits et al.*, 2007a], and use of commercially available sensors [*Wang et al.*, 2015]. Other techniques include isotopic fractionation (oxygen-18 and deuterium values) between throughfall and stream water, which is related to forest floor evaporation [*Kubota and Tsuboyama*, 2004]. Drainage experiments can underestimate litter interception of rainfall if litter is not saturated or drained excessively, and overestimate interception if the time available for drainage is limited such as in rain-events occurring at short time intervals [*Neto et al.*, 2012]. Large rain events that saturate litter and unnatural drainage underestimated litter interception of rainfall, whereas location of litter trays in open area hastened evaporation and overestimated interception in hardwood forest [*Helvey*, 1964]. Forest floor mapping was used to infer laboratory based estimates of litter interception from simulated rainfall draining to field condition. Although samples were mimicked as in field, the approach was disturbing, applicable for same plant species and required large litter mass sampling [*Putuhena and Cordery*, 1996]. Interception basins had valves to empty water, which were congested by sand and leaves; thereby producing gaps in interception data [*Gerrits et al.*, 2007b]. Sensor-based approaches are particularly important if the goal is to estimate the overall loss of throughfall to litter for a given period of time. Recently, the wetting and drying process of *Quercus serrata* litter in Japan was studied by *Ataka et al.* [2014] using a Decagon EC-5 capacitance sensor. In that study, the EC-5 output voltage was calibrated against gravimetric water content of litter under a laboratory setting. The gradient of water content of litter was achieved by drying saturated litter to different water levels. Although saturated litter condition does occur under certain conditions, our approach of wetting down dried litter samples to calibrate sensor output is a more realistic representation of litter interception for a field

setting. Hydrophobic phenomenon exists widely for dry litter [*Robinson et al.*, 2010; *Wine et al.*, 2012]. Water entry into a dry litter differs from a wet litter. In semi-arid and sub-humid regions, the litter layer rarely gets fully saturated in the field as it would be in most laboratory studies.

Wilson et al. [2014] evaluated the use of a simple commercial soil moisture probe to provide long-term leaf litter estimates for a deciduous forest near Oak Ridge in eastern Tennessee. The voltage output of the capacitance probe with fiberglass grid was linearly correlated to the gravimetric moisture content. We found a similar relationship with leaf wetness sensor counts of the Decagon probe. Relative humidity measurements monitored with iButton temperature and relative humidity loggers were also strongly correlated to gravimetric litter moisture for both broadleaf and conifer litter. These commercially available sensors and probes which have been shown to be able to measure litter water content thus show promise to be applied to monitoring litter interception. However, due to the high variability of litter characteristics and difference of meteorological conditions, robust and vigorous calibration under controlled conditions is critically important. In-situ application of LWS sensors requires a thick litter layer and their use is therefore especially suitable for use under conifer forest. This approach might be less appropriate for broadleaf litter due to larger pore spaces and poor contact between litter and sensor.

We faced logistical problems with rodents chewing on the LWS cables and the sensing element for the litter wetness. In some cases, they completely destroyed the sensors, and in other cases, they damaged the sensor housing for the electrical components and caused rain water to seep in and eventually destroy the sensor. The latter

case resulted in erratic, inconsistent, and faulty C_{LWS} values. After some initial damage we subsequently attempted to protect the cables from the rodents by enclosing them inside flexible plastic conduit. This did protect the cable, but not the sensor housing. In our future work we intend to form a protective cage made of 6 mm hardware cloth around the location of the sensor. This will allow rain to pass through easily and not only deter the rodents but also keep the litter and probe placement from being disturbed.

S, C_{max}, and C_{min}

In this study, the maximum water storage capacity (S) showed a linear relationship with the mass of litter. Similar relationship was found by *Putuhena and Cordery*, [1996], *Sato et al.* [2004] and *Li et al.* [2013]. The S values were within the range reported by *Li et al.* [2013]. The mean S value of 8 mm for our average litter mass was close to C_{max} values ranging between 9 to 12 mm at field condition.

The C_{max} and C_{min} values were relatively smaller but within the range reported by *Li et al.* [2013]. *Putuhena and Cordery*, [1996] observed no clear relationship between C_{max} and rainfall intensity. However, *Sato et al.* [2004] observed that C_{min} increased with rainfall intensity and litter mass. We observed no clear relationship between C_{min} and rainfall intensity, similar to *Li et al.* [2013]. In another study, the C_{min} values remained fairly constant with rainfall intensity in poplar leaves [*Guevara-Escobar et al.*, 2007]. Our C_{max} and C_{min} values were dervied from *in situ* litter water content and natural highly-variable (both within and among) rain events and are thus more realistic compared to simulated rain experiments. Interception storage capacity depends on litter mass, morphological characterstics of vegetation types, surface tension, viscosity, and rainfall

intensity [*Li et al.*, 2013]. For example, leaf trichomes can modify boundary layer resistance [*Guevara-Escobar et al.,* 2007], and fragmanted pinnae and tubular petioles in bracken litter decrease water loss and increases water retention [*Putuhena and Cordery,* 1996]. Broadleaf litter can facilitate lateral movement of water and may store more water than needle leaf litter [*Li et al.,* 2013; *Sato et al.,* 2004]. Small voids in litter are important for water retention whereas large voids between litter particles govern gravity drainage [*Dunkerley,* 2015]. The *S* values were greater than C_{min} values. It is important to note that C_{min} values were obtained under natural rain events but S values were obtained from full saturation of litter under laboratory conditions. The *S* values are determined primarily by litter types and water adhesion on litter surface and can be used as a parameter in hydrological models, or as an approach to predict evaporation [*Li et al.*, 2013; *Sato et al.,* 2004].

Interception loss

A classic study estimated annual interception loss of approximately 3% of the annual rainfall by hardwood litter in the southern Appalachians [*Helvey,* 1964]. Owens et al. (2004) reported a slightly higher litter interception of 5% for Ashe juniper (*Juniperus ashei*) in Texas. Redcedar litter has characteristics very similar to Ashe juniper and our estimated litter interception loss by redcedar for part of one year was equivalent to 10% of gross precipitation. The higher litter interception by these two juniper species may be the result of the species specific litter characteristics. Juniper species have scale-like leaf structure that can retain substantial amounts of water [*Owens et al.,* 2006]. Interception storage capacity varies with plant species and rainfall intensity [*Keim et al.,* 2006; *Li et*

al., 2013; *Tsiko et al.*, 2012] and rainfall size affects the percentage of rainfall being intercepted. *Owens et al.* [2006] reported that more than 60% of small amounts of rainfall (<12.5 mm of rain over 24h) is intercepted by the canopy and litter layers combined and that the percent interception loss decreases as storm size increases [*Owens et al.*, 2006].

In this study, for all events of <12.5 mm of rain, litter interception loss based on sensor I and sensor IV was 31 mm and 24 mm out of 157 mm of rain, respectively. For all events of >12.5 mm of rain, litter interception loss based on sensor I and sensor IV was 23 mm and 14 mm out of 316 mm of rain, respectively. The overall litter interception loss (I_{loss}) was 18% for small events and 6% for bigger events of >12.5 mm of rain. Factors such as below canopy atmospheric conditions (e.g. wind exposure, radiation and temperature) affect evaporation potential before and after rainfall events. *Bulcock and Jewitt* [2012b] reported that in South Africa litter interception by *Eucalyptus grandis*, *Pinus patula* and *Acacia mearnsii* was 8.5%, 6.6% and 12.1% of gross precipitation, respectively. These high interception ratios could be associated with the high below canopy atmospheric demand.

Our litter interception estimation at the small catchment scale was calculated based on average litter mass (2,931 g/ m^2) taken from a previous unpublished study. The large variation in litter biomass in that study was a result of the redcedar stands being interspersed with grassland. Therefore, the truly random samples picked up locations of little to no litter of any kind, low levels of grass litter, and low to high levels of redcedar litter under the trees. Our non-random grab sampling done on representative patches of redcedar litter during the field verification process had average litter mass of 3091 g/ m^2.

Therefore, our assumed litter biomass was a reasonable number to use for estimating litter interception. The need to leave the LWS in the litter undisturbed for the long-term *in situ* monitoring of litter moisture prevented us from obtaining the precise biomass measurement for that litter. Heterogeneity in litter mass, canopy structure, and canopy boundary layer are major constraints to precisely determining the true litter interception on landscape.

Interception losses by either canopy or litter are typically reported as an annual loss due to the natural variations which occur throughout the year by month or season and influenced by climatic conditions such as temperature, wind, relative humidity, etc. Our reported estimate of 10% interception loss by redcedar is based only on a partial year and must therefore be used with caution. Considerable changes in percent litter interception and mm interception loss were observed for the different months of this study. December, January, and February are the three coldest and driest months of the year for Payne County OK, while June, July, and August, with moderate rainfall amounts, are the three hottest months and have the highest evaporation rates. Therefore, it is still unknown how much rainfall will be lost to litter interception during the other months of the year.

For the same locations as our *in situ* litter interception monitoring, we had access to 15-minute volumetric water content (VWC) values at 5-cm soil depth and we were able to compare changes in soil water with changes in litter water for the individual rain events. We observed an increase in soil moisture content for rain events with a peak of rainfall intensity greater than 12 mm h^{-1}. This increase may be due to drainage from litter during and after the rainfall event. Three mm of rain in a 15-minute period seemed to

overwhelm the capacity of the litter and allowed water to percolate through the litter and enter the soil. For a May 5 rain event, the average VWC was 0.146 m^3 m^{-3} before the rain event. After 11.2 mm of rain fell within a 15-minute period, followed by 5.1 mm in the next 15-minute period, the LWS I recorded a maximum C_{LWS} of 1023 and the VWC rose to 0.208 m^3 m^{-3} rainfall (Figure 2.7). One hour later, 8.6 mm fell in 15-minutes and again LWS I and V recorded maximum C_{LWS} which represent 10.77 mm of water depth. The VWC increased further to a mean of 0.263 m^3 m^{-3}. We also observed increases in soil moisture which occurred with rainfall intensities less than 12 mm h^{-1} but those increases were associated with prolonged rainfall events with durations longer than 6 hours

We estimated that 10% of gross rainfall was intercepted by redcedar litter after accounting for drainage. *Sharafatnandrad et al.* [2010] found that in the arid environment of Iran, litter may actually serve to conserve water by reducing evaporation from the soil itself and thereby allows water to stay in the soil longer after rainfall. Litter layer protects the soil by reducing the direct impact of rainfall, and erosion and overland flow [*Sayer,* 2006]. More studies should examine the direct relationship between litter interception, soil water content in the upper layers of soil, and run-off and overland flow.

Implications

A large portion of the Great Plains of the United States is located at the transition zone between grassland and forest. This region exhibits a semi-arid to sub-humid climate and encompasses a diverse mosaic of vegetation and land use. Vegetation in this zone is susceptible to land-use and climate change variability which potentially alters catchment water budgets [*Huxman et al.,* 2005; *Zhang et al.,* 2001]. Transformation of grassland to

woodland or woody dominated savanna, as has occurred on portions of the south-central Great Plains [*Briggs et al.*, 2002; *Smith*, 2011], reduces water availability for streamflow and recharge [*Zou et al.*, 2014]. Estimation of water budget, therefore, requires a better understanding of incoming water loss to canopy interception [*Caterina et al.*, 2014], and more importantly, rainfall interception by vegetation litter. A major advantage of this novel approach is that with event rainfall information, interception loss can be calculated with reasonable accuracy for a whole year. The LWS method can be used to continuously monitor litter water which provides an estimate of interception loss to redcedar litter and thus will assist us in understanding surface soil moisture variability and help us improve ecohydrological models to simulate catchment water budget.

CONCLUSION

Our study has demonstrated how Decagon leaf wetness sensor counts correlate linearly with the gravimetric water content of litter layers under both controlled wetting conditions in the laboratory and natural rainfall events in the field. Under field validation conditions, the correlation of determination of this relationship is reduced by 45%; yet the LWS counts still explain 48% of the observed variance in litter water content. Considering the heterogeneity in litter mass, depth of litter, canopy structure, and exposure to variable throughfall amounts under field conditions, it is encouraging that the Decagon leaf wetness sensor has performed adequately for the measurement of litter water content and therefore forest floor water flux. Rainfall loss to the litter layer atop the soil can constitute a substantial component of the water budget in a sub-humid environment and a leaf wetness sensor can be calibrated to assist with *in situ*

measurement of that litter interception loss. Future studies should investigate the feasibility of using leaf wetness sensors in litter of different types and shapes and examine the sensitivity of leaf wetness sensors to below canopy temperature, relative humidity, wind, and solar radiation variations.

ACKNOWLEDGEMENT

The field equipment installation and data collection were completed with support from USGS OWRRI grants and USDA NIFA award (2014-67010-216530). The data analysis and paper writing were partially supported with funding from NSF EPSCoR (NSF-1301789) and NSF Dynamics of Coupled Natural and Human Systems (CNH) program (DEB-1413900). The authors extend their appreciation to Dr. Ning Wang from Biosystems and Agricultural Engineering, Oklahoma State University for her technical assistance.

REFERENCES

Ataka M, Kominami Y, Miyama T, Yoshimura K, Jomura M, Tani M. 2014. Using Capacitance Sensors for the Continuous Measurement of the Water Content in the Litter Layer of Forest Soil. Applied and Environmental Soil Science, **2014**.

Briggs JM, Hoch GA, Johnson LC. 2002. Assessing the rate, mechanisms, and consequences of the conversion of tallgrass prairie to Juniperus virginiana forest. Ecosystems, **5**: 578-586.

Bulcock H, Jewitt G. 2012. Field data collection and analysis of canopy and litter interception in commercial forest plantations in the KwaZulu-Natal Midlands, South Africa. Hydrology and Earth System Sciences, **16**: 3717-3728.

Bulcock H, Jewitt G. 2012. Field data collection and analysis of canopy and litter interception in commercial forest plantations in the KwaZulu-Natal Midlands, South Africa. Hydrology and Earth System Sciences, **9**.

Caterina GL, Will RE, Turton DJ, Wilson DS, Zou CB. 2014. Water use of Juniperus virginiana trees encroached into mesic prairies in Oklahoma, USA. Ecohydrology, **7**: 1124-1134. DOI: DOI: 10.1002/eco.1444.

Decagon Devices I. 2014. Dielectric Leaf Wetness Sensor, Operator's Manual, 2014.

Dunkerley D. 2015. Percolation through leaf litter: What happens during rainfall events of varying intensity? Journal of Hydrology, **525**: 737-746.

Engle DM, Coppedge BR, Fuhlendorf SD. 2008. From the dust bowl to the green glacier: human activity and environmental change in Great Plains grasslands. In: Western North American Juniperus Communities, Springer, pp: 253-271.

Gerrits A, Savenije H, Hoffmann L, Pfister L. 2007. New technique to measure forest floor interception–an application in a beech forest in Luxembourg. Hydrology and Earth System Sciences, **11**: 695-701.

Gerrits A, Savenije H, Hoffmann L, Pfister L. 2007. New technique to measure forest floor interception: an application in a beech forest in Luxembourg. Hydrology and Earth Systems Sciences.

Helvey J. 1964. Rainfall interception by hardwood forest litter in the southern Appalachians. US Department of Agriculture, Forest Service, Southeastern Forest Experiment Station.

Helvey J, Patric J. 1965. Canopy and litter interception of rainfall by hardwoods of eastern United States. Water Resources Research, **1**: 193-206.

Helvey J, Patric J. 1965. Design criteria for interception studies. In: Design of Hydrological Networks; Proceedings of a symposium, pp: 131-137.

Huffman JA, Pöhlker C, Prenni A, DeMott P, Mason R, Robinson N, Fröhlich-Nowoisky J, Tobo Y, Després V, Garcia E. 2013. High concentrations of biological aerosol particles and ice nuclei during and after rain. Atmospheric Chemistry and Physics, **13**: 1767-1793.

Huxman TE, Wilcox BP, Breshears DD, Scott RL, Snyder KA, Small EE, Hultine K, Pockman WT, Jackson RB. 2005. Ecohydrological implications of woody plant encroachment. Ecology, **86**: 308-319.

Junk J, Görgen K, Jarroudi ME, Delfosse P, Pfister L, Hoffmann L. 2008. Operational application and improvements of the disease risk forecast model PROCULTURE to optimize fungicides spray for the septoria leaf blotch disease in winter wheat in Luxembourg. Advances in Science and Research, **2**: 57-60.

Keim RF, Skaugset AE, Weiler M. 2006. Storage of water on vegetation under simulated rainfall of varying intensity. Advances in Water Resources, **29**: 974-986. DOI: http://dx.doi.org/10.1016/j.advwatres.2005.07.017.

Kittredge J. 1955. Litter and forest floor of the chaparral in parts of the San Dimas Experimental Forest, California. University of California.

Kubota T, Tsuboyama Y. 2004. Estimation of evaporation rate from the forest floor using oxygen-18 and deuterium compositions of throughfall and stream water during a non-storm runoff period. Journal of Forest Research, **9**: 51-59.

Li X, Niu J, Xie B. 2013. Study on Hydrological Functions of Litter Layers in North China. PLoS ONE, **8**: e70328.

Llorens P, Poch R, Latron J, Gallart F. 1997. Rainfall interception by a Pinus sylvestris forest patch overgrown in a Mediterranean mountainous abandoned area I. Monitoring design and results down to the event scale. Journal of Hydrology, **199**: 331-345.

McPherson RA, Fiebrich CA, Crawford KC, Kilby JR, Grimsley DL, Martinez JE, Basara JB, Illston BG, Morris DA, Kloesel KA. 2007. Statewide monitoring of the mesoscale environment: A technical update on the Oklahoma Mesonet. Journal of Atmospheric and Oceanic Technology, **24**: 301-321.

Naeth M, Bailey A, Chanasyk D, Pluth D. 1991. Water holding capacity of litter and soil organic matter in mixed prairie and fescue grassland ecosystems of Alberta. Journal of Range Management, **44**: 13-17.

Oklahoma Climatological Survey. 2012. Payne County Climate Summary. http://climate.ok.gov/county_climate/Products/QuickFacts/payne.pdf.

Owens MK, Lyons R, Kneuper C. 2004. Evaporation and interception water loss from juniper communities on the Edwards Aquifer Recharge Area. Report Texas A&M University System.

Owens MK, Lyons RK, Alejandro CL. 2006. Rainfall partitioning within semi-arid juniper communities: effects of event size and canopy cover. Hydrological Processes, **20**: 3179-3189.

Pathak P, Pandey A, Singh J. 1985. Apportionment of rainfall in central Himalayan forests (India). Journal of Hydrology, **76**: 319-332.

Putuhena WM, Cordery I. 1996. Estimation of interception capacity of the forest floor. Journal of Hydrology, **180**: 283-299. DOI: 10.1016/0022-1694(95)02883-8.

Questad EJ, Kellner JR, Kinney K, Cordell S, Asner GP, Thaxton JM, Diep J, Uowolo A, Brooks S, Inman-Narahari N. 2013. Mapping habitat suitability for at-risk plant species and its implications for restoration and reintroduction. Ecological Applications.

Reynolds JF, Knight DH. 1973. The magnitude of snowmelt and rainfall interception by litter in Lodgepole pine and Spruce-fir forest in Wyoming. Northwest Science, **47**: 50-60.

Robinson DA, Lebron I, Ryel RJ, Jones SB. 2010. Soil water repellency: A method of soil moisture sequestration in pinyon–juniper woodland. Soil Science Society of America Journal, **74**: 624-634.

Sato Y, Kumagai T, Kume A, Otsuki K, Ogawa S. 2004. Experimental analysis of moisture dynamics of litter layers - the effects of rainfall conditions and leaf shapes. Hydrol. Process., **18**: 3007-3018. DOI: 10.1002/hyp.5746.

Savage M. 2012. Estimation of frost occurrence and duration of frost for a short-grass surface. South African Journal of Plant and Soil, **29**: 173-181.

Sayer EJ. 2006. Using experimental manipulation to assess the roles of leaf litter in the functioning of forest ecosystems. Biological Reviews, **81**: 1-31.

Schaetzl R, Thompson ML. 2015. Soils. Cambridge University Press.

Sharafatmandrad M, Mesdaghi M, Bahremand A, Barani H. 2010. The Role of Litter in Rainfall Interception and Maintenance of Superficial Soil Water Content in an

Arid Rangeland in Khabr National Park in South-Eastern Iran. Arid Land Research and Management, **24**: 213-222. DOI: 10.1080/15324981003762422.

Smith S. 2011. Eastern red-cedar: positives, negatives and management. The Samuel Roberts Noble Foundation: Ardmore, OK.

Steidle Neto AJ, Ribeiro A, Lopes DdC, Neto S, Souza WG, Santana MO. 2012. Simulation of rainfall interception of canopy and litter in eucalyptus plantation in tropical climate. Forest Science, **58**: 54-60.

Thurow T, Blackburn W, Warren S, Taylor Jr C. 1987. Rainfall interception by midgrass, shortgrass, and live oak mottes. Journal of Range Management: 455-460.

Tsiko CT, Makurira H, Gerrits AMJ, Savenije HHG. 2012. Measuring forest floor and canopy interception in a savannah ecosystem. Physics and Chemistry of the Earth, Parts A/B/C, **47–48**: 122-127. DOI: http://dx.doi.org/10.1016/j.pce.2011.06.009.

Viney NR. 1991. A review of fine fuel moisture modelling. International Journal of Wildland Fire, **1**: 215-234.

Walsh R, Voigt P. 1977. Vegetation litter: an underestimated variable in hydrology and geomorphology. Journal of Biogeography: 253-274.

Wang L, Throop HL, Gill T. 2015. A novel method to continuously monitor litter moisture – A microcosm-based experiment. Journal of Arid Environments, **115**: 10-13. DOI: http://dx.doi.org/10.1016/j.jaridenv.2014.12.011.

Wilson T, Kochendorfer J, Meyers T, Heuer M, Sloop K, Miller J. 2014. Leaf litter water content and soil surface CO_2 fluxes in a deciduous forest. Agricultural and Forest Meteorology, **192**: 42-50.

Wine ML, Ochsner TE, Sutradhar A, Pepin R. 2012. Effects of eastern redcedar encroachment on soil hydraulic properties along Oklahoma's grassland-forest ecotone. Hydrological Processes, **26**: 1720-1728.

Wine ML, Zou CB. 2012. Long-term streamflow relations with riparian gallery forest expansion into tallgrass prairie in the Southern Great Plains, USA. Forest Ecology and Management, **266**: 170-179.

Yoshikawa K, Overduin PP, Harden JW. 2004. Moisture content measurements of moss (Sphagnum spp.) using commercial sensors. Permafrost and Periglacial Processes, **15**: 309-318.

Zhang L, Dawes W, Walker G. 2001. Response of mean annual evapotranspiration to vegetation changes at catchment scale. Water Resources Research, **37**: 701-708.

Zou CB, Caterina GL, Will RE, Stebler E, Turton D. 2015. Canopy Interception for a Tallgrass Prairie under Juniper Encroachment. PLoS ONE, **10**: e0141422.

Zou CB, Turton DJ, Will RE, Engle DM, Fuhlendorf SD. 2014. Alteration of hydrological processes and streamflow with juniper (Juniperus virginiana) encroachment in a mesic grassland catchment. Hydrol. Process., **28**: 6173-6182. DOI: 10.1002/hyp.10102.

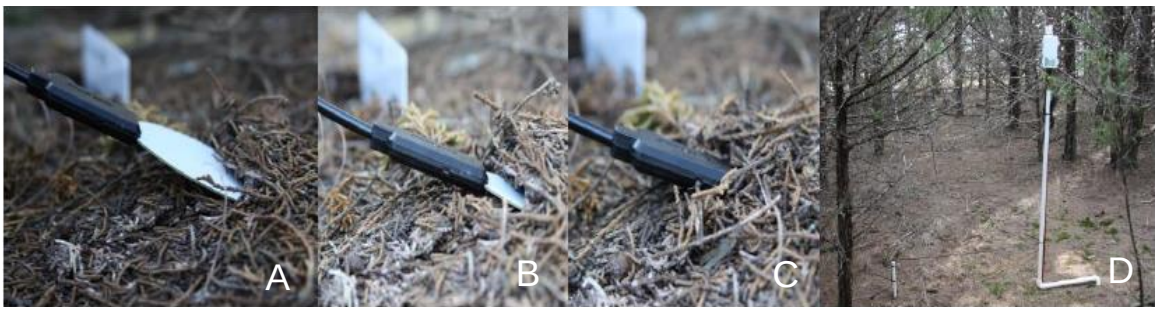

Figure 2.1. Illustration of stepwise installation (from A to C) of Leaf Wetness Sensor (LWS) into litter under juniper canopy. LWS was deployed at a 45° angle to the soil surface to measure change in dielectric constant of litter. Output signals were logged at 15-minute intervals as LWS counts with an EM50 data logger fixed to a T-Post (D).

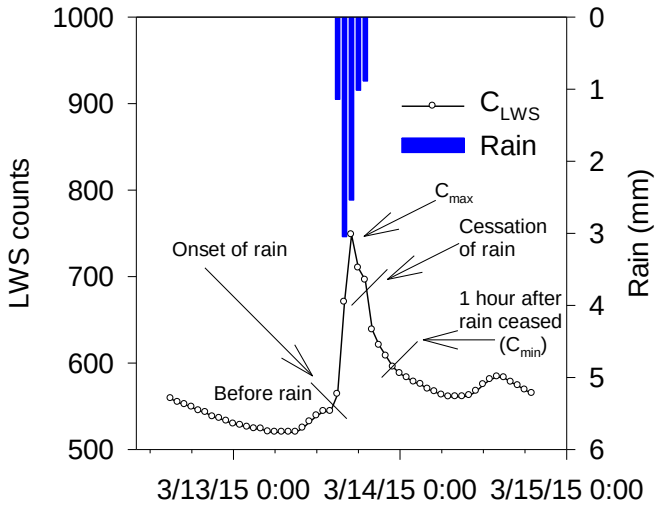

Figure 2.2. Determination of maximum and minimum interception capacities and litter interception loss used the Leaf Wetness Sensor counts (C_{LWS}) values from immediately before the onset of a rain event, the maximum C_{LWS} values during the rain event, and the C_{LWS} values one hour after the cessation of the rainfall event. Each dot or bar represents one 15-minute interval.

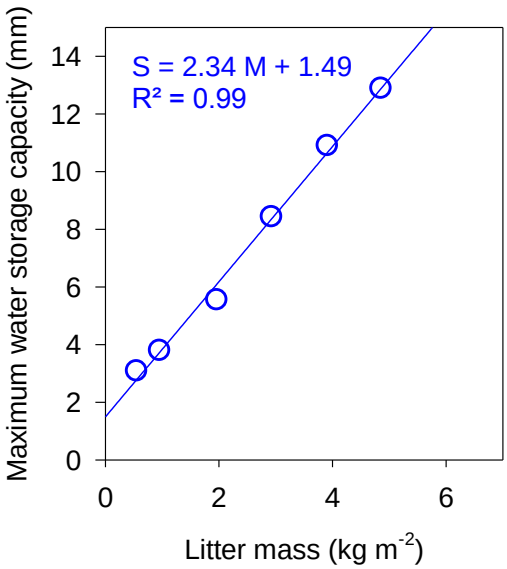

Figure 2.3. Relationship between maximum water storage capacity (*S*) and litter mass (M)

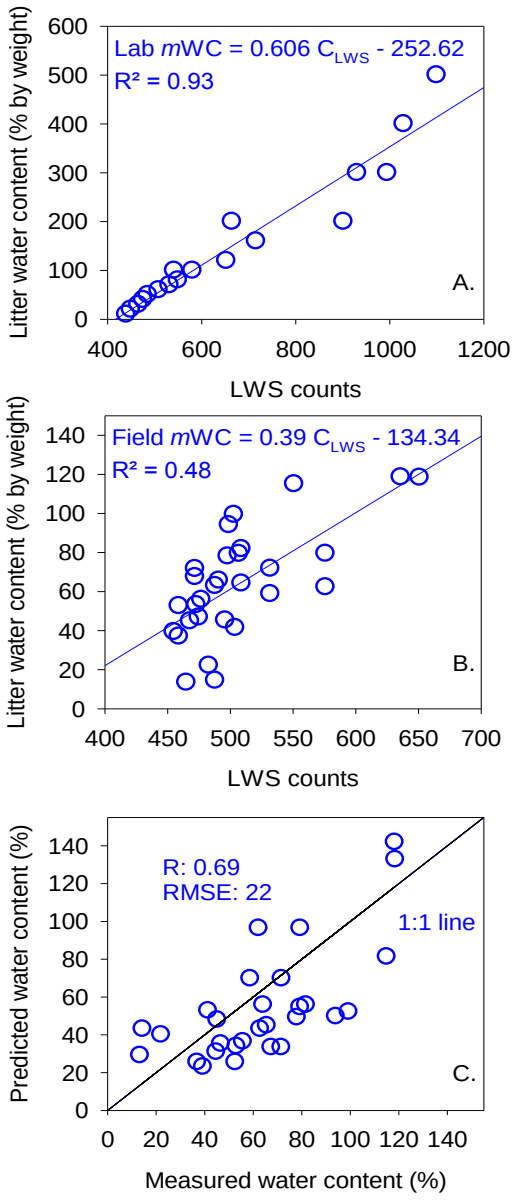

Figure 2.4. Relationship between Leaf Wetness Sensor counts (C_{LWS}) and measured litter water content (*m*WC) under laboratory setting using point comparisons for known litter water content series (A). Relationship between Leaf Wetness Sensor counts (C_{LWS}) and measured litter water content (*m*WC) under field setting (B), and comparison of the measured and the predicted litter water content with the 1:1 line (C).

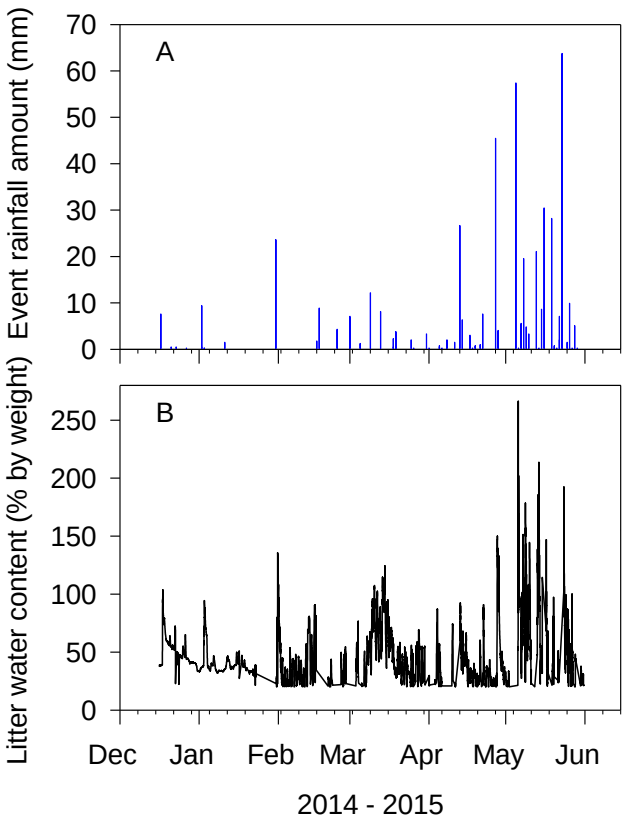

Figure 2.5. Event rainfall amount (mm) recorded at a weather station at the Oklahoma State University Range Research Station (A) and values of predicted litter water content (% by weight) (B)

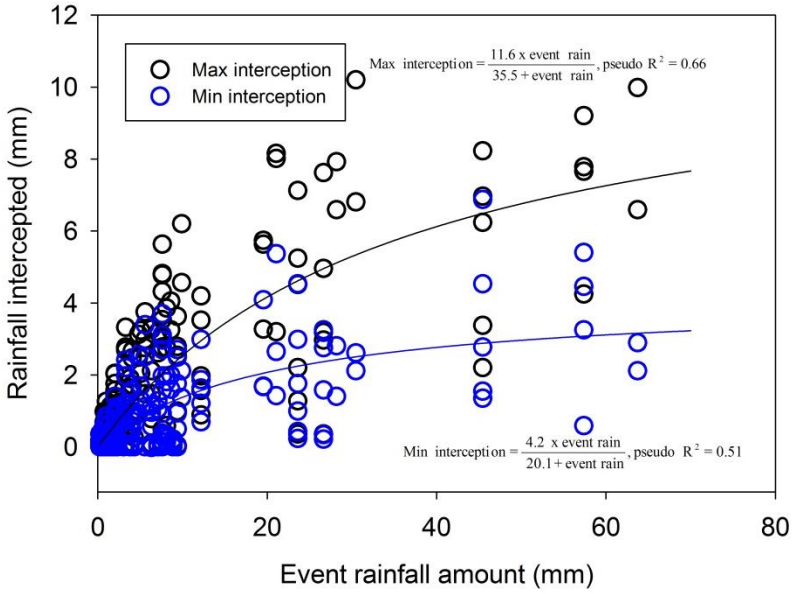

Figure 2.6. Relationship between event rainfall amount and maximum and minimum values for mm of rainfall intercepted

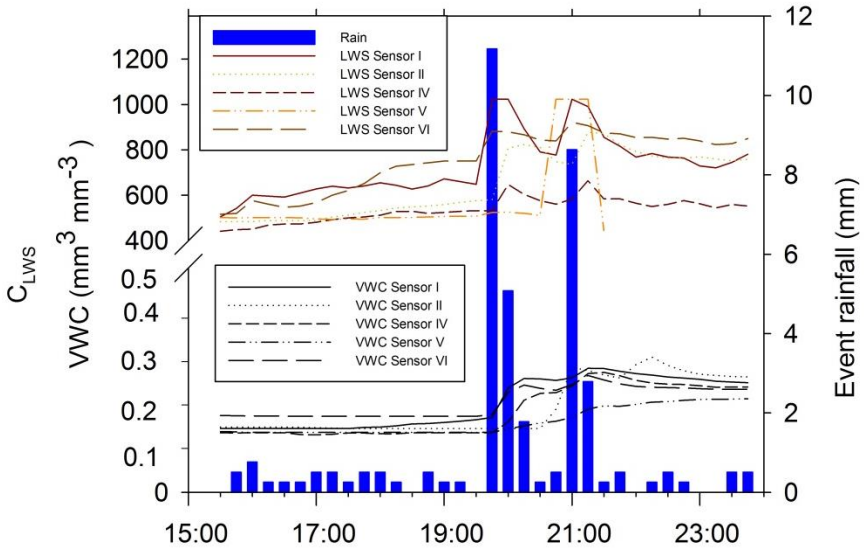

Figure 2.7. Increase in volumetric water content (VWC) and C_{LWS} associated with short intense rainfall within the larger rain event of 5 May 2015. Rain amounts greater than 3 mm in a 15-minute period generated increase in VWC. Soil water content was measured by EC-5 soil water content sensors at 5-cm soil depth.

CHAPTER III

VEGETATION CONTROLS ON THE SPATIO-TEMPORAL HETEROGENEITY OF DEEP MOISTURE IN BEDROCK: HYDROGEOPHYSICAL EVALUATION IN TALLGRASS PRAIRIE, JUNIPER WOODLANDS AND OAK FOREST

ABSTRACT

Information on soil moisture and its spatio-temporal variability in the vadose zone is important to detect the existence and assess the magnitude of deep drainage and flow pathways under different vegetation cover types. Time-lapse electrical resistivity imaging (ERI) was used to monitor water dynamics to a depth of 9 m in a tallgrass prairie, a prairie encroached by a juniper species (*Juniperus virigiana*), a full juniper woodland and an oak forest in the south-central Great Plains, Oklahoma, US. ERI indicated (a) vegetation induced differences in vertical bulk conductivity profiling, (b) increased spatial-temporal variability in root zone bulk conductivity under juniper-encroachment compared to grassland cover type and (c) two-layered bulk conductivity profiles. Electrical resistivity difference images were converted to volumetric moisture difference maps based on site-specific relationship between moisture content and inverted resistivity

differences. Although volumetric moisture content was lower in the top 3 m than deeper depths in tallgrass prairie, the moisture increased in deep soil layers and ranged between 25 and 45%. Volumetric moisture in juniper-encroached catchment ranged between 0 and 5% in deep soil layers. Oak forest showed 15 to 35% moisture content below 2.5 m depth. Two groundwater monitoring wells of 3 m depth were drilled in a tallgrass prairie and a juniper-encroached catchment. In a perched aquifer, water level in the monitoring well was higher under the tallgrass prairie than under the juniper-encroached catchment. Vegetation type resulted in heterogeneity in deep moisture levels and distribution, and hydrogeophysical methods such as electrical signatures and monitoring wells can be used for broader understanding of subsurface hydrology for land-use and groundwater management.

KEY WORDS: Electrical resistivity imaging, time-lapse ERI, grassland, juniper, oak, monitoring wells, vadose zone moisture, deep water dynamics, recharge

INTRODUCTION

Deep drainage and recharge occur when soil water percolates vertically, passes the active root extracting zone and through the vadose zone [*Allison et al.*, 1994; *M Sophocleous*, 2004]. The vadose zone in water-limited regions is usually thick [*McCord et al.*, 1997; *Nimmo et al.*, 2002; *Vauclin et al.*, 1979] and deep percolation of water and storage is sensitive to the depth of the rooting system. Change in water use pattern, and rooting depth and architecture [*Bleby et al.*, 2010] associated with changes in vegetation functional type, such as transition of grassland to woodland, is likely to affect the deep percolation dynamics and local recharge process [*M Sophocleous*, 2004; *Marios Sophocleous*, 2005; *Winter*, 1999]. A global synthesis of groundwater recharge showed that grasslands produce higher recharge compared to woodlands [*Kim and Jackson*, 2012]. Lower annual recharge rate was estimated after a grassland was encroached by woody vegetation in southwest Texas [*Moore et al.*, 2012].

Information on soil moisture and its spatial and temporal changes through the vadose zone are pivotal to detect the existence and assess the magnitude of deep drainage and flow pathways under contrasting vegetation types. Soil moisture can be determined by using moisture probes or dielectric sensors, cosmic ray neutrons, gamma ray attenuation, disturbed temperature sensing, and/or by using remote sensing methods [*Ochsner et al.*, 2013]. However, they fail to provide adequate information on deep soil moisture due to limits of coring depth [*Jayawickreme et al.*, 2014] and calibration techniques [*Ochsner et al.*, 2013], especially where competent rock is shallow. Electrical resistivity imaging (ERI), a non-intrusive technique, has been used since the 1830's [*Van*

Nostrand and Cook, 1966] to characterize and monitor water distribution, contaminant plumes, contaminations and remediation, fluid transport, groundwater flow and reactions, and subsurface heterogeneity and anisotropy, to map soil texture and to monitor geo-hazards [*Bentley and Gharibi*, 2004; *Beresnev et al.*, 2002; *Halihan et al.*, 2012; *Halihan et al.*, 2005; *Ong et al.*, 2010], but its use in monitoring vadose zone soil moisture dynamics and groundwater recharge is still limited [*Jayawickreme et al.*, 2014; *Ma et al.*, 2014; *Miller et al.*, 2014].

Electrical resistivity imaging is a geophysical technique in which surface electrodes are used for measurement and acquisition of apparent resistivity [*Halihan et al.*, 2005; *Jayawickreme et al.*, 2010; *Loke*, 1999; *Ma et al.*, 2014]. Changes in resistivity are derived by collecting apparent resistivity from same location at different time intervals [*Nijland et al.*, 2010]. The change in resistivity is due largely to soil water content in the absence of other subsurface reactions. The apparent resistivity data are inverted using an inversion model and developed into two-dimensional and three-dimensional images [*Halihan et al.*, 2005]. Electrical resistivity data are influenced by soil particle size, form and distribution of voids, soil water content, fluid properties, and temperature [*Samouëlian et al.*, 2005].

Limited studies have utilized ERI to estimate deep drainage of water and understand the dynamic interaction between vegetation and vadose zone moisture. *Jayawickreme et al.* [2008] used time-lapse ERI to understand the interaction between vegetation, climate and root zone moisture in a grassland-forest ecotone of Michigan, USA. In a recent study, spatial-temporal dynamics of near-surface soil moisture was

investigated using ERI in deciduous woodland [*Yuteng Ma et al.*, 2014]. One of the complications in using such geophysical methods is to accurately transform resistivity to volumetric moisture. Moisture values are underestimated when inverted resistivity values are converted into soil water based on petrophysical relations [*Michot et al.*, 2003]. Despite this limitation, no alternative method is currently feasible for non-intrusive estimation of subsurface moisture distribution and migration.

The objectives of this study were to evaluate the ability of two-dimensional time-lapse ERI to track soil moisture changes and to determine spatio-temporal variability in deep moisture in four different vegetated areas (tallgrass prairie, juniper encroached, full juniper woodland, and oak forest) in the south-central Great Plains, USA. Results will be used to help assess the effects of woody plant encroachment on the water cycle. Previous research indicates that encroachment by junipers reduces runoff and soil moisture in the rooting zone. We currently do not know how encroachment affects deep water migration or the differences between prairie, woodland, and oak forest. This understanding will allow us to better estimate changes in land use on a previously poorly understood portion of the water cycle.

METHODS

Experimental Site

The study was conducted at the Cross-Timber Research Station, Oklahoma State University. The study area is located about 11 km southwest of Stillwater, Payne County, Oklahoma, USA (36^{o} 03’47” N, 97^{o}11’03” W, and 331 m-asl) in the lower Cimarron

River watershed. It has a continental climate with mean annual temperature of 15.2 ^{o}C, and mean annual precipitation of 900 mm during 1994 to 2011 [*Zou et al.*, 2014].

Dominated by the Wellington formation of Permian age, the geology of the experimental site largely consists of red-brown shale, fine-grained sandstone and mudstone conglomerate (http://www.owrb.ok.gov/). Major soil types in the study site include Stephenville-Darnell complex, Grainola-Lucien complex, and Coyle soil series approximately one meter thick. Stephenville are fine-loamy, siliceous, active, thermic Ultic Haplustalfs; Darnell are loamy, siliceous, thermic, shallow, Udic Ustochrepts; Grainola are fine, mixed, thermic, Vertic Haplustalfs; Lucien are shallow fine sandy loam, mixed, thermic, shallow Typic Haplustolls; and Coyle series are fine-loamy, siliceous, thermic, Udic Argiustolls [*Henley et al.*, 1987; *Soil Survey Staff*, 1999].

Two major vegetation types in the site include tallgrass prairie and oak woodland. Prairie areas consist of C_4 grasses, including little bluestem (*Schizachyrium scoparium*), big bluestem (*Andropogon gerardii*), Indiangrass (*Sorghastrum nutans*), switchgrass (*Panicum virgatum*), and tall dropseed (*Sporobolus asper*) [*Limb et al.*, 2010]. Major forbs include western ragweed (*Ambrosia psilostachya)* and broomweed (*Gutierrezia dracunculoides*). Grasses are often found in Grainola-Lucien complex and Coyle soil series. Oak woodland is associated with Stephenville-Darnell complex and is dominated by post oak (*Quercus stellata* Wangenh.), blackjack oak (*Q. mailandica* Muenchh.) [*Engle et al.*, 2006]. In recent years, a juniper species (*J. virigiana*, eastern redcedar) is rapidly encroaching and expanding in tall- and mixed-grass prairies, thereby converting prairie patches into woodland. The mean basal area of juniper at the juniper encroached

site ranges from 15.9 to 17.0 m^2 ha^{-1}. Four experimental catchments, prairie, juniper encroached, juniper woodland and oak forest were selected for the study (Fig. 3.1). The catchments are between 2.0 and 2.7 ha with a mean slope between 5 and 6%.

Electrical Resistivity Imaging (ERI)

Electrical resistivity in the subsurface can be quantified using a multielectrode array to collect apparent resistivity data which can then be inverted into model or true resistivity values of the subsurface (Advanced Geoscience, Inc. SuperSting 8-channel resistivity instrument). Low-frequency alternating current is induced in two current electrodes and the potential difference is measured between two electrodes in an induced electric field. Typical range of current vary from 100 to 300 mA in these experiments. Contact resistance between soil and electrode was below 2000 ohms around the electrodes. Contact resistance tests were completed prior to initiating the survey to identify poor electrical contact between the electrodes and soil. Apparent resistivity ρ_a (Ω-m) is defined as the ratio between measured potential difference (ΔV) and induced electric current (I) into the ground.

$$\rho_a = \frac{\Delta V}{I} \tag{1}$$

Soil electrical conductivity σ (Sm^{-1}) is defined as the reciprocal of resistivity:

$$\sigma = \frac{1}{\rho} \tag{2}$$

Subsurface electrical resistivity is significantly influenced by different factors such as porosity, soil cavities and cracks, degree of water saturation, and concentration of dissolved salts [*Loke*, 1999; *Samouëlian et al.*, 2005].

Surface soil temperature

Soil temperature increases electrical conductivity by decreasing pore fluid resistivity and increasing mobility of ions [*Jayawickreme et al.*, 2014; *Samouëlian et al.*, 2005]. Therefore, diurnal and seasonal fluctuations in soil temperature alter electrical resistivity. Resistivity values are often expressed at standard temperature to facilitate comparison across time. Electrical resistivity is corrected to 25^{o}C using the *Keller and Frischknecht* [1966] equation:

$$\rho_{25^{\circ}C} = \rho_T \left[1 + 0.025\left(T - 25\right)\right] \quad (3)$$

where, $\rho_{25^{o}C}$ is the electrical resistivity at 25^{o}C, ρ_T is the electrical resistivity at temperature, T (^{o}C), and 0.025 is the correction factor.

Surface soil temperature was measured randomly across the transects in proximity to electrodes to a depth of 12 cm using a reference thermometer (Thermoworks, USA) (*accuracy* $\pm$ 0.05^{o}C) to detect temperature variability, and to determine the necessity of temperature correction for resistivity values. Daily soil temperature averaged over 5 minutes was also reported from a nearby weather station. We however did not correct resistivity values for temperature because as diurnal soil surface temperature minimally fluctuated (max=28^{o}C, min=24^{o}C, mean ± SD; 26^{o} ± 1.3^{o}C) throughout the months of data acquisition (Fig. 3.2).

Transect locations and description

A digital elevation model (DEM) was generated for the site from Light Detection and Ranging (LiDAR) bare earth elevation dataset-2 m for projected in North American horizontal datum of 1983 obtained from USDA NRCS. DEM's produced from LiDAR dataset are of higher resolution and provide greater accuracy for base layer for terrain mapping, watershed evaluations and hydrological modelling. The vertical accuracy of LiDAR bare earth elevation dataset was approximately 12.5 cm RMSE (G. Utley, personal communication, NRCS, OK, January 13, 2014). Transects were subjectively selected to follow the elevation contour line, to ensure that the soil profile is perpendicular to the flow paths and to adequately represent the vegetation cover. An attention was made to cover sufficient and different size class of juniper trees in the encroached site (Table 3.1), and oak trees in oak forest (Fig. 3.1).

The permanent latitudinal transects were 42 m long and oriented along the contour lines. All of the transects were located and deployed with electrodes of 48.3 cm length and 1.6 cm diameter made up of copper coated steel lightning rods permanently installed to a depth of 15 to 30 cm in June 2014. Electrode installation was completed a week prior to first ERI measurement to ensure good contact between soil and electrodes. Installation of permanent electrode lines prevents and/or minimizes any alterations in near-surface soil properties [*Amidu and Dunbar*, 2007]. Thus, a total of 56 electrodes were permanently deployed on the surface across each latitudinal transect with 0.75 m electrode spacing.

Acquisition of apparent resistivity

Apparent resistivity data were collected following rainfall events in June 2014, and after drier conditions in June, July and August 2014 to understand and image deep drainage of water (Table 3.2). The 42 m long ERI line provided data acquisition to infer subsurface process and anomalies and deep moisture to the depth of approximately 9 m. Hundreds of data points were collected in an automated mode following Oklahoma State University (OSU) proprietary method (the Halihan-Fenstemaker, HF, method). The OSU proprietary method provides better data quality and increases the sensitivity of subsurface images by approximately an order of magnitude [*Halihan and Fenstemaker*, 2004; *Miller et al.*, 2014]. The resolution of electrical resistivity images were half of the stake spacing (0.38 m). Data collection included repetitive measurements. The average error in apparent resistivity data ranged was 0.4%.

Conversion of resistivity to soil water content

Surface volumetric soil moisture (12 cm) near electrodes was determined using HydroSense II (Campbell Scientific, USA) randomly during ERI data acquisition. The relationship between soil electrical resistivity and volumetric soil water content in the near surface is typically described using Archie's relationship [*Daily et al.*, 2004; *Samouëlian et al.*, 2005], which may follow a power, logarithmic or non-linear trend [*Calamita et al.*, 2012]:

$$s = \left(\frac{\rho_s}{\rho} \right)^{\frac{1}{m}} \tag{4}$$

Where, S is the volumetric water content, m is the power law coefficient between saturation and resistivity (sand 1.16 and clay loam 0.67), ρ is the resistivity values from inversion data, and ρ_s is the bulk resistivity of soil at 100% saturation [*Jayawickreme et al.*, 2010]. Archie's relationship and laboratory-based petro-physical models are only appropriate for certain soil types (e.g. coarse to medium grained), rely on small soil sample volume and controlled conditions, and exhibit narrow field application [*Michot et al.*, 2003]. Thus, we developed a field scale relationship to calculate spatial heterogeneity in volumetric moisture (Fig. 3.3). The site-specific relationship between volumetric moisture and inverted resistivity was determined based on surface moisture content using HydroSense II. Resistivity was converted and mapped as volumetric water content [*Fan et al.*, 2015b; *Yuteng Ma et al.*, 2014].

Temporal variability in water level

Two monitoring wells of 3 m depth and 5.1 cm diameter were drilled in a hydraulically conductive location as indicated by electrical resistivity imaging (ERI); one in each tallgrass prairie site and juniper-encroached catchment site using a trailer-mounted Geoprobe (6200 TMP, Kejr, Inc. Salina, KS), and the piezometers were instrumented with CTD-10 sensors for monitoring. The sensor was connected to the EM50 data logger (Decagon, Pullman, WA, USA) to measure water level (*accuracy* $\pm$ 0.05%) at 15-minutes intervals.

Data analysis

Field data were corrected for topography to adjust the change in distance between the electrodes. Three applications of topographic correction included (a) compensation for alterations in surface elevation [*Schwartz and Zhang*, 2003], (b) discerning lateral heterogeneity in electrical properties and comparison of subsurface images in three-dimensional, and (c) dealing with lines orthogonal to the contour line. A base station was established in each site, and a TOPCON Hyperlite Plus Global Positioning System and a rover with Bluetooth connected handheld unit was set to record latitude, longitude and elevation for each electrode with 1 cm accuracy. The location of each electrode was thus corrected based on the easting, northing and elevation of base station obtained from Online Positioning User Service (OPUS), which is operated by National Oceanic and Atmospheric Administration (NOAA).

Pseudo-sections of electrical resistivity images were developed in two-dimensions using an inversion algorithm following the HF method. Random noise error was eliminated prior to inversion iterations to prevent extreme values. Data repeatability error in excess of 2% was minimized by removing values prior to inversion. The apparent resistivity data, collected in field, were inverted to create a model space of resistivity values to replicate the collected data [*Halihan et al.*, 2005]. The later values are also called true resistivity values. The RMS inversion error was reported in percent for pseudo-sections of electrical resistivity to illustrate goodness of fit. The lower RMS inversion error represents better input data, inverted model and model fit [*Travelletti et al.*, 2012]. The RMS inversion error ranged from 3.82 to 5.07% (Table 3.1).

$$RMS = \sqrt{\frac{\sum_{i=1}^{N}\left(\frac{d_i^{pred} - d_i^{meas}}{d_i^{meas}}\right)^2}{N}} \times 100 \quad (5)$$

where, N = total no of data points, and d_i^{pred} and d_i^{meas} are predicted and measured values of data point i respectively [*Gasperikova et al.*, 2012].

Given that the lithology and soil texture were unchanged, background ERI was used to compare and characterize spatio-temporal variability in subsurface resistivity. Percent change in conductivity was imaged based on the difference in resistivity between background image and each subsequent date. Spatial and temporal distribution of volumetric moisture content was developed from regular resistivity images. Images were contoured using Surfer 8 (Golden Software Inc), and presented with a consistent color scheme.

RESULTS

Baseline ERI for 4 sites

The background resistivity images for the prairie and juniper-encroached catchments were G1LO066 and E1LO613, respectively (Table 3.2). Background ERI from the prairie site showed a resistive layer (100 to 500 Ohm-m) running across the line to a depth of 3.5 m (Fig. 3.4, top panel). The volumetric moisture content ranged between 0 to 10% (Fig. 3.5). An interface between the shallow resistive and deeper conductive zone (hereafter referred to as the interface only) was observed at 325 m in the background ERI (3.5 m deep). Irregular resistive zones appeared at the corners of the

pseudo-section with resistivity of 500 Ω-m and 5% volumetric moisture, but may be the effects of boundary conditions on the inversion. The soil below 3.5 m was highly conductive except for a small resistive layer (200 Ohm-m, and 10% moisture) near 9 m. The bottommost layer at the depth below 6 m showed higher lateral heterogeneity in resistivity along the 42 m long profile.

In contrast, the juniper-encroached site showed highly conductive upper layer and resistive lower soil profile (Fig. 3.6, top panel). The soil was highly conductive (0 to 90 Ω-m) up to 3.5 m depth. The volumetric moisture content in the top 3.5 m ranged between 20 to 45% (Fig. 3.7, top panel). Peak resistivity of 2500 Ω-m (0 to 5% moisture) appeared at the distance of 36 m from the LHS across the line. Resistivity below 6 m was highly variable with a range from 500 to 5000 Ω-m. A highly resistive layer (5000 Ω-m) appeared at the lowermost elevation (314 to 316 m) of the pseudo-section. However, background electrical properties in oak forest showed higher resistivity up to 4.5 m depth (100 to 2500 Ω-m and 5 to 15% moisture) and lower resistivity below 4.5 m (25 to 90 Ω-m) (Fig. 3.8, top panel). The moisture distribution appeared similar to prairie site and juniper woodland (Fig. 3.9). The background electrical resistivity image in the juniper woodland shows greater resistivity up to 2.5 m depth (100 to 2500 Ω-m) but conductive subsurface (5 to 90 Ω-m) below the resistive layer. However, resistivity at 2.5 m depth continuously increased at right hand side (RHS) along the 42 m line (Fig. 3.10, top panel).

Transient resistivity and moisture

Transient conductivity images showed a two-layer moisture migration profile: non-wetted and wetted in all catchments after a rainfall event. Percent change in conductivity and volumetric water content was lower in the top 3 m and higher below the 3 m depth in the electrical resistivity and moisture images. Thus, tallgrass prairie and oak forest were dry on the top and wet below 3 m depth. In contrast, juniper-encroached site was wet on the top but dry below 3 m depth.

Prairie

No change in electrical conductivity below 323 m elevation (5.5 m deep) was detected in the pseudosection G1LO0606T-0624, which was collected 18 days after the baseline image. Thus, the gray region in the pseudosection between 319 to 323 m elevations epitomizes the zone with no apparent change in conductivity. The volumetric moisture content of this zone during the time ranged between 10 to 45%. However, the conductivity increased by 5 to 25% up to 323 m elevation. The volumetric moisture for the zone ranged between 5 to 10% (Fig. 3.5). A few dry spots with 0 to 5% moisture occurred on surface at 327.5 m elevation after 18 days in the electrical image leaving no change in conductivity in the remaining area. In July 2014, the top horizon in the electrical image G1LO0606T-0703 completely dried with up to 25% decrease in conductivity corresponding to 5% volumetric moisture. However, conductivity increased by 25 to 50% between 322 to 327 m. No change in conductivity was detected below 322 m. Distinct changes in conductivity were apparent in the month of August as indicated by the electrical image G1LO0606T-0801. The top surface was very dry (5% moisture) resulting in 25% decrease in conductivity (Fig. 3.5). The change in conductivity below

the top horizon was negligible. However, water accrued beneath the preceding thin layer. A circular anomaly at 5.5 m deep had 20% increases in conductivity.

Juniper-encroached

A large portion of transient image E1LO0613-0624, which was collected 11 days after the baseline image showed no change in conductivity through time (Fig. 3.6). Few spots at the corner of pseudosection at 317 to 322 m elevation, and at 10, 20 and 35 m distance along the transects between 320 to 322 m elevation showed 5 to 10% increase in conductivity (Fig. 3.6). Those regions had 35 to 45% volumetric moisture (Fig. 3.7). A 5% decrease in conductivity was also detected between 30 to 35 m transect distance at 318 m elevation. A few dry areas occurred near the surface of the image. The conductive area of the image showed an irregular increase during July 2014. The vertical and horizontal increase in conductive region was observed at 317 m elevation. Two circular anomalies near 321 m elevation (2.5 m deep) from left hand side (LHS) of the pseudosection E1LO0613-0703 were inferred as a conductive zone. The conductivity of the anomalies increased by 20%. The volumetric moisture content was 20 to 25% for the anomalies (Fig. 3.7). The upper 1 m thick layer in pseudo-section of E1LO0613-0801 showed 20% decrease in conductivity. Below this resistive layer, the conductivity remained unchanged throughout the transect length for nearly half meters thickness. Below this horizontal layer, conductivity increased by 20% to a depth of 9 m. The volumetric moisture content was between 0 to 5% towards the corners of image. Two distinct nuclei with depth extent of 2 m and 25% increase in conductivity were observed at 293 m elevation. Between 15 to 25 m distances along the pseudo-section of

E1LO0613-0801 at 314 to 316 m elevation, there was no apparent change in conductivity and 0 to 5% volumetric moisture. The overall volumetric water content was higher for the top 5 m and lower below 5 m depth.

Oak forest

First two transient images from 27 June and 05 July 2014 showed 25 to 100% decrease in conductivity up to 2.5 m depth, and 0.5 m thick gray region delimited the zone with no change in conductivity (Fig. 3.8). The gray zone had 10% volumetric moisture. The volumetric moisture content for top 2.5 m ranged between 5 to 10%. Volumetric ranged between 15 to 35% below 2.5 m depth (Fig. 3.9). Transient image demonstrated on July 2014 showed 50 to 75% increase in conductivity.

Juniper woodland

The first transient image from 04 July 2014 showed no change in conductivity except a small patch at the left corner of image, which clearly exhibits 10 to 15% decrease in conductivity (Fig. 3.10). The moisture image demonstrated complete drying of surface with 0 to 10% volumetric moisture (Fig. 3.11). At the end of July, the top 3 m showed either 10 to 20% decrease in conductivity or no change in conductivity as indicated by gray region. Few areas on the surface also showed no change in conductivity. Conductivity increased by 15 to 20% below the top 3 m profile across 42 m line. However, no apparent change in conductivity was detected below 7 m in LHS of the pseudosection. Moisture images showed 15 to 35% volumetric moisture below 3 m depth.

Temporal variability in water level in a tallgrass prairie and juniper-encroached catchment

Climate, vegetation and lithologic properties are likely to govern the seasonal fluctuations in water level. Water level was higher under the tallgrass prairie than under the juniper-encroached catchment. Peak water level was recorded on 25-June 2015 in the prairie, but the water level in the juniper-encroached catchment peaked during 28-November 2015 (Fig. 3.12 and 3.13).

DISCUSSION

There were substantial difference in resistivity under tallgrass prairie, juniper-encroached catchment, juniper woodland and oak forest. High bulk conductivity zones were developed in tallgrass prairie and oak forest after rainfall events. Results indicate two-layered moisture migration profiles: non-wetted and wetted across the vegetation cover types. Grass and oak forest reduced volumetric moisture content in the top 3 m of the critical zone but increased deep water content.

Background ERI

Background ERI provided initial images of resistivity based on inversion model from measurements taken at time step 1. In other words, they refer to reference pseudo-sections developed prior to actual measurements to better describe temporal anomalies in resistivity [*Halihan et al.,* 2012; *Travelletti et al.,* 2012]. Background ERI from the grassland showed a resistive layer across the line to a depth of 3.5 m. Evaporation from soil surface and/or plant water extraction during the data acquisition period could

potentially lower moisture content and increase resistivity in the shallow zone. In contrast, higher subsurface resistivity below 3.5 m depth in the background image for juniper-encroached catchment indicates that trees are expected to tap water from greater depth. The oak forest showed a higher moisture content below 4.5 m depth indicating deep drainage of infiltrated water. Studies indicate that trees play an important role in increasing the preferential flow of water [*Alaoui et al.*, 2011], and improving soil infiltration capacity [*van Dijk and Keenan*, 2007; *Zou et al.*, 2014]. Surface evaporation however can dominate juniper woodland with thick litter mass to produce lower volumetric moisture content. Annual evapotranspiration (ET) is also higher in woody plants compared to grasslands [*Heilman et al.*, 2009; *Liu et al.*, 2010; *Zhang et al.*, 2001], and ET and near surface moisture content are highly correlated in woodland [*Heilman et al.*, 2009].

Time-lapse ERI in 2D: change in conductivity, and volumetric water

Time lapse images are necessary to understand the influence of weather, vegetation and lithology on subsurface moisture distribution [*Jayawickreme et al.*, 2008]. The influence of weather and vegetation on water content can be seen from the pseudosection G1LO0606T-0624 for the prairie cover type. The data acquisition for this pseudosection followed a major rainfall event on 2nd June 2014, but volumetric moisture (5 to 10%) near soil surface was lower, which implies that most of the water was either used by plants or lost to evaporation, or drained deeper within the profile. *Jayawickreme et al.* [2008] observed a resistive layer near the surface following a rainfall event in a grassland from Michigan, USA wherein water drained deeper into the profile. Recent

studies also indicate that woody plants rely on shallow soil water during the wet season and deep water during the dry season [*Rossatto et al.*, 2012; *Verweij et al.*, 2011].

The influence of lithology can be seen from the pseudosection G1LO0606T-0703 for the prairie cover type. A pattern of potential lateral flow was observed in the image. Barriers to vertical flow of water by subsurface features like shallow bedrock interfaces and argillic horizons and the formation of perched water tables by subsurface ponding of water may contribute to the development of horizontal flow [*Hardie et al.*, 2012; *Mulholland et al.*, 1990]. *Jayawickreme et al.* [2008] observed no apparent change in conductivity between 2.5 to 5 m depth during early summer but increased conductivity following rain water percolation during early fall 2007.

The juniper-encroached catchment was however highly conductive in the top layer up to 3.5 m depth as notable in background image E1LO613. The rooting depth for shrubs may extend up to 5.1 ± 0.8 m which is greater than for grasses or herbaceous plants (2.6 ± 0.1 m) [*Canadell et al.*, 1996]. The higher moisture content in the rooting zone, as observed to the depth of 3.5 m, in the juniper-encroached catchment compared to prairie suggests that moisture was retained in the surface and trees access deep horizons and tap into deep moisture. *Zou et al.* [2014] also reported substantially higher initial and steady state infiltration rate under juniper compared to grassland catchment. We reported that most of the juniper trees existed towards the end of pseudosection. A substantial part (> 70 %) of this latitudinal transect was free of vegetation, and thus limited canopy cover and juniper litter was present along the distance up to 35 m to intercept rainfall (Fig. 3.8). Areas directly and/or closely below the trees were resistive and showed complete loss of

water. However, trees could increase infiltration [*van Dijk and Keenan*, 2007] and facilitate downward movement of water [*Alaoui et al.*, 2011]. Trees may redirect and funnel intercepted water into the soil as stemflow [*Zou et al.*, 2015]. Similarly, the occurrence of small storm events during July and August in partly moist soils (Fig. 3.2) can significantly alter deep drainage of water. Volumetric moisture in the deep layer (below 5 m depth) ranged 0 to 5% for all images in juniper-encroached compared to grassland catchment. *Caterina et al.* [2014] indicated that water use by individual juniper trees, as indicated by sap flow measurement, ranged from 2 to 80 liters per day, which was largely explained by tree characteristics, environmental variables (temperature and solar radiation), and volumetric moisture extending up to 10 cm. Plant water use can be high during favorable moisture content and for larger trees.

Transient images in the oak forest indicate deep drainage of infiltrated water (Fig. 3.9). Higher electrical conductivity, and a stable moisture profile were observed in an oak-pine forest in New Jersey after a rain event; suggesting the role of oak roots on soil moisture regulation [*J L Robinson et al.*, 2012]. Our oak forest has an undisturbed land use history but juniper-encroached catchments were cultivated prior 1950s' and soils may have been compacted. The surface was completely dry in the juniper woodland (Fig. 3.10 and 3.11). Entire rainfall may have been intercepted by canopy or evaporated from litter layer but after a couple of rain events in July water is likely to infiltrate deep as indicated by conductive subsurface below 3 m. Salts are also likely to flush down deep under precipitation events; thereby increasing salt concentration and electrical conductivity below 3 m [*Moore et al.*, 2010]. Overall, the electrical resistivity images showed a two-

layer moisture migration profile in all experimental catchments and heterogeneity in soil moisture across vegetation and months indicate differential water use pattern. It is important to mention that one transect was used for each cover type in this study. It is therefore likely that some of the differences are due to the specific soil types that were under the specific transects, not the vegetation. However, the length of transect enabled us to capture spatial heterogeneities in soil types, and thus were representative of the vegetation cover type.

Temporal variability in water level

Water level in two monitoring wells indicates that vegetation can modulate recharge processes, and woody plants can decrease the water table in a perched aquifer by a significant amount. The results are akin to and support electrical conductivity from the time-lapse ERI. Woody plants intercept rainfall via plant canopy and litter [*Zou et al.*, 2015], affect ET differently [*Dawson*, 1996] and/or tap into deep water to reduce water level [*Rossatto et al.*, 2012]. Water extraction can however vary with vegetation structure, slope positions and depth of water table, and a minimal of 30% of total water use such as in cerrado woody community may arise from deeper layers [*Rossatto et al.*, 2012]. Monitoring wells and spatio-temporal variability in groundwater level are therefore important to understand the effects of land-use and vegetation cover on deep water dynamics.

Land management implications

Woody plant encroachment in grasslands and savannas is a global phenomenon, which results in biogeochemical, ecophysiological and ecohydrological changes [*Hibbard et al.*, 2001; *Huxman et al.*, 2005; *McClain et al.*, 2003; *Sala and Maestre*, 2014; *Williams et al.*, 2013]. Grasslands in the south-central Great Plains are rapidly being transformed from herbaceous-dominated systems to woodlands or woody-dominated savanna [*Archer et al.*, 1995; *Briggs et al.*, 2002]. Proliferation of woody plants into rangelands previously dominated by herbaceous plants in Oklahoma, USA [*Smith*, 2011] is predicted to decrease albedo and increase latent heat partitioning to evapotranspiration (ET) at the landscape level [*Heilman et al.*, 2009]. As a result, the physiognomy transition from grassland to shrub is associated with increased ET due to greater leaf area, deeper roots, and greater canopy interception, and potential loss of water available for streamflow and recharge, especially in the semi-arid and sub-humid regions [*Bridget R Scanlon et al.*, 2002a; *Bridget R Scanlon et al.*, 2002b; *Seyfried and Wilcox*, 2006; *Wilcox and Thurow*, 2006]. Similarly, crown area and leaf area index in deciduous forest such as oak are negatively correlated to soil moisture at the beginning of growing season, but water content may increase with higher throughfall after leaves abscise [*Yuteng Ma et al.*, 2014].

Understanding the impact of vegetation and vegetation transition is pivotal to manage land cover for water supply. Groundwater depletion in the United states [*Konikow*, 2015] is evident in the south and south-central Great Plains as indicated by water shortage issues resulting from loss of streams and water in reservoirs and presumably higher water extraction from groundwater aquifers [*Murray*, 2012]. Such

issues are often exacerbated by long and intense droughts and increasing demand of water for irrigation purpose. It is predicted that the one-third of southern Great Plains will fail to support irrigation activities by 2042 due largely to depleting fossil groundwater [*Bridget R Scanlon et al.*, 2012]. Thus, information on deep moisture is important to understand deep drainage and groundwater recharge under different land use and cover [*Bridget R Scanlon et al.*, 2005]; this is critical to manage water resources and to adapt to climatic variability and extreme events like droughts.

The results contextualize and highlight the ability of time-lapse ERI to detect moisture dynamics and localized recharge sites. Results indicate that grass may reduce volumetric moisture in the top 3 m of the critical zone but increase deep water content. Vegetation transition such as woody encroachment is likely to reduce deep drainage and recharge in the experimental catchments but grasslands and oak trees as land cover can potentially improve ground water recharge. An in-depth study on the effect of vegetation and vegetation transition on regional groundwater systems is equally essential. It is important to mention that one transect was used for each cover type in this study. It is therefore likely that some of the differences are due to the specific soil types, and lithology that was under the specific transects, not the vegetation. Future studies should monitor subsurface physical properties, identify hydraulic properties of unconsolidated materials and directly quantify groundwater recharge using isotopes or chloride mass balance.

ACKNOWLEDGEMENT

This study was supported by the USGS 104B through Oklahoma Water Resources Center, Oklahoma Agricultural Experiment Station, Boone Pickens School of Geology, NSF EPSCoR (NSF-1301789), NSF Dynamics of Coupled Natural and Human Systems (CNH) program (DEB-1413900) and USDA National Institute of Food and Agriculture AFRI Sustainable Bioenergy program (2014-67010-21653). We gratefully acknowledge Elaine Stebler and Chris Stanberry for the field assistance and logistic support. The Halihan-Fenstemaker method used in this paper is the property of Oklahoma State University. The technique is also commercially available by Aestus, LLC.

REFERENCES

Alaoui, A., U. Caduff, H. H. Gerke, and R. Weingartner (2011), A Preferential Flow Effects on Infiltration and Runoff in Grassland and Forest Soils, *Vadose Zone J.*, *10*(1), 367-377.

Allison, G., G. Gee, and S. Tyler (1994), Vadose-zone techniques for estimating groundwater recharge in arid and semi-arid regions, *Soil Sci. Soc. Am. J.*, *58*(1), 6-14.

Amidu, S. A., and J. A. Dunbar (2007), Geoelectric studies of seasonal wetting and drying of a Texas vertisol, *Vadose Zone J.*, *6*(3), 511-523.

Archer, S., D. S. Schimel, and E. A. Holland (1995), Mechanisms of shrubland expansion: land use, climate or CO2?, *Clim. Change*, *29*(1), 91-99.

Bentley, L. R., and M. Gharibi (2004), Two-and three-dimensional electrical resistivity imaging at a heterogeneous remediation site, *Geop.*, *69*(3), 674-680.

Beresnev, I. A., C. E. Hruby, and C. A. Davis (2002), The use of multi-electrode resistivity imaging in gravel prospecting, *JAG*, *49*(4), 245-254.

Bleby, T. M., A. J. Mcelrone, and R. B. Jackson (2010), Water uptake and hydraulic redistribution across large woody root systems to 20 m depth, *Plant, Cell Environ.*, *33*(12), 2132-2148.

Briggs, J. M., G. A. Hoch, and L. C. Johnson (2002), Assessing the rate, mechanisms, and consequences of the conversion of tallgrass prairie to Juniperus virginiana forest, *Ecosystems*, *5*(6), 578-586.

Calamita, G., L. Brocca, A. Perrone, S. Piscitelli, V. Lapenna, F. Melone, and T. Moramarco (2012), Electrical resistivity and TDR methods for soil moisture estimation in central Italy test-sites, *J. Hydrol., 454*, 101-112.

Canadell, J., R. Jackson, J. Ehleringer, H. Mooney, O. Sala, and E.-D. Schulze (1996), Maximum rooting depth of vegetation types at the global scale, *Oecologia*, *108*(4), 583-595.

Caterina, G. L., R. E. Will, D. J. Turton, D. S. Wilson, and C. B. Zou (2014), Water use of Juniperus virginiana trees encroached into mesic prairies in Oklahoma, USA, *Ecohydrology*, *7*, 1124-1134.

Daily, W., A. Ramirez, A. Binley, and D. LeBrecque (2004), Electrical resistance tomography, *The Leading Edge*, *23*(5), 438-442.

Dawson, T. E. (1996), Determining water use by trees and forests from isotopic, energy balance and transpiration analyses: the roles of tree size and hydraulic lift, *Tree Physiology*, *16*(1-2), 263-272.

Engle, D. M., T. N. Bodine, and J. Stritzke (2006), Woody plant community in the cross timbers over two decades of brush treatments, *Rangeland Ecol. Manage.*, *59*(2), 153-162.

Fan, J., A. Scheuermann, A. Guyot, T. Baumgartl, and D. A. Lockington (2015), Quantifying spatiotemporal dynamics of root-zone soil water in a mixed forest on subtropical coastal sand dune using surface ERT and spatial TDR, *J. Hydrol.*, *523*, 475-488.

Gasperikova, E., S. S. Hubbard, D. B. Watson, G. S. Baker, J. E. Peterson, M. B. Kowalsky, M. Smith, and S. Brooks (2012), Long-term electrical resistivity monitoring of recharge-induced contaminant plume behavior, *J. Contam. Hydrol.*, *142*, 33-49.

Halihan, T., and T. Fenstemaker (2004), Proprietary electrical resistivity imaging method, 2nd ed. Stillwater, Oklahoma, in *Oklahoma State University Office of Intellectual Property* edited.

Halihan, T., J. Albano, S. D. Comfort, and V. A. Zlotnik (2012), Electrical Resistivity Imaging of a Permanganate Injection During In Situ Treatment of RDX-Contaminated Groundwater, *Ground Water Monit. R.*, *32*(1), 43-52.

Halihan, T., S. Paxton, I. Graham, T. Fenstemaker, and M. Riley (2005), Post-remediation evaluation of a LNAPL site using electrical resistivity imaging, *J. Environ. Monit.*, *7*(4), 283-287.

Hardie, M. A., R. B. Doyle, W. E. Cotching, and S. Lisson (2012), Subsurface lateral flow in texture-contrast (duplex) soils and catchments with shallow bedrock, *Appl. Environ. Soil Sci.*, *2012*.

Heilman, J., K. McInnes, J. Kjelgaard, M. Keith Owens, and S. Schwinning (2009), Energy balance and water use in a subtropical karst woodland on the Edwards Plateau, Texas, *J. Hydrol*, *373*(3), 426-435.

Henley, J., R. Gelnar, and R. E. Mayhugh (1987), *Soil survey of Payne County, Oklahoma*, US Government Printing Office.

Hibbard, K. A., S. Archer, D. S. Schimel, and D. W. Valentine (2001), Biogeochemical changes accompanying woody plant encroachment in a subtropical savanna, *Ecology*, *82*(7), 1999-2011.

Huxman, T. E., B. P. Wilcox, D. D. Breshears, R. L. Scott, K. A. Snyder, E. E. Small, K. Hultine, W. T. Pockman, and R. B. Jackson (2005), Ecohydrological implications of woody plant encroachment, *Ecology*, *86*(2), 308-319.

Jayawickreme, D. H., R. L. Van Dam, and D. W. Hyndman (2008), Subsurface imaging of vegetation, climate, and root-zone moisture interactions, *Geophys. Res. Lett.*, *35*(18).

Jayawickreme, D. H., R. L. Van Dam, and D. W. Hyndman (2010), Hydrological consequences of land-cover change: Quantifying the influence of plants on soil moisture with time-lapse electrical resistivity, *Geop.*, *75*(4), WA43-WA50.

Jayawickreme, D. H., E. G. Jobbágy, and R. B. Jackson (2014), Geophysical subsurface imaging for ecological applications, *New Phytol.*, *201*(4), 1170-1175.

Keller, G. V., and F. C. Frischknecht (1966), Electrical methods in geophysical prospecting.

Kim, J. H., and R. B. Jackson (2012), A global analysis of groundwater recharge for vegetation, climate, and soils, *Vadose Zone J.*, *11*(1), 0-0.

Konikow, L. F. (2015), Long-Term Groundwater Depletion in the United States, *Groundwater*, *53*(1), 2-9.

Limb, R. F., D. M. Engle, A. L. Alford, and E. C. Hellgren (2010), Tallgrass prairie plant community dynamics along a canopy cover gradient of eastern redcedar (Juniperus virginiana L.), *Rangeland Ecol. Manage.*, *63*(6), 638-644.

Liu, W., Y. Hong, S. I. Khan, M. Huang, B. Vieux, S. Caliskan, and T. Grout (2010), Actual evapotranspiration estimation for different land use and land cover in urban regions using Landsat 5 data, *J. Appl. Remote Sens.*, *4*(1), 041873-041873-041814.

Loke, M. (1999), Electrical imaging surveys for environmental and engineering studies, *A practical guide to, 2*.

Ma, Y., R. L. Van Dam, and D. H. Jayawickreme (2014), Soil moisture variability in a temperate deciduous forest: insights from electrical resistivity and throughfall data, *Environ. Earth Sci., 72*(5), 1367-1381.

McClain, M. E., E. W. Boyer, C. L. Dent, S. E. Gergel, N. B. Grimm, P. M. Groffman, S. C. Hart, J. W. Harvey, C. A. Johnston, and E. Mayorga (2003), Biogeochemical hot spots and hot moments at the interface of terrestrial and aquatic ecosystems, *Ecosystems, 6*(4), 301-312.

McCord, J., C. Gotway, and S. Conrad (1997), Impact of geologic heterogeneity on recharge estimation using environmental tracers: Numerical modeling investigation, *Water Resour. Res., 33*(6), 1229-1240.

Michot, D., Y. Benderitter, A. Dorigny, B. Nicoullaud, D. King, and A. Tabbagh (2003), Spatial and temporal monitoring of soil water content with an irrigated corn crop cover using surface electrical resistivity tomography, *Water Resour. Res., 39*(5).

Miller, R. B., D. M. Heeren, G. A. Fox, T. Halihan, D. E. Storm, and A. R. Mittelstet (2014), The hydraulic conductivity structure of gravel-dominated vadose zones within alluvial floodplains, *J. Hydrol., 513*, 229-240.

Moore, G. W., D. A. Barre, and M. K. Owens (2010), Changes in soil chloride following shrub removal and subsequent regrowth, *Geoderma, 158*(3), 148-155.

Moore, G. W., D. A. Barre, and M. K. Owens (2012), Does Shrub Removal Increase Groundwater Recharge in Southwestern Texas Semi-arid Rangelands?, *Rangeland Ecol. Manage., 65*(1), 1-10.

Mulholland, P. J., G. V. Wilson, and P. M. Jardine (1990), Hydrogeochemical response of a forested watershed to storms: effects of preferential flow along shallow and deep pathways, *Water Resour. Res.*, *26*(12), 3021-3036.

Murray, K. (2012), Geologic Controls on Groundwater Recharge to the Central Oklahoma Aquifer, *Okla Geol Notes*, *72*(2), 2.

Nijland, W., M. Van der Meijde, E. A. Addink, and S. M. De Jong (2010), Detection of soil moisture and vegetation water abstraction in a Mediterranean natural area using electrical resistivity tomography, *Catena*, *81*(3), 209-216.

Nimmo, J. R., J. A. Deason, J. A. Izbicki, and P. Martin (2002), Evaluation of unsaturated zone water fluxes in heterogeneous alluvium at a Mojave Basin site, *Water Resour. Res.*, *38*(10), 33-31-33-13.

Ochsner, T. E., M. H. Cosh, R. H. Cuenca, W. A. Dorigo, C. S. Draper, Y. Hagimoto, Y. H. Kerr, E. G. Njoku, E. E. Small, and M. Zreda (2013), State of the art in large-scale soil moisture monitoring, *Soil Sci. Soc. Am. J.*, *77*(6), 1888-1919.

Ong, J. B., J. W. Lane Jr, V. A. Zlotnik, T. Halihan, and E. A. White (2010), Combined use of frequency-domain electromagnetic and electrical resistivity surveys to delineate near-lake groundwater flow in the semi-arid Nebraska Sand Hills, USA, *J. Hydrol.*, *18*(6), 1539-1545.

Robinson, J. L., L. D. Slater, and K. V. Schäfer (2012), Evidence for spatial variability in hydraulic redistribution within an oak–pine forest from resistivity imaging, *J. Hydrol.*, *430*, 69-79.

Rossatto, D. R., L. d. C. R. Silva, R. Villalobos-Vega, L. d. S. L. Sternberg, and A. C. Franco (2012), Depth of water uptake in woody plants relates to groundwater level

and vegetation structure along a topographic gradient in a neotropical savanna, *Environ. Exp. Bot.*, *77*, 259-266.

Sala, O. E., and F. T. Maestre (2014), Grass–woodland transitions: determinants and consequences for ecosystem functioning and provisioning of services, *J. Ecol.*, *102*(6), 1357-1362.

Samouëlian, A., I. Cousin, A. Tabbagh, A. Bruand, and G. Richard (2005), Electrical resistivity survey in soil science: a review, *Soil Till. Res.*, *83*(2), 173-193.

Scanlon, B. R., A. R. Dutton, and M. A. Sophocleous (2002a), *Groundwater recharge in Texas*, Bureau of Economic Geology, University of Texas at Austin.

Scanlon, B. R., R. W. Healy, and P. G. Cook (2002b), Choosing appropriate techniques for quantifying groundwater recharge, *J. Hydrol. 10*(1), 18-39.

Scanlon, B. R., R. C. Reedy, D. A. Stonestrom, D. E. Prudic, and K. F. Dennehy (2005), Impact of land use and land cover change on groundwater recharge and quality in the southwestern US, *Global Change Biol.*, *11*(10), 1577-1593.

Scanlon, B. R., C. C. Faunt, L. Longuevergne, R. C. Reedy, W. M. Alley, V. L. McGuire, and P. B. McMahon (2012), Groundwater depletion and sustainability of irrigation in the US High Plains and Central Valley, *PNAS*, *109*(24), 9320-9325.

Schwartz, F. W., and H. Zhang (2003), *Fundamentals of ground water*, Wiley New York.

Seyfried, M. S., and B. P. Wilcox (2006), Soil water storage and rooting depth: key factors controlling recharge on rangelands, *Hydrol. Process.*, *20*(15), 3261-3275.

Smith, S. (2011), Eastern red-cedar: positives, negatives and management.

Soil Survey Staff. (1999), *Soil taxonomy: a basic system of soil classification for making and interpreting soil surveys*, United States Department of Agriculture.

Sophocleous, M. (2004), Groundwater recharge, in *Encyclopedia of Life Support Systems (EOLSS)*, edited, Oxford, UK (UNESCO, Eolss).

Sophocleous, M. (2005), Groundwater recharge and sustainability in the High Plains aquifer in Kansas, USA, *J. Hydrol.*, *13*(2), 351-365.

Travelletti, J., P. Sailhac, J. P. Malet, G. Grandjean, and J. Ponton (2012), Hydrological response of weathered clay-shale slopes: water infiltration monitoring with time-lapse electrical resistivity tomography, *Hydrol. Process.*, *26*(14), 2106-2119.

van Dijk, A. I., and R. J. Keenan (2007), Planted forests and water in perspective, *For. Ecol. Manage.*, *251*(1), 1-9.

Van Nostrand, R. G., and K. L. Cook (1966), Interpretation of resistivity data*Rep. 2330-7102*, US Govt. Print. Off.

Vauclin, M., D. Khanji, and G. Vachaud (1979), Experimental and numerical study of a transient, two-dimensional unsaturated-saturated water table recharge problem, *Water Resour. Res.*, *15*(5), 1089-1101.

Verweij, R. J., S. I. Higgins, W. J. Bond, and E. C. February (2011), Water sourcing by trees in a mesic savanna: Responses to severing deep and shallow roots, *Environ. Exp. Bot.*, *74*, 229-236.

Wilcox, B. P., and T. L. Thurow (2006), Emerging issues in rangeland ecohydrology: vegetation change and the water cycle, *Rangeland Ecol. Manage.*, *59*(2), 220-224.

Williams, R. J., S. W. Hallgren, G. W. T. Wilson, and M. W. Palmer (2013), Juniperus virginiana encroachment into upland oak forests alters arbuscular mycorrhizal abundance and litter chemistry, *Appl. Soil Ecol.*, *65*(0), 23-30.

Winter, T. C. (1999), *Ground water and surface water: a single resource*, DIANE Publishing.

Zhang, L., W. Dawes, and G. Walker (2001), Response of mean annual evapotranspiration to vegetation changes at catchment scale, *Water Resour. Res.*, *37*(3), 701-708.

Zou, C. B., D. J. Turton, R. E. Will, D. M. Engle, and S. D. Fuhlendorf (2014), Alteration of hydrological processes and streamflow with juniper (Juniperus virginiana) encroachment in a mesic grassland catchment, *Hydrol. Process.*, *28*, 6173-6182.

Zou, C. B., G. L. Caterina, R. E. Will, E. Stebler, and D. Turton (2015), Canopy Interception for a Tallgrass Prairie under Juniper Encroachment, *PLoS ONE*, *10*(11), e0141422.

Table 3.1: Biophysical attributes of juniper trees along the latitudinal transect in the juniper-encroached catchment.

Tree	Nearest electrode	Distance between tree and nearest electrode (m)	Plant height (m)	DBH (cm)
T1	E28	0.98	2.6	2.8
T2	E40	1.35	1.5	0.2
T3	E51	1.07	4.4	13
T4	E54	0.06	3.2	8
T5	E56	1.7	5.5	14.9

†DBH = Diameter at breast height, T = Tree, E = Electrode

Table 3.2: Measurements of electrical resistivity in 2014. Root mean square errors of inverted images (refer to file name for images) are shown in percentage.

Site Name	Line Name	Date	Total Electrodes	Image Name	RMS Error (%)	Time Step
G1	LO	6/06/2014	56	G1LO-0606	4.85	1
E1	LO	6/13/2014	56	C1LO-0613	4.68	1
G1	LO	6/24/2014	56	G1LO-0624	4.95	2
E1	LO	6/24/2014	56	E1LO-0624	4.57	2
G1	LO	7/03/2014	56	G1LO-0703	3.84	3
E1	LO	7/03/2014	56	E1LO-0703	4.52	3
G1	LO	8/01/2014	56	G1LO-0801	3.82	4
E1	LO	8/01/2014	56	E1LO-0801	4.16	4
O1	LO	6/13/2014	56	O1LO-0613	3.51	1
O1	LO	6/27/2014	56	O1LO-0627	3.9	2
O1	LO	7/05/2014	56	O1LO-0705	4.08	3
F1	LO	6/27/2014	56	F1LO-0627	4.39	1
F1	LO	7/04/2014	56	F1LO-0704	4.46	2
F1	LO	7/29/2014	56	F1LO-0729	5.07	3

†E = Juniper-encroached, G = Tallgrass prairie, O = Oak forest, F = Juniper woodland, LO = Latitudinal, RMS = Root mean square

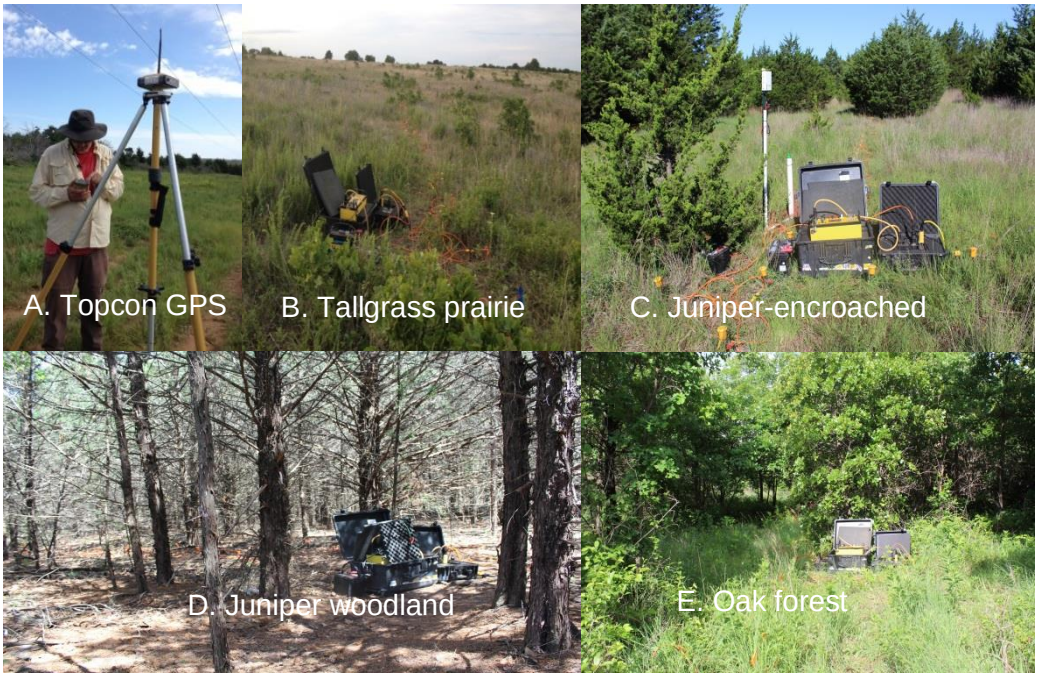

Fig. 3.1. General view of field instrumentation and research site: base station for the TOPCON Hyperlite Plus Global Positioning System to obtain coordinates and elevation for each electrode (A), the prairie with SuperString 8-channel resistivity meter and switchbox (B), and the juniper-encroached catchment (C), juniper forest (D), and oak forest (E).

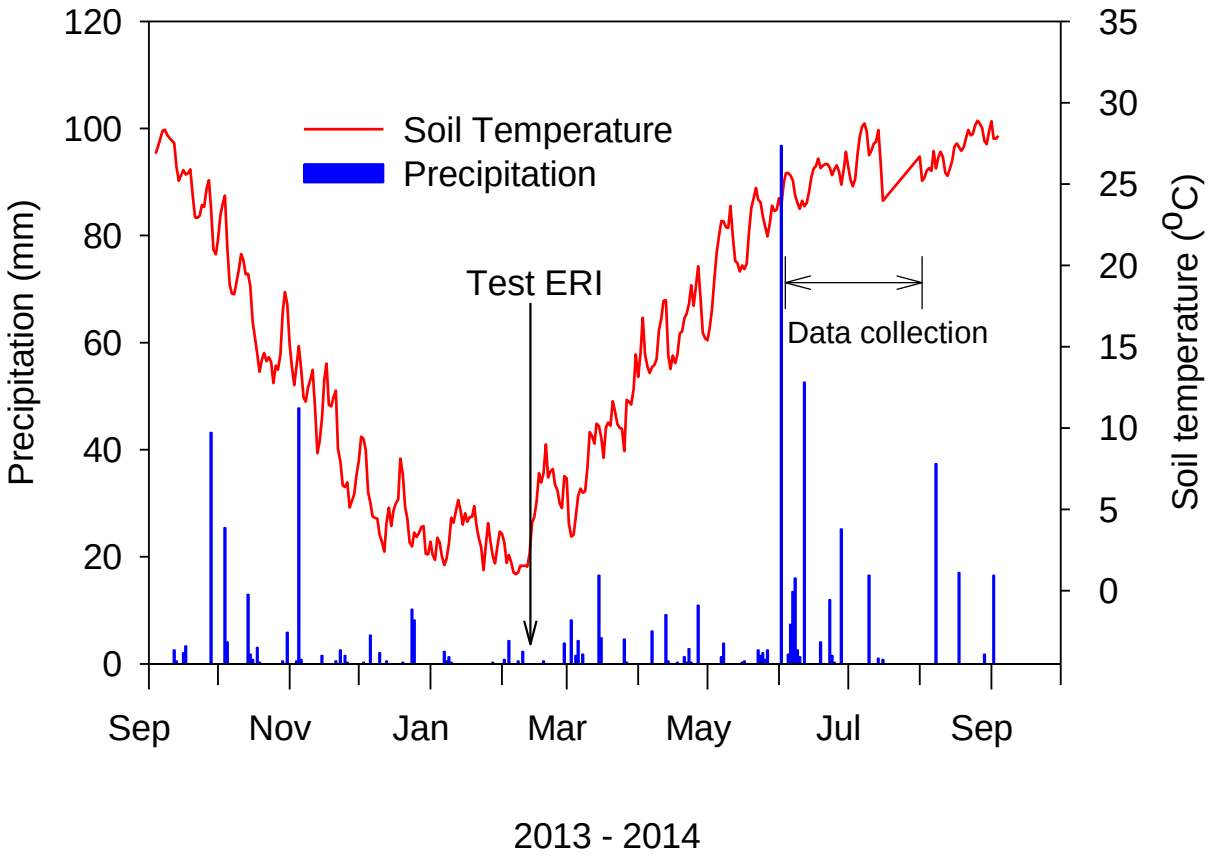

Fig. 3.2. Daily precipitation in mm (TB3 siphoning tipping bucket rain gauge with a 0.254 mm tip; Hydrological Services America, Lake Worth, FL) and soil temperature in ^{o}C (107-L temperature probe; Campbell Scientific, Logan UT) from a weather station at Cross-Timber Research Station during September 2013 to September 2014. Soil temperature values are averaged over 5 minute and recorded. Different arrows indicate time of ERI data acquisition.

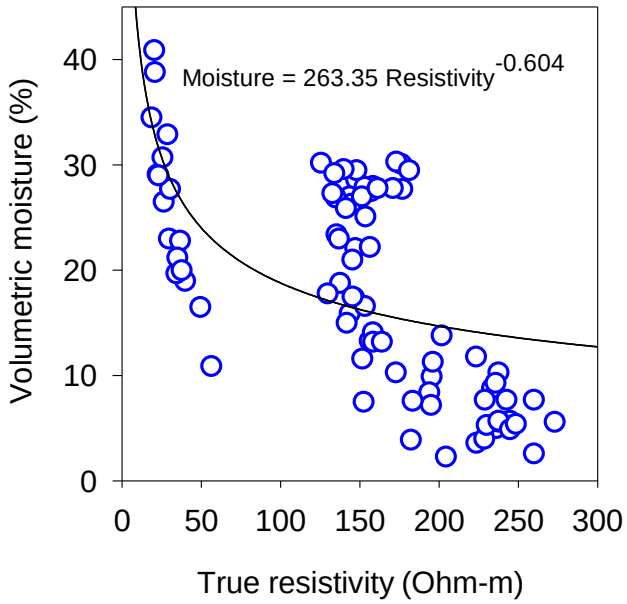

Fig. 3.3. The power law relation between true resistivity after inversion and the volumetric soil moisture content across all vegetation cover types measured by using HydroSense II (Campbell Scientific, USA).

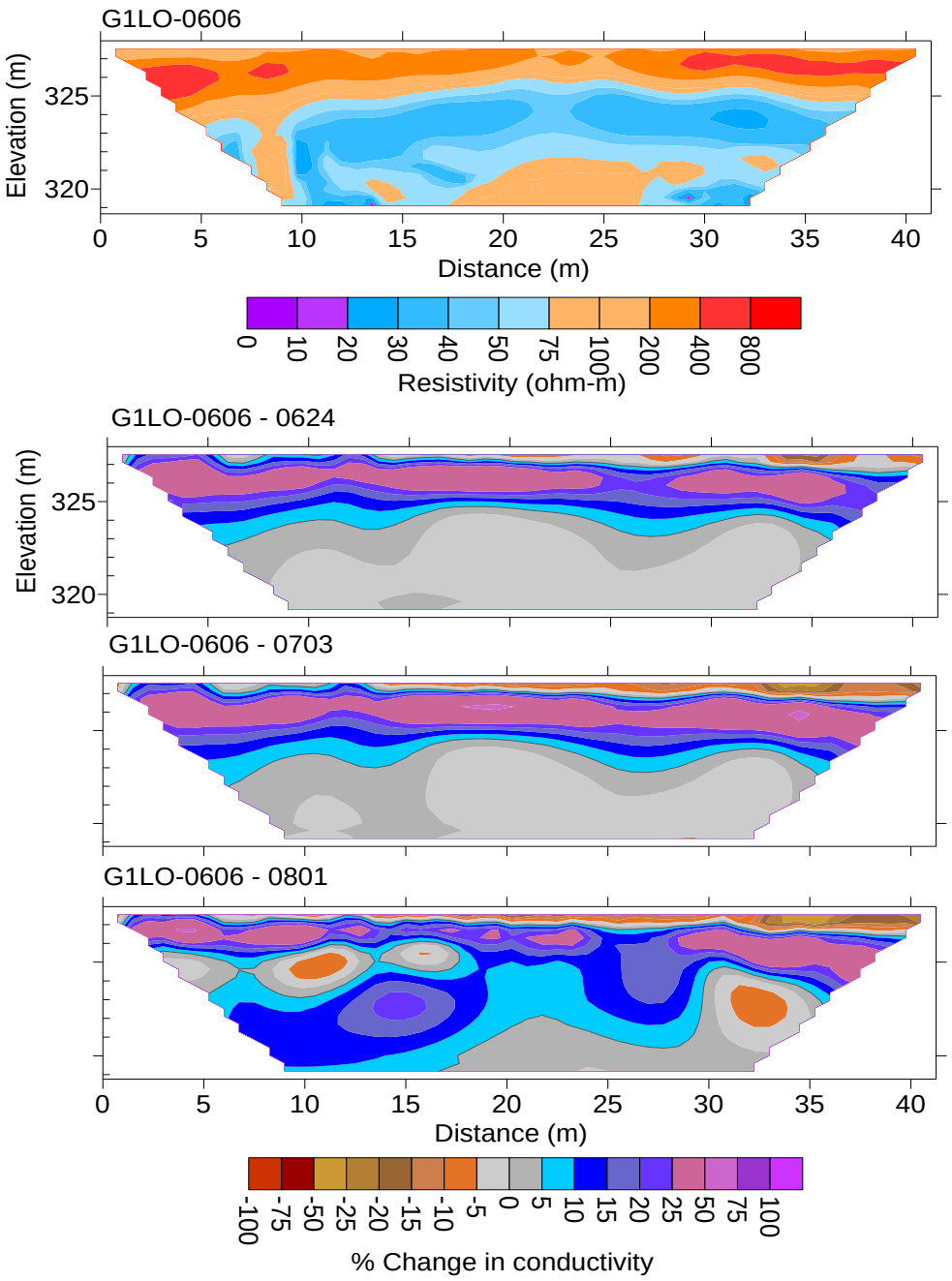

Fig. 3.4. Electrical resistivity images from the tallgrass prairie. Time lapse images were developed from latitudinal transect deployed with 56 electrodes. The top image represents background image and subsequent images are time-lapse pseudosections showing percent change in conductivity.

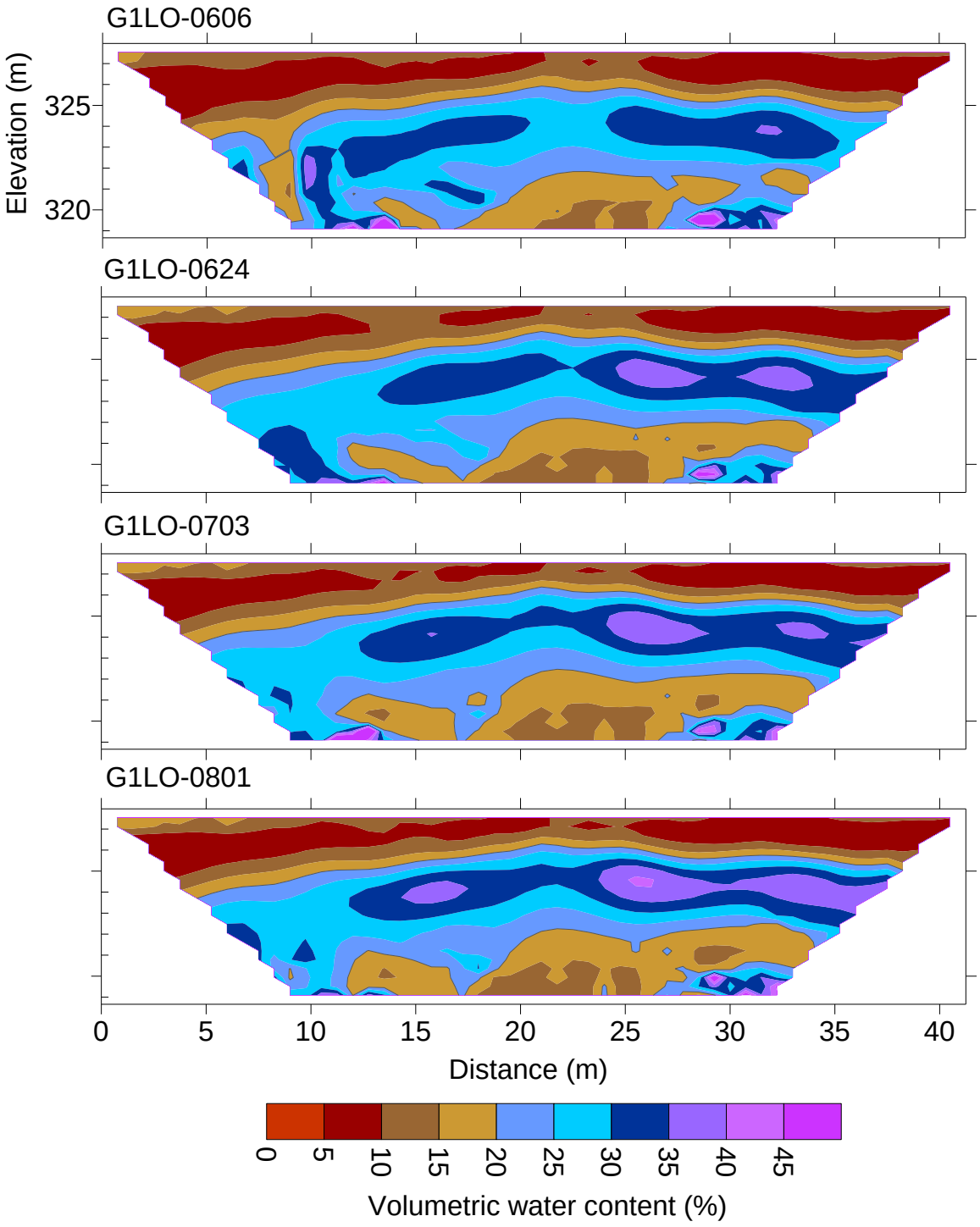

Fig. 3.5. Time-lapse pseudosections showing spatial and temporal distribution of volumetric moisture content in the tallgrass prairie.

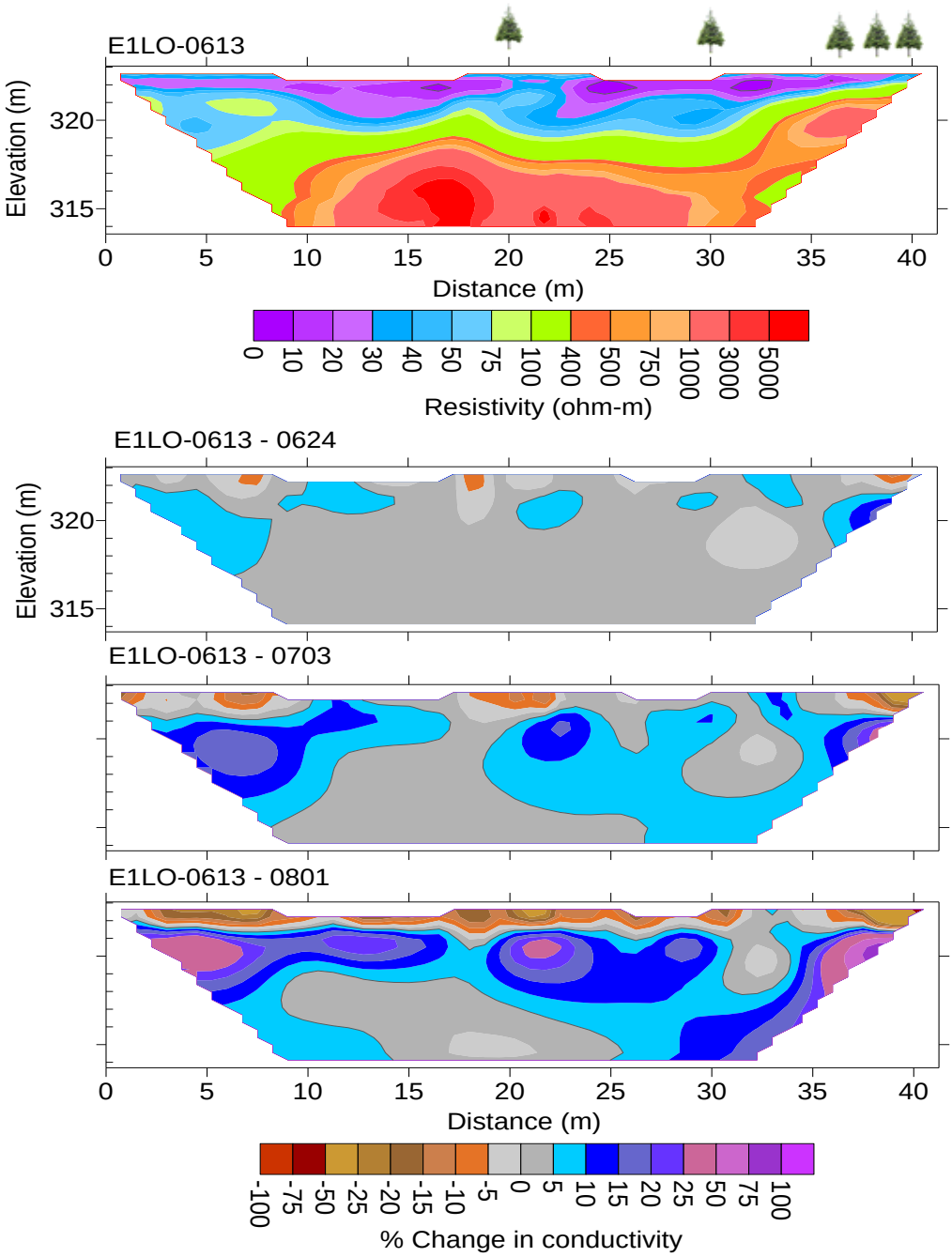

Fig. 3.6. Electrical resistivity images from the juniper-encroached catchment. Time lapse images were developed from latitudinal transect deployed with 56 electrodes. The top image represents background image and subsequent images are time-lapse pseudosections showing percent change in conductivity.

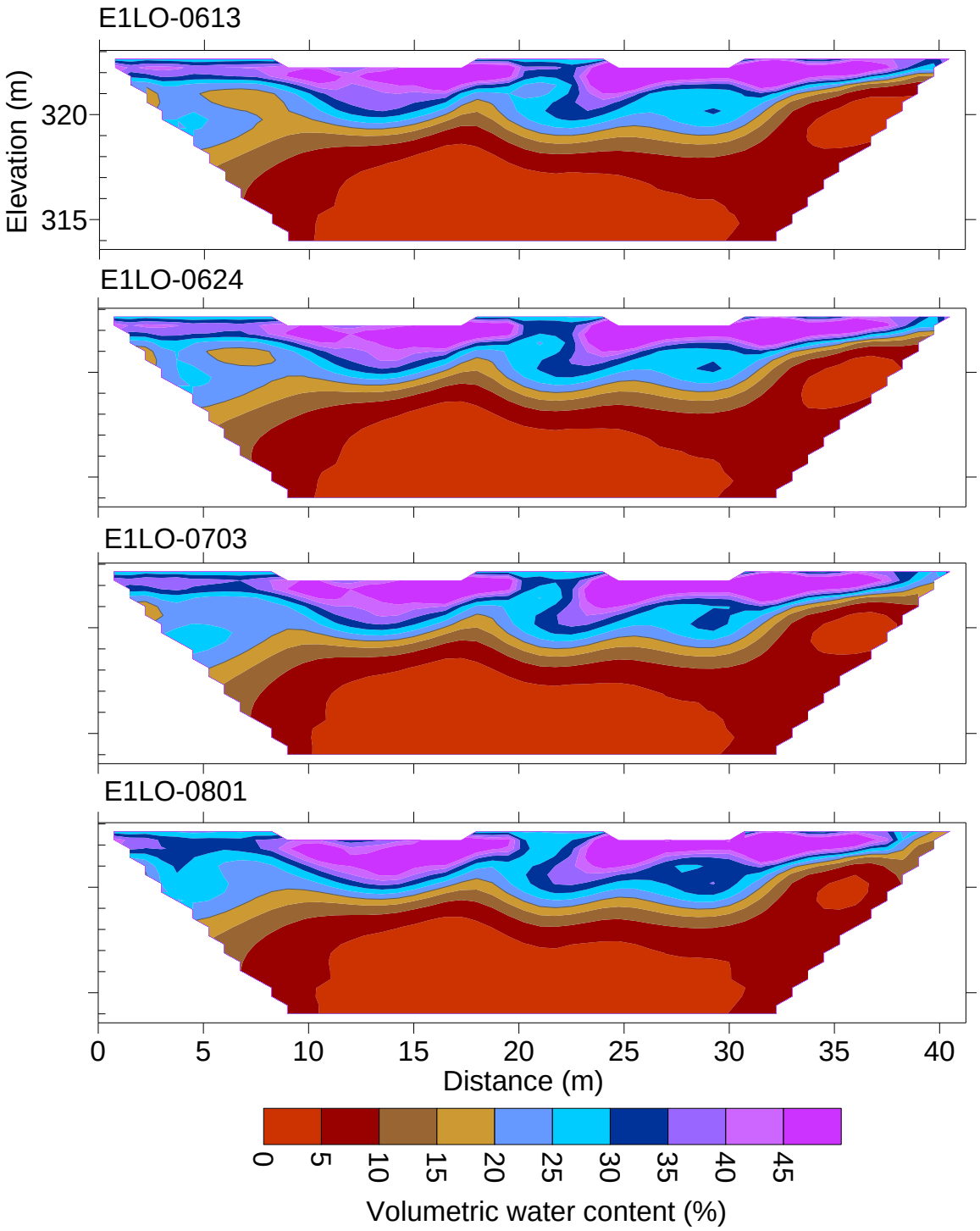

Fig. 3.7. Time-lapse pseudosections showing spatial and temporal distribution of volumetric moisture content in juniper-encroached catchment.

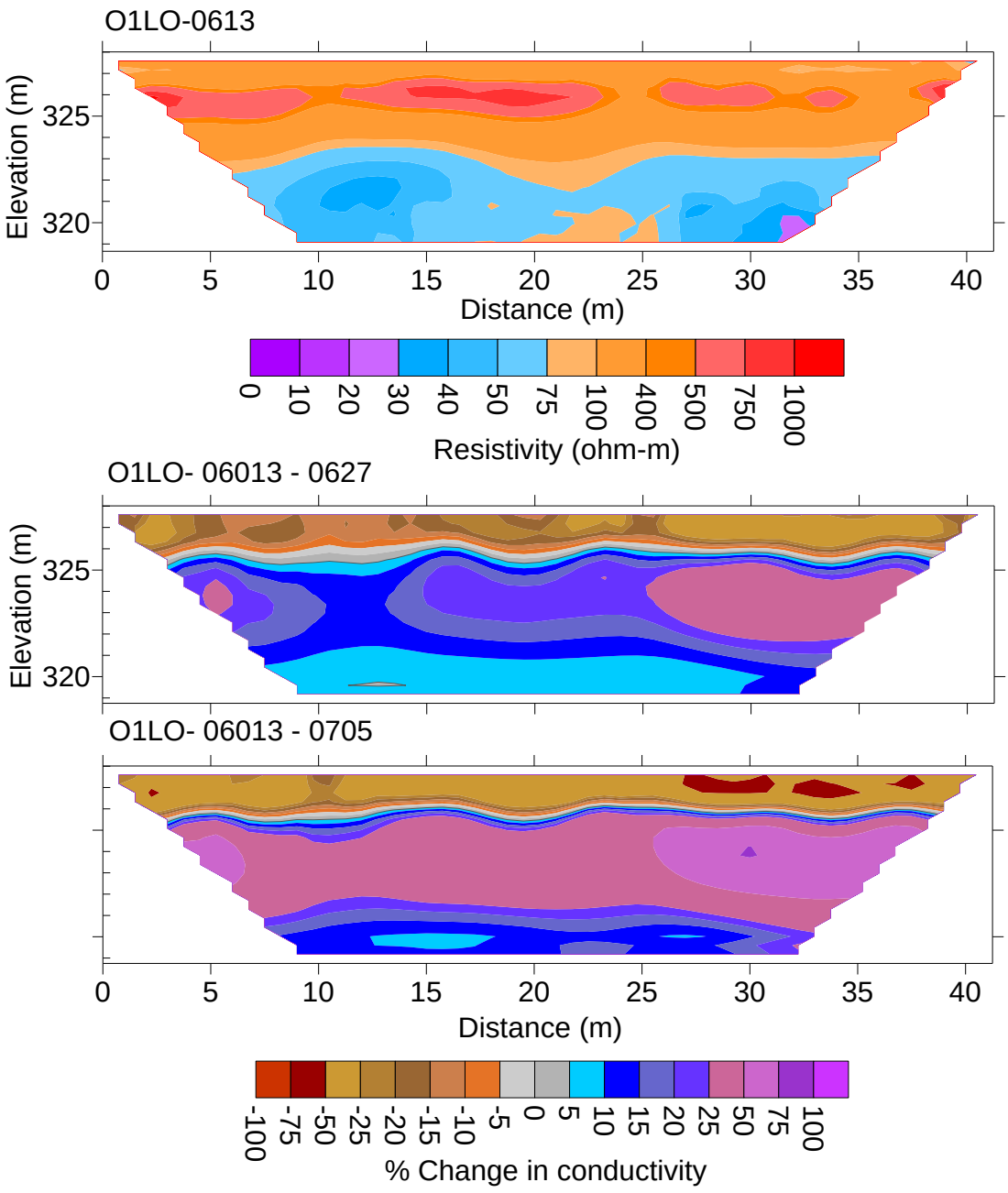

Fig. 3.8. Electrical resistivity images from oak forest. Time lapse images were developed from latitudinal transect deployed with 56 electrodes. The top images represents background image and subsequent images are time-lapse pseudosections showing percent change in conductivity.

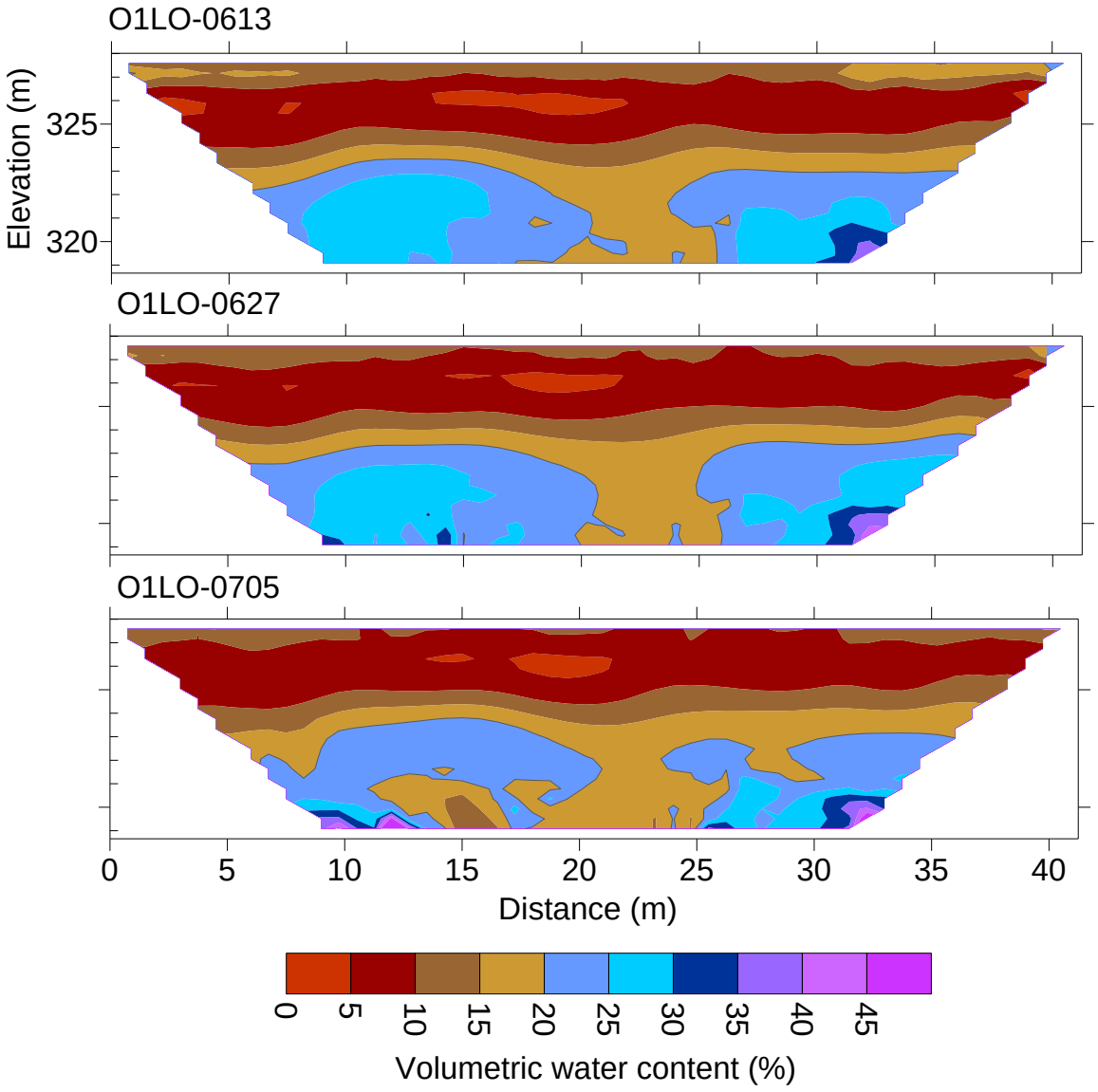

Fig. 3.9. Time-lapse pseudosections showing spatial and temporal distribution of volumetric moisture content in oak forest.

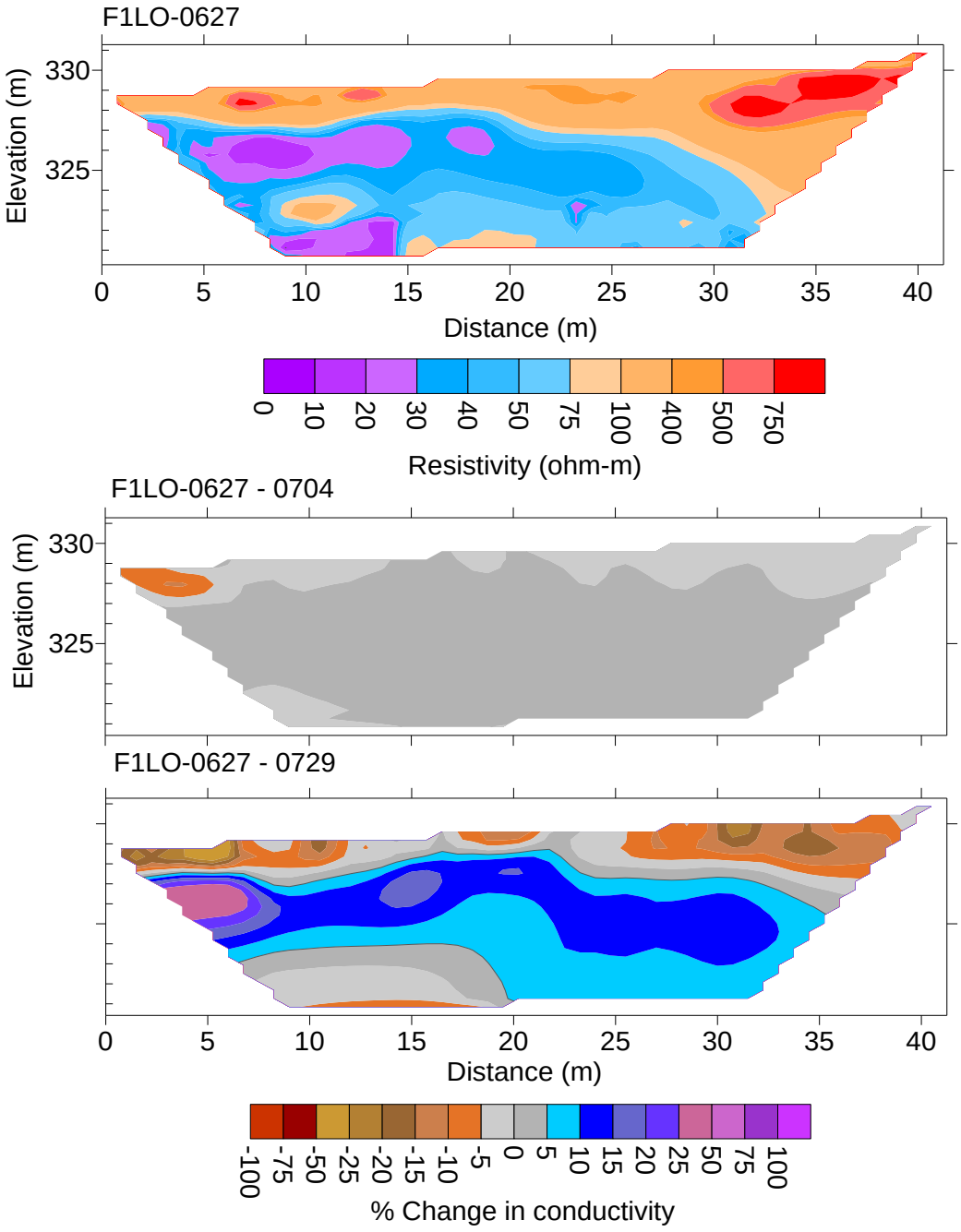

Fig. 3.10. Electrical resistivity images from juniper woodland. Time lapse images were developed from latitudinal transect deployed with 56 electrodes. The top images represents background image and subsequent images are time-lapse images showing percent change in conductivity.

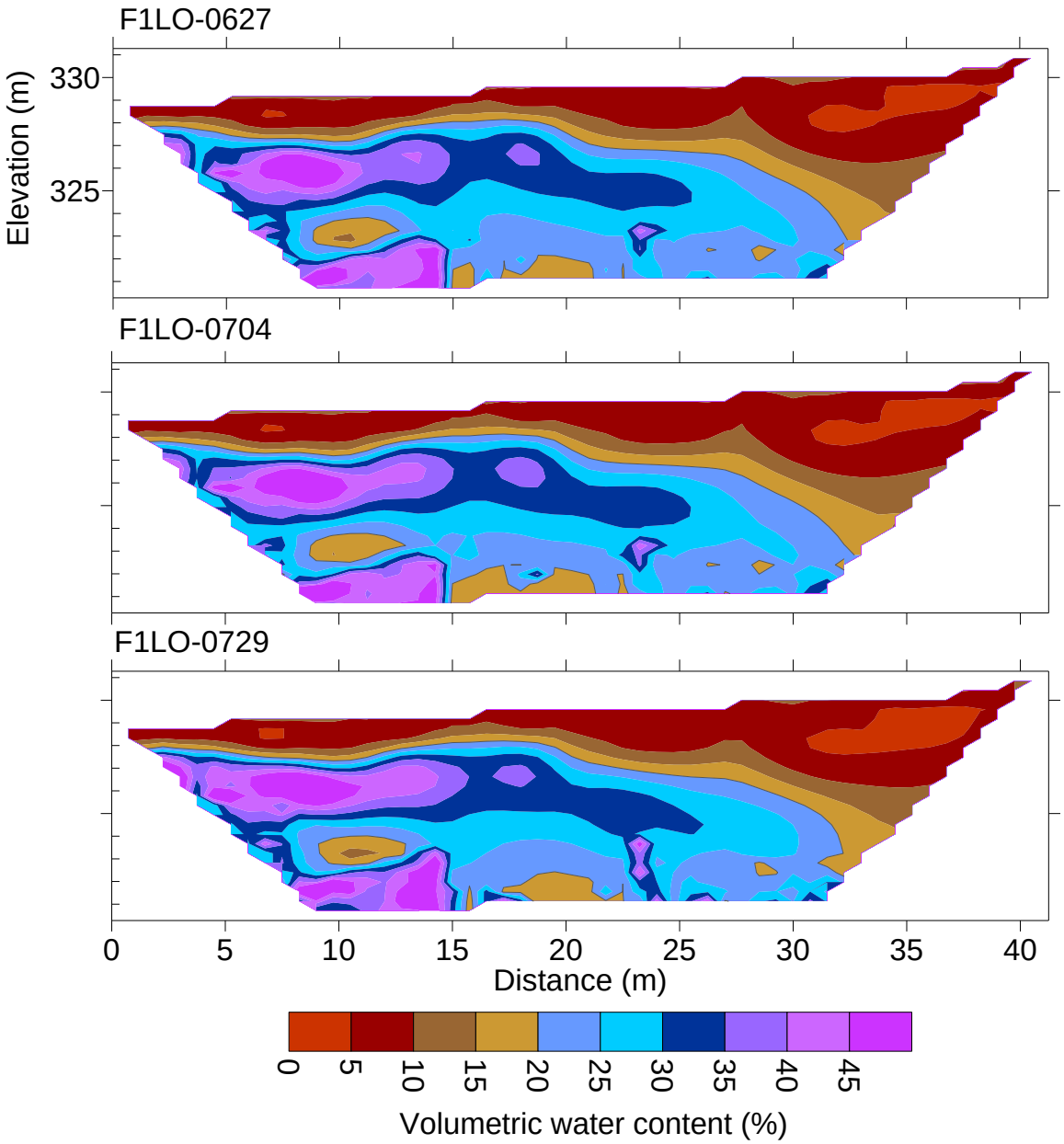

Fig. 3.11. Time-lapse pseudosections showing spatial and temporal distribution of volumetric moisture content in juniper woodland.

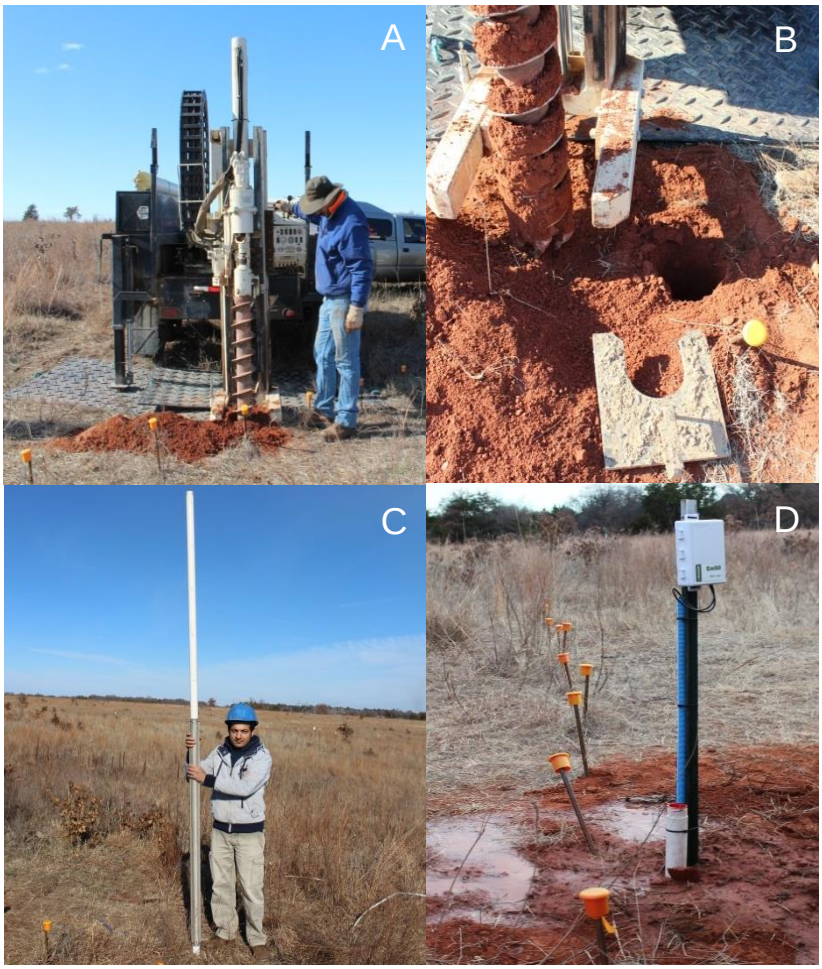

Fig. 3.12. Photos show solid-stem auger mounted in Geoprobe 6200 TMP (A) to drill hole of 3 m depth (B) in the tallgrass prairie. A piezometer constructed with a screen, sand pack around the screen and a casing protector was installed (C) and instrumented with CTD-10 sensor. The sensor was connected to the EM50 data logger (Decagon, Pullman, WA, USA) fixed to a T Post to measure water level (*accuracy* $\pm$ 0.05%), electrical conductivity (accuracy $\pm$0.01 dS/m) and temperature (accuracy $\pm$ 1°C) at 15-minutes interval (D).

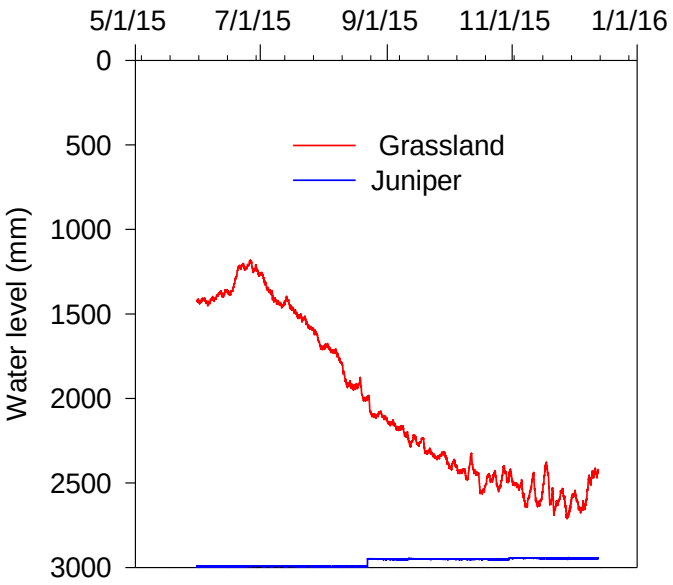

Fig. 3.13. Water level recorded at 15-minutes interval during 31 May to 12 Dec 2015 from two monitoring wells of 3 m depth in a tallgrass prairie and a juniper-encroached catchment

CHAPTER IV

TEMPORAL ELECTRICAL RESISTIVITY IMAGING AND BERM INFILTRATION REVEALS SUBSURFACE LATERAL FLOW PATHWAYS IN GRASSLAND

ABSTRACT

Subsurface hydrologic flow pathways are difficult to trace and visualize, especially for ecosystems underlain by sandstone layer. We evaluated subsurface flow for a grassland underlain by porous standstone using passive seasonal temporal electrical resistivity imaging (ERI) after natural precipitation event and short-term temporal ERI during a berm infiltration experiment. Passive seasonal temporal ERI indicated two-layered moisture migration profile and lateral flow of water in grassland. Infiltrated water migrated vertically through the soil but moved laterally at approximately 1 m below ground surface due to a hydraulically restrictive layer associated with bedrock. Lateral migration rates were faster than vertical migration rates. Under natural precipitation events, soil water migrated laterally at a velocity of 0.5 m/day along the soil and base rock interface. However, a lateral velocity of as high as 3.3 m/day was observed under

ponding water with a berm infiltration. The results suggest that in an ecosystem with shallow sandstone bedrock, lateral movement of water along the soil bedrock interface retained water in the rooting zone or perched shallow aquifers and therefore strengthened the vegetation and subsurface soil moisture connectivity. Time-lapse ERI has the potential to be used for broader understanding of subsurface anisotropy and hydrology in ecosystem studies.

Keywords: Lateral flow, electrical resistivity imaging, time-lapse ERI, grassland, berm

INTRODUCTION

Stormwater runoff and stream flow generation at the catchment scale is influenced by lateral movement of water in the unsaturated zone [*Samper et al.*, 2015]. The lateral movement of water is referred to as lateral flow or horizontal flow and may occur during or shortly after a rainfall event. Subsurface lateral flow is reported to significantly affect nutrients and contaminant transport, water quality, groundwater depth, and preferential recharge [*Fox et al.*, 2011; *Maxwell and Kollet*, 2008; *Mulholland et al.*, 1990; *M Sophocleous*, 2004].

Lateral flow is often assumed to depend upon preferential flow of infiltrating water in macropores [*Hardie et al.*, 2012]. Macropores are macrovoids formed by soil fauna, plant roots, cracks and fissures, vary in effective pore size and shape, and affect water and solute transport [*Beven and Germann*, 1982; *Flury et al.*, 1994; *Gerke*, 2006]. Natural soil pipes are macropores developed by subsurface erosion process in highly permeable system, or by desiccation cracking in steep slopes and bedrock channels [*Beven and Germann*, 1982]. Subsurface features like shallow bedrock and argillic horizons may contribute to the development of preferential flow. Interference of vertical flow by bedrock or confining layers, alone or coupled with steep slopes and intense rains and ponding of water over confining layers with low permeability, result in perched water tables [*Fox et al.*, 2011; *Hardie et al.*, 2012; *Mulholland et al.*, 1990], and stimulate lateral flow of perched water [*Hardie et al.*, 2012]. An improved understanding of subsurface flow is necessary to understand streamflow component, groundwater recharge, and to improve management of water resource.

A large portion of the Great Plains of the United States is located at the transition zone between grassland and forest. The ecotone exhibits a dry sub-humid climate and encloses a mosaic vegetation primarily delineated by soil texture. Grassland, a major vegetation cover type in the south and south-central Great Plains, is usually delineated by fine texture clay or clayey loam soil and maintained by fire. It is unclear how percolation interfaces with porous sandstone substrates to drive vertical and lateral water movement. Understanding this process is important for study the potential impact of vegetation changes such as woody encroachment into the grassland on alteration of runoff and recharge generation mechanisms.

Field-based, direct observations of subsurface flow are often limited [*Burke and Kasahara*, 2011; *Guo et al.*, 2014]. Field approaches to study subsurface flow often include isotope and dye tracers experiments [*Samper et al.*, 2015]. The technique can be substantially destructive as plots are excavated to detect staining patterns [*Flury et al.*, 1994]. More recently, non-intrusive hydrogeophysical methods such as electrical resistivity imaging (ERI) are increasingly used for subsurface hydrological investigations, which can be a promising alternative to traditional methods to monitor water flow pathways.

Electrical resistivity imaging is a geophysical technique in which surface electrodes are used for measurement and acquisition of apparent resistivity [*Halihan et al.*, 2005; *Jayawickreme et al.*, 2010; *Loke*, 1999; *Miller et al.*, 2014; *Samouëlian et al.*, 2005]. A time-lapse ERI allows the collection of apparent resistivity from same locations at different time intervals [*Jayawickreme et al.*, 2010]. Changes in resistivity are typically derived from alteration in soil water content assuming no change in lithology [*Nijland et*

al., 2010]. Time-lapse ERI has been used to monitor, image and/or characterize surface water, groundwater, groundwater aquifers, landfills sites (contaminant transport), saltwater intrusion along the coastal areas [*Kuras et al.*, 2009; *Singha et al.*, 2014], landslides [*Perrone et al.*, 2014; *Wilkinson et al.*, 2011] and permafrost [*Wilkinson et al.*, 2011]. An Automated Time-Lapse Electrical Resistivity Tomography (ALERT) controls the data acquisition of subsurface anomalies, data transfer, and image visualization remotely using wireless telemetry [*Kuras et al.*, 2009; *Ogilvy et al.*, 2008].

Electrical resistivity is measured using a quadrapole measurement with two current electrodes and two potential electrodes [*Jayawickreme et al.*, 2010; *Jayawickreme et al.*, 2014; *Loke*, 1999]. Electrical resistivity can vary from 0.1 to several 1000 Ω-m and is affected by physical and chemical properties of substrates including stable properties such as lithology and mineralogy and transient properties such as temperature and soil water content [*Samouëlian et al.*, 2005]. Temperature could increase electrical conductivity by increasing the ions' mobility [*Jayawickreme et al.*, 2014; *Samouëlian et al.*, 2005]. Soil moisture has high electric conductivity compared with soil minerals and the resistivity decreases with increasing water content. The spatial resolution of ERI can be manipulated according to the spacing of electrodes with resolution equal to half of the stake spacing.

The objective of this study was to evaluate and elucidate the manifestation of subsurface lateral flow in grassland underlain by sandstone layer using electrical resistivity imaging (ERI). First, ERI images were developed for both rainfall events and dry down processes to detect lateral flow using passive seasonal temporal ERI. Next, subsurface lateral flow was confirmed by a short-term temporal ERI during and after

berm infiltrometer test. Finally, the data were compared to evaluate lateral and vertical migration rates on both the short and long time scales to determine if the observed processes correlated with results from previous modeling and field evaluation efforts.

METHODS

Experimental Site and Hydrogeological Setting

The study was conducted at the Cross-Timber Research Station (CTER), Oklahoma State University. The study area is located about 11 km southwest of Stillwater, Payne County, Oklahoma, USA (36^{o} 03'47" N, 97^{o}11'03" W, and 331 m-asl) in the lower Cimarron watershed. It has a continental climate with mean annual temperature of 15.2^{o} C. The mean annual precipitation is 900 mm during 1994 to 2011 with 65% occurring during May to October [*Caterina et al.*, 2014; *Zou et al.*, 2014].

The bedrock geology of the study site consists of Wellington formation of Permian age. The northern part of the site is dominated by red-brown shale, and southern part largely consists of fine-grained sandstone and mudstone conglomerate [Stoeser et al., 2005]. The thickness of the formation is 259 m. There are no groundwater wells in the study site or within its periphery, but the water table in Payne County is estimated at a depth of 12 m below the surface (http://ogs.ou.edu/docs/hydrologicatlases/).

The dominating soil types in the study site include Grainola-Lucien complex, and Coyle soil series. Grainola are fine, mixed, thermic, Vertic Haplustalfs; and Lucien are shallow fine sandy loam, mixed, thermic, shallow Typic Haplustolls; and Coyle series are fine-loamy, siliceous, thermic, Udic Argiustolls [*Henley et al.*, 1987; *Soil Survey Staff*, 1999]. The initial and steady-state infiltration rates reported in the study site were 10 and 5 cm h^{-1}, respectively [*Zou et al.*, 2014].

Grassland is one of the main vegetation types in non-cultivated landscape in the research site. Grassland is dominated by C_4 grasses, including little bluestem (*Schizachyrium scoparium*), big bluestem (*Andropogon gerardii*), Indiangrass (*Sorghastrum nutans*), switchgrass (*Panicum virgatum*), and tall dropseed (*Sporobolus asper*) [*Limb et al.*, 2010]. Major forbs include western ragweed (*Ambrosia psilostachya)* and broomweed (*Gutierrezia dracunculoides*).

Electrical Resistivity Imaging

Apparent resistivity (ρ_a) (Ω-m) is defined as the ratio between measured potential difference (ΔV) and induced electric current (I) into the ground:

$$\rho_a = \frac{\Delta V}{I} \qquad [1]$$

The ρ_a was quantified using a battery-operated multichannel multielectrode resistivity instrument (Advanced Geoscience, Inc. SuperSting 8-channel instrument). This instrument uses direct current or low-frequency alternating current (typical ranging from 100 mA to 350 mA here) in two current electrodes and measure the potential difference between two electrodes in an electric field. The ρ_a can be converted into true resistivity (ρ_t) using an inversion process. Soil electrical conductivity σ (Sm^{-1}) is equivalent to the reciprocal of its resistivity:

$$\sigma = \frac{1}{\rho} \qquad [2]$$

Transect Locations and Description

The Light Detection and Ranging (LiDAR) bare earth digital elevation dataset-2 m projected in North American horizontal datum of 1983 was obtained from USDA

NRCS for four bounding coordinates (-97.21083, 36.04306 by -97.15917, 36.07879 Decimal Degrees). A digital elevation model (DEM) was generated for the site from the LiDAR dataset. The elevation model is of higher resolution and provides greater accuracy for base layer to anchor terrain mapping, watershed evaluation and hydrological modelling. Similarly, National Agriculture *Imagery* Program (NAIP) aerial imagery, projected at UTM NAD83 Native Image, was obtained for Payne County, Oklahoma, USA. Both of these dataset were used to produce a site map, delineate the watershed and draw contour lines. The experimental watershed in the OSU Range Research Station covers an area of 2.1 ha and has mean elevation of 328 m and slope of 5.5%. Transects were subjectively selected to follow the elevation contour line, to ensure that the soil profile is perpendicular to the surface flow paths, and to adequately represent the vegetation cover (Figure 4.1).

A permanent transect (L1) was established; L1 was 21 m long and oriented along the contour line. An orthogonal transect (L0) of 21 m ran through the center of the latitudinal line to dissect L1 (Figure 4.1). All of the transects were located and deployed with surface electrodes of 48.3 cm length and 1.6 cm diameter made up of copper coated steel lightning rods permanently to a depth of 15 to 30 cm in June 2014. Electrodes installation was completed a week prior to first ERI measurement to ensure good contact between soil and electrodes. The permanent electrode line prevented and/or minimized any alterations in near-surface soil properties [*Amidu and Dunbar*, 2007]. Thus, a total of 28 electrodes were permanently deployed on the surface across L0 and L1 transects with 0.75 m electrode spacing.

Data Acquisition

The data acquisition for apparent resistivity was conducted following rainfall events in June 2014 to capture soil moisture conditions at the study site. The electrical resistivity measurement across the L0 ERI line provided data acquisition to infer subsurface process and anomalies including deep moisture to the depth of approximately 4 m. The resistivity images had a resolution of 0.38 m. ERI surveys were also conducted during drier conditions in June, July and August 2014 to characterize deep drainage and water-flow. Overall, June was interpreted as a wet month with July and August as drier months. A contact resistance test was completed prior to initiating the survey to identify poor electrical contact between the electrodes and the soil, breaks in the circuit, and signal strength [*Hesse et al.*, 1986; *PB Wilkinson et al.*, 2010]. Hundreds of data points were collected in an automated mode following an OSU method (the Halihan-Fenstemaker method) [*OSU*, 2004]. The method provides better data quality, and increases the sensitivity of subsurface images by approximately an order of magnitude [*Halihan and Fenstemaker*, 2004; *Miller et al.*, 2014]. A switchbox was used to perform switching at the electrodes. Apparent resistivity data were collected in the orthogonal transects during one ERI data acquisition. Data quality was tested by repetitive measurements. The average error in apparent resistivity data ranged up to 0.4%.

Surface Soil Temperature

Soil temperature increases electrical conductivity by either decreasing pore fluid resistivity or increasing mobility of ions [*Jayawickreme et al.*, 2014; *Samouëlian et al.*, 2005]. Therefore, diurnal and seasonal fluctuations in soil temperature alter electrical resistivity. Resistivity values are often expressed at standard temperature to facilitate

comparison across time. Electrical resistivity is corrected to 25^{o}C using the *Keller and Frischknecht* [1966] equation

$$\rho_{25^{\circ}C} = \rho_T \left[1 + 0.025\left(T - 25\right)\right] \quad [3]$$

where, $\rho_{25^{0}C}$ is the electrical resistivity at 25^{o}C, ρ_T is the electrical resistivity at temperature, T (^{o}C), and 0.025 is the correction factor.

Surface soil temperature was measured randomly across the transects in proximity to electrodes using a reference thermometer (Thermoworks, USA) (*accuracy* $\pm$ 0.05 ^{0}C) to detect temperature variability, and to determine the necessity of temperature correction for resistivity values. Daily soil temperature averaged over 5 minute was also reported from a nearby weather station (Figure 4.2). No temperature correction was warranted for our resistivity data, as diurnal surface temperature minimally fluctuated throughout the months of data acquisition (max=28^{o} C, min=24^{o} C, mean ± SD; 26^{o} ± 1.3^{o} C).

Berm Infiltration and Short-term temporal ERI

Three temporary ERI lines of 21 m length were constructed at 2 m intervals from L1 line to track water migration. The ERI lines (L0, L+1, and L-1) run parallel to the permanent line (hereafter referred as L+2) and a total of 28 electrodes were deployed in each line at an electrode spacing of 0.75 m. A berm infiltrometer was located at the L0 line at the distance of 1 m from adjacent lines. The berm infiltrometer of 1 x 1 m was constructed using 15 cm Vinyl hoses following *Heeren et al.*, [2013]. The hoses were attached to four steel elbows at 90 degrees and tightly secured using stainless steel hose clamps, and sealed with silicone sealant. Weight was imparted to the berm by partially filling with tap water, and transported to field and installed in the grassland site by cutting

a shallow trench of 5 cm. Granules of bentonite were soaked in water for 20 minutes and applied underneath and around the berm to ensure close contact of vinyl hose to the ground and to further minimize surface flow of water. The berm infiltrometer provided a constant head infiltration, and was easy to operate in field [*Heeren et al.*, 2013]. A 200 gallon water tank was used to supply water in the berm by gravity flow via a garden hose that ran into the float valve. A truck with a reservoir was used to fill the water tank periodically (Figure 4.3). A constant head of 4 cm was considered for berm infiltration. Temperature and electrical conductivity were measured inside the berm using a HANNA Combo pH/EC/TDS/C tester (HI98130; Hanna Instruments) (accuracy ±0.05 pH, ±2% F.S., ±0.5°C) to evaluate the necessity of temperature correction and assess conductivity of transient images, respectively (Figure 4.4).

Background electrical resistivity data were collected a day prior to the berm infiltration experiment from all 5 lines/transects. During the infiltration experiment, daily electrical resistivity data were collected for about a week to produce short-term temporal ER images. Resistivity data were later collected at a week interval for about a month thereby producing a total of 43 ERI profiles or nine sets [one set is equivalent to five ERI profiles measured from five transect].

Data Analysis

Field data were corrected for topography to adjust for change in distance between the electrodes. Three applications of topographic correction included (a) an adjustment for surface elevation [*Schwartz and Zhang*, 2003], (b) discerning lateral heterogeneity in electrical properties and comparison of subsurface images in 3D, and (c) dealing with line orthogonal to the contour line. On 14th July 2014, a base station was established at the

study site near ERI line, and a TOPCON Hyperlite Plus Global Positioning System and a rover with Bluetooth connected handheld unit was set to record latitude, longitude and elevation for each electrode with centimeter-scale accuracy. In 30 July, 2015, a laser survey instrument was used to record the elevations of all electrodes in the three new ERI lines. Data from Topcon GPS was downloaded to a computer and base data was sent to Online Positioning User Service (OPUS). The easting, northing and elevation of base station obtained from OPUS were used to correct the location data of each electrodes. The location data of electrodes in the three new lines in 2015 were also corrected using TOPCON information.

Pseudo-sections of the electrical resistivity images were developed in two-dimensions using an inversion algorithm. Inversion is largely dependent on a rectangular grid method consisting of horizontal and vertical grid cells, and is used to estimate true resistivity in each grid nodes. Random noise error must be eliminated prior to inversion iterations to prevent extreme values. Data repeatability error in excess of 2% was minimized by removing values prior to inversion. The apparent resistivity data, collected in field, were inverted to create a model space of resistivity values to replicate the collected data [*Halihan et al.,* 2005]. The later values are referred as true resistivity values. The RMS inversion error was reported in percent for pseudo-sections of electrical resistivity to illustrate goodness of fit. The lower RMS inversion error represents better input data, inverted model and model fit [*Travelletti et al.,* 2012]. Percent change in conductivity was imaged based on the resistivity difference between background/baseline image and each subsequent date. Transient images resulting from passive seasonal temporal ERI in the L+2 transect showed uniform change in moisture at each depth;

thereby elucidating low lateral variability (data not shown). As a result, temporal images from L_v transect were analyzed for lateral flow that showed non-uniform change in moisture. For short-term temporal ERI, the structure of the data after a week became too difficult to correlate to the berm, so the first week data were utilized for analysis. Velocity for an image in short-term temporal ERI was calculated as the change in distance covered by a conductive layer over time comparing to the preceding image. Wedge shaped images that resolve boundary conditions were developed using Surfer 8 (Golden Software Inc), and presented with consistent color scheme.

RESULTS

Passive seasonal temporal ERI

The inversion root mean square error (RMSE) between resistivity model and apparent resistivity ranged from 1.8 to 5.0% for the resistivity images. The background ERI for the site showed a thick resistive upper layer running from 326 to 327 m elevation (Figure 4.5 A). Peak resistivity values of 700 to 750 Ω-m appeared at the right corner of the layer in the pseudo-section. An interface between the upper resistive and the lower conductive zone was observed at 325 m in the background ERI image.

Transient images showed two-layered, non-wetted and wetted, moisture migration profiles (Figure 4.5 B to D). The first layer was about a meter thick with either 10 to 20% decrease in conductivity or no change in conductivity. This layer was followed by a 3 m thick and wet conductive layer. The top stratum of transient electrical image in 24 June 2014 was drier, similar to background image, with 5 to 10% decrease in conductivity. Conductivity increased laterally by 15 to 25% from 324 to 326.5 m elevation. Conductivity increased by 20% from 324 to 326 m elevation for a distance of 10 m from

the left hand side (LHS) of the line. In July, the conductive zone observed in June further expanded discerning three distinct layers. The left corner of pseudo-section near the interface had 75% increases in conductivity. In August, the top layer of the site dried to 5%, a site minimum, with a further decrease in conductivity of 10 to 15%. A thin layer, with no change in conductivity, appeared below the top layer. However, conductivity increased by 15 to 25% up to 324 m elevation and the region showing 75% increase in conductivity during July continued to exist as a "convex" layer. Water content along the orthogonal line showed both an increasing and widening conductive layer down the hillslope. Thus, water accumulated below 1.7 m soil depth can form a transient recharge zone in grassland, and may result in lateral flow of water.

Short-term temporal ERI

A total of 3030 liters of water infiltrated within the berm in 24 hours. The infiltration rate in grassland was 13 cm/hour. There was strong electrical connection between soil and electrodes as indicated by low contact resistance. As a result, inversion data loss was relatively low. The inversion RMS error ranged from 2.6% to 6.5% for the resistivity images and 1.2% to 5.3% for transient images. The L2 and L4 transects had best data with RMS error in the range of 1.1 to 4.1%. This range of RMSE indicates better data quality and calculated data fit between resistivity model and apparent resistivity.

Lateral flow of water

Short-term temporal ERI showed lateral migration of water to left hand side in transient images (Figure 4.6 A) and to right hand side (RHS) in a few images once they encountered preferential flow pathways (Figure 4.6 B). Lateral flow was distinct for the

L0 transect. Approximately one day after the start of infiltration, electrical conductivity increased laterally by 5 to 15% for a distance of 3 to 9 m from the LHS of the L0 transect at 325 to 327m elevation (Figure 4.6 A). Similarly, on approximately day 6, conductivity increased at the LHS of the image below 325 m elevation. An increase in conductivity by up to 15% was observed for a distance of 3 m at the 325 m elevation and by 20 to 25% at RHS of image for a distance of 15 to 17 m at the 324 to 326 m elevation (Figure 4.6 A).

Vertical and lateral velocity of water

Vertical and horizontal migration of water was observed for the L-1 transect. Approximately two days since the start of infiltration, conductivity increased by 30% vertically near 10 m from the LHS of the transect at the 326 to 327 m elevation (Figure 4.6 B). The conductivity increased by 5 % laterally on the RHS of the image between 12 and 18 m transect distance at the 323.5 to 326 m elevation. The horizontal velocity of water was 2.1 m/day and was much higher than the lateral velocity of water moving towards the LHS (1.6 m/day), but lower than water moving towards the RHS (2.7 m/day) (Figure 4.6 B, middle panel). The lateral velocity of water migrating in both directions for the L0 transect was 3.3 m/day. Thus, the lateral migration rates were higher than vertical migration rates through the porous sandstone.

DISCUSSION

The data acquisition for passive seasonal temporal ERI was conducted during June to August 2014, wherein June and July were fairly wet and August was drier with only a few rain events (Figure 4.2). The background ERI at 6 June 2014 indicates a resistive upper layer in the grassland site (Figure 4.5 A). The shallow soil in all seasonal temporal images showed a pronounced 5 to 10% decrease in conductivity. Lower

conductivity could potentially occur from plant water use, evaporation and/or deep drainage of water. *Zou et al.* [2014] indicated longer wetting duration for soil water content at 80 cm depth during summer at the same site. Such antecedent moisture plays important function of producing flow in the vadose zone [*Kienzler and Naef*, 2008].

So far, only a few studies report subsurface lateral flow from direct field observations [*Fox et al.,* 2011]. For example, dye tracer experiments show macropore flow in forest, and overland flow in grassland as characterized by lower number of macropore and higher tortuosity, and reduced interaction between macropore and soil matrix [*Alaoui et al.*, 2011]. Macropores are largely formed in soils rich with organic matter and biological activity. Lateral flow may occur under lower moisture when soil water bypasses the soil matrix for macropore flow [*Gerke*, 2006; *Newman et al.*, 1998]. Our short-term temporal ERI showed consistent lateral migration of fluid to left hand side in temporal images due to hydraulically restrictive layer associated with bedrock (Figure 4.6 A) and to right hand side (RHS) once the fluid encountered preferential flow pathways (Figure 4.6 B).

The lateral flow was largely controlled by differences in lithologic properties with depth. As a result, discrete recharge might have been occurring. Depth to refusal tests and soil sampling using a handheld auger indicates soil depth ranging from 0.8 to 1.0 m in the site, and soil layers below 1 m primarily consist of sandstone deposits; thereby interfering with the vertical flow of water. *Dietrich et al.* [2014] used electrical resistivity tomography in Azul Creek basin, Argentina and observed lateral flow when vertical fluxes of water were restricted due to argillic horizon at 60 cm below soil surface. We observed an increase in conductivity in the downslope direction. Similar flow direction

was reported in an experimental mountain watershed, which indicated the effects of rainfall amount, surface and bedrock topography, and perched water levels to determine flow direction [*Meerveld et al.*, 2015]. The direction may follow bedrock topography at low water levels and surface topography at higher water levels. Studies also report alterations in subsurface flow directions between storm events such as in alluvial floodplains [*Heeren et al.*, 2014]. The direction of subsurface lateral flow at watershed scales is influenced by different factors such as root types and their orientation and position, presence/absence of soil cracks, and bedrock. The orientation and mass of roots is likely to affect pore-water pressure and flow of water. For example, if the mass of root at downslope is greater than mass at upslope from the stem, water is likely to flow downslope and vice versa [*Ghestem et al.*, 2011].

Attempts have been made to understand subsurface lateral flow and its response to rainfall, antecedent moisture and hillslope lengths in tracer studies using flow velocities [*Anderson et al.*, 2009]. To test the apparent subsurface lateral flow in the grassland site, electrical images from short-term temporal data were analyzed for migration of water during and following a berm infiltration experiment. This approach is fairly easy and has great potential to improve the understanding of flow patterns and eliminate uncertainties associated with the passive seasonal temporal ERI approach. The short-term temporal ERI approach clearly demonstrated the evolution of lateral flow of water following infiltration experiment. However, the L_v transect showed physically non-realizable result during one to six days after the start of infiltration (Figure 4.6 C top panel). Areas below the berm showed decrease in conductivity by 50 to 100%. This is unexpected and unlikely given that the L0 transect showed considerable increase in

conductive area below the berm. Under natural precipitation events (passive seasonal temporal images), lateral flow took 10 days to appear with a velocity of 0.5 m/day but in short-term temporal ERI, the flow was seen immediately after berm water infiltrated the soil below 1 m soil depth as observed in L0 transect approximately one day since the start of infiltration. These differences could be attributed to higher pressure head under berm infiltration forcing water into the ground and higher soil moisture content, which may facilitate interconnection between pores, compared to natural rain events. The observed velocities since infiltration were higher than under natural rain events and within the range of maximum subsurface flow velocities in a grassland as indicated by *Anderson et al.* [2009] who gave a range of 0.5 to 331 m/h. Saturated hydraulic conductivity is more likely to develop under constant head experiments such as with the berm, thereby, more likely forming a perched layer than under natural rainfall events [*Mosley*, 1982].

Hydrologic flow models are frequently used to describe spatial and temporal variability of subsurface flow [*Steward et al.*, 2014]. Because soil is not necessarily a homogenous medium as described on such theoretical models, subsurface studies should rely on the use of field techniques [*Guo et al.*, 2014; *Swarowsky et al.*, 2012]. An earlier study at this site indicated that streamflow in the grassland is associated with saturation excess overland flow when soil water storage in grassland approach 380 mm [*Zou et al.*, 2014]. Lateral flow is equally important in determining streamflow and its potential contribution needs to be established based on these experiments. Our results also indicate that water movement may not be one-dimensional as that of moving piston. Thus, two-dimensional or three-dimensional imaging is necessary to understand sub-surface flow patterns.

CONCLUSIONS

In this study, passive seasonal temporal ERI and short-term temporal ERI were used as non-invasive tool to monitor water migration in grassland. Passive seasonal temporal ERI indicated two-layered moisture migration profiles and lateral flow of water. Temporal ERI experiment tracked the movement of water from a berm infiltrometer and confirmed the occurrence lateral flow. Based on the results, the following conclusions were drawn:

- Under natural precipitation events, lateral flow took several days to appear and showed a velocity of 0.5 m/day. However, the flow was observed after 23 hours of berm infiltration with a lateral velocity of 3.3 m/day.
- The lateral flow resulted from a hydraulically restrictive layer associated with bedrock at 1m depth. Infiltrated water migrated vertically through the soil but moved laterally below 1 m soil depth in both directions in the images.
- Lateral migration rates were higher than vertical migration rates through the porous sandstone.

Thus, our results showed the evidence of hydraulic barrier control on water flow and confirmed subsurface lateral flow in grassland. Results highlight the importance of short-term controlled temporal electrical resistivity imaging to infer subsurface flow in the unsaturated zone and to act as confirmation for observations from passive ERI. In an ecosystem with shallow sandstone layer, lateral movement of water along the soil bedrock interface is likely to retain water in the rooting zone; indicating the connectivity between vegetation and subsurface soil moisture.

ACKNOWLEDGEMENTS

This study was supported by the USGS 104B through Oklahoma Water Resources Center, Oklahoma Agricultural Experiment Station, Boone Pickens School of Geology, NSF EPSCoR (NSF-1301789), NSF Dynamics of Coupled Natural and Human Systems (CNH) program (DEB-1413900) and USDA National Institute of Food and Agriculture AFRI Sustainable Bioenergy program (2014-67010-21653). Special thanks are given to Elaine Stebler and Chris Stanberry for the field assistance and logistic support. The data used in this paper are available at http://datagateway.nrcs.usda.gov/, given in the table and/or shown in the images itself. The Halihan-Fenstemaker method used in this paper is the property of Oklahoma State University. The technique is also commercially available by Aestus, LLC.

REFERENCES

Alaoui, A., U. Caduff, H. H. Gerke, and R. Weingartner (2011), A Preferential Flow Effects on Infiltration and Runoff in Grassland and Forest Soils, *Vadose Zone J.*, *10*(1), 367-377.

Amidu, S. A., and J. A. Dunbar (2007), Geoelectric studies of seasonal wetting and drying of a Texas vertisol, *Vadose Zone J.*, *6*(3), 511-523.

Anderson, A., M. Weiler, Y. Alila, and R. Hudson (2009), Subsurface flow velocities in a hillslope with lateral preferential flow, *Water Resour. Res.*, *45*(11).

Beven, K., and P. Germann (1982), Macropores and water flow in soils, *Water Resour. Res.*, *18*(5), 1311-1325.

Briggs, J. M., A. K. Knapp, J. M. Blair, J. L. Heisler, G. A. Hoch, M. S. Lett, and J. K. McCARRON (2005), An ecosystem in transition: causes and consequences of the conversion of mesic grassland to shrubland, *Bioscience*, *55*(3), 243-254.

Burke, A. R., and T. Kasahara (2011), Subsurface lateral flow generation in aspen and conifer-dominated hillslopes of a first order catchment in northern Utah, *Hydrol. Process.*, *25*(9), 1407-1417.

Caterina, G. L., R. E. Will, D. J. Turton, D. S. Wilson, and C. B. Zou (2014), Water use of Juniperus virginiana trees encroached into mesic prairies in Oklahoma, USA, *Ecohydrology*, *7*, 1124-1134.

Dietrich, S., P. A. Weinzettel, and M. Varni (2014), Infiltration and drainage analysis in a heterogeneous soil by electrical resistivity tomography, *Soil Sci. Soc. Am. J.*, *78*(4), 1153-1167.

Engle, D. M., B. R. Coppedge, and S. D. Fuhlendorf (2008), From the dust bowl to the green glacier: human activity and environmental change in Great Plains grasslands, in *Western North American Juniperus Communities*, edited, pp. 253-271, Springer.

Flury, M., H. Flühler, W. A. Jury, and J. Leuenberger (1994), Susceptibility of soils to preferential flow of water: A field study, *Water resources research*, *30*(7), 1945-1954.

Fox, G. A., D. M. Heeren, R. B. Miller, A. R. Mittelstet, and D. E. Storm (2011), Flow and transport experiments for a streambank seep originating from a preferential flow pathway, *JHyd*, *403*(3), 360-366.

Gerke, H. H. (2006), Preferential flow descriptions for structured soils, *J. Plant Nutr. Soil Sci.*, *169*(3), 382-400.

Ghestem, M., R. C. Sidle, and A. Stokes (2011), The influence of plant root systems on subsurface flow: implications for slope stability, *Bioscience*, *61*(11), 869-879.

Guo, L., J. Chen, and H. Lin (2014), Subsurface lateral preferential flow network revealed by time-lapse ground-penetrating radar in a hillslope, *Water Resour. Res.*, *50*, 9127-9147.

Halihan, T., and T. Fenstemaker (2004), Proprietary electrical resistivity imaging method, 2nd ed. Stillwater, Oklahoma, in *Oklahoma State University Office of Intellectual Property* edited.

Halihan, T., S. Paxton, I. Graham, T. Fenstemaker, and M. Riley (2005), Post-remediation evaluation of a LNAPL site using electrical resistivity imaging, *J. Environ. Monit.*, *7*(4), 283-287.

Hardie, M. A., R. B. Doyle, W. E. Cotching, and S. Lisson (2012), Subsurface lateral flow in texture-contrast (duplex) soils and catchments with shallow bedrock, *Appl. Environ. Soil Sci.*, *2012*.

Heeren, D. M., G. A. Fox, and D. E. Storm (2013), Berm Method for Quantification of Infiltration at the Plot Scale in High Conductivity Soils, *J. Hydrol. Eng.*, *19*(2), 457-461.

Heeren, D. M., G. A. Fox, A. K. Fox, D. E. Storm, R. B. Miller, and A. R. Mittelstet (2014), Divergence and flow direction as indicators of subsurface heterogeneity and stage-dependent storage in alluvial floodplains, *Hydrol. Process.*, *28*(3), 1307-1317.

Henley, J., R. Gelnar, and R. E. Mayhugh (1987), *Soil survey of Payne County, Oklahoma*, US Government Printing Office.

Hesse, A., A. Jolivet, and A. Tabbagh (1986), New prospects in shallow depth electrical surveying for archaeological and pedological applications, *Geop*, *51*(3), 585-594.

Jayawickreme, D. H., R. L. Van Dam, and D. W. Hyndman (2010), Hydrological consequences of land-cover change: Quantifying the influence of plants on soil moisture with time-lapse electrical resistivity, *Geop.*, *75*(4), WA43-WA50.

Jayawickreme, D. H., E. G. Jobbágy, and R. B. Jackson (2014), Geophysical subsurface imaging for ecological applications, *New Phytol.*, *201*(4), 1170-1175.

Keller, G. V., and F. C. Frischknecht (1966), Electrical methods in geophysical prospecting.

Kienzler, P. M., and F. Naef (2008), Subsurface storm flow formation at different hillslopes and implications for the 'old water paradox', *Hydrol. Process.*, *22*(1), 104-116.

Kuras, O., J. D. Pritchard, P. I. Meldrum, J. E. Chambers, P. B. Wilkinson, R. D. Ogilvy, and G. P. Wealthall (2009), Monitoring hydraulic processes with automated time-lapse electrical resistivity tomography (ALERT), *C R Geoscience*, *341*(10–11), 868-885.

Limb, R. F., D. M. Engle, A. L. Alford, and E. C. Hellgren (2010), Tallgrass prairie plant community dynamics along a canopy cover gradient of eastern redcedar (Juniperus virginiana L.), *Rangeland Ecol. Manage.*, *63*(6), 638-644.

Loke, M. (1999), Electrical imaging surveys for environmental and engineering studies, *A practical guide to*, *2*.

Maxwell, R. M., and S. J. Kollet (2008), Interdependence of groundwater dynamics and land-energy feedbacks under climate change, *Nature Geosci.*, *1*(10), 665-669.

Meerveld, H., J. Seibert, and N. Peters (2015), Hillslope–riparian-stream connectivity and flow directions at the Panola Mountain Research Watershed, *Hydrol. Process.*, *29*, 3556–3574.

Miller, R. B., D. M. Heeren, G. A. Fox, T. Halihan, D. E. Storm, and A. R. Mittelstet (2014), The hydraulic conductivity structure of gravel-dominated vadose zones within alluvial floodplains, *Journal of Hydrology*, *513*, 229-240.

Mosley, M. P. (1982), Subsurface flow velocities through selected forest soils, South Island, New Zealand, *J. Hydrol.*, *55*(1), 65-92.

Mulholland, P. J., G. V. Wilson, and P. M. Jardine (1990), Hydrogeochemical response of a forested watershed to storms: effects of preferential flow along shallow and deep pathways, *Water Resour. Res.*, *26*(12), 3021-3036.

Newman, B. D., A. R. Campbell, and B. P. Wilcox (1998), Lateral subsurface flow pathways in a semi-arid ponderosa pine hillslope, *Water Resour. Res.*, *34*(12), 3485-3496.

Nijland, W., M. Van der Meijde, E. A. Addink, and S. M. De Jong (2010), Detection of soil moisture and vegetation water abstraction in a Mediterranean natural area using electrical resistivity tomography, *Catena*, *81*(3), 209-216.

Ogilvy, R., P. Meldrum, O. Kuras, P. Wilkinson, and J. Chambers (2008), *Advances in geoelectric imaging technologies for the measurement and monitoring of complex earth systems and processes*, International Union of Geological Sciences.

OSU (2004), Improved method for Electrical Resistivity Imaging, edited.

Perrone, A., V. Lapenna, and S. Piscitelli (2014), Electrical resistivity tomography technique for landslide investigation: A review, *Earth-Sci. Rev.*, *135*, 65-82.

Samouëlian, A., I. Cousin, A. Tabbagh, A. Bruand, and G. Richard (2005), Electrical resistivity survey in soil science: a review, *Soil Till. Res.*, *83*(2), 173-193.

Samper, J., B. Pisani, and J. E. Marques (2015), Hydrological models of interflow in three Iberian mountain basins, *Environ. Earth Sci.*, *73*, 2645-2656.

Schwartz, F. W., and H. Zhang (2003), *Fundamentals of ground water*, Wiley New York.

Singha, K., F. D. Day-Lewis, T. Johnson, and L. D. Slater (2014), Advances in interpretation of subsurface processes with time-lapse electrical imaging, *Hydrol. Process.*, *29*, 1549-1576.

Soil Survey Staff. (1999), *Soil taxonomy: a basic system of soil classification for making and interpreting soil surveys*, United States Department of Agriculture.

Sophocleous, M. (2002), Interactions between groundwater and surface water: the state of the science, *HydJ*, *10*(1), 52-67.

Sophocleous, M. (2004), Groundwater recharge, in *Encyclopedia of Life Support Systems (EOLSS)*, edited, Oxford, UK (UNESCO, Eolss).

Steward, D. R., X. Yang, S. Lauwo, S. A. Staggenborg, G. Macpherson, and S. M. Welch (2014), From precipitation to groundwater baseflow in a native prairie ecosystem: a regional study of the Konza LTER in the Flint Hills of Kansas, USA.

Stoeser, D. B., G. N. Green, L. C. Morath, W. D. Heran, A. B. Wilson, D. W. Moore, and B. Gosen (2005), Preliminary integrated geologic map databases for the United States, *US Geological Survey, Open-File Report*, *1351*.

Swarowsky, A., R. Dahlgren, and A. O'Geen (2012), Linking Subsurface Lateral Flowpath Activity with Streamflow Characteristics in a Semi-arid Headwater Catchment, *Soil Sci. Soc. Am. J.*, *76*(2), 532-547.

Travelletti, J., P. Sailhac, J. P. Malet, G. Grandjean, and J. Ponton (2012), Hydrological response of weathered clay-shale slopes: water infiltration monitoring with time-lapse electrical resistivity tomography, *Hydrol. Process.*, *26*(14), 2106-2119.

Wilkinson, P., J. Chambers, O. Kuras, P. Meldrum, and D. Gunn (2011), Long-term time-lapse geoelectrical monitoring, *FiBr.*, *29*(8), 77-84.

Wilkinson, P., P. Meldrum, O. Kuras, J. Chambers, S. Holyoake, and R. Ogilvy (2010), High-resolution electrical resistivity tomography monitoring of a tracer test in a confined aquifer, *JAG*, *70*(4), 268-276.

Zou, C. B., D. J. Turton, R. E. Will, D. M. Engle, and S. D. Fuhlendorf (2014), Alteration of hydrological processes and streamflow with juniper (Juniperus virginiana) encroachment in a mesic grassland catchment, *Hydrol. Process.*, *28*, 6173-6182.

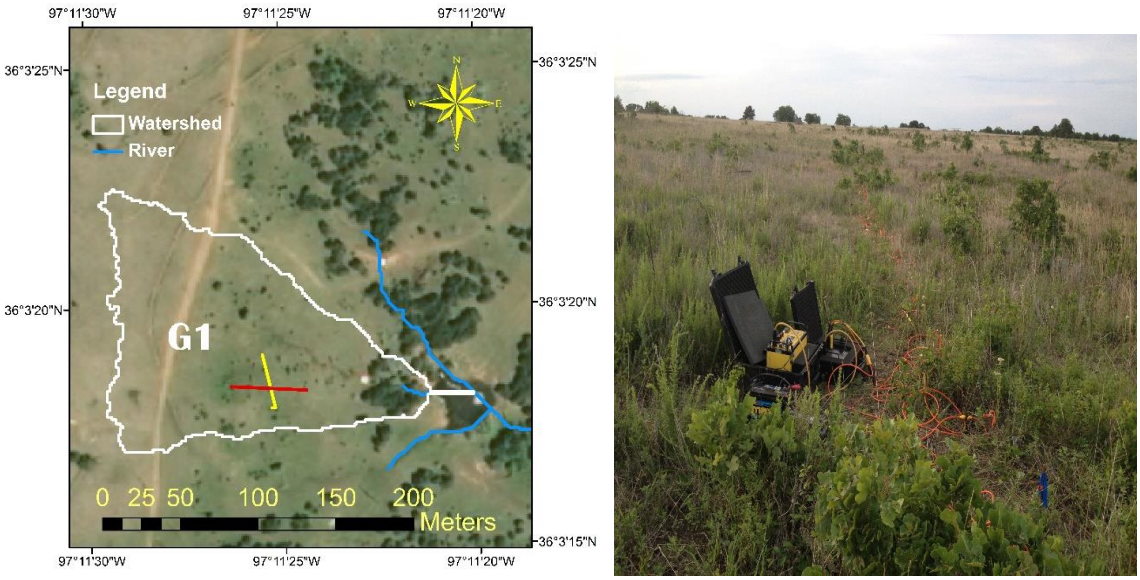

Figure 4.1. Map of experimental site based on LiDAR bare earth digital elevation dataset-2 meters and National Agriculture Imagery Program (NAIP) image from USDA/ NRCS- National Geospatial Center of Excellence. The white outline and G1 label indicates the grassland watershed for this study. Yellow and red lines indicate latitudinal and orthogonal seasonal ERI transects respectively. The photo in the right panel shows the grassland watershed with battery, AGI SuperString R8/IP Resistivity Instrument and switchbox collecting data from the orthogonal line.

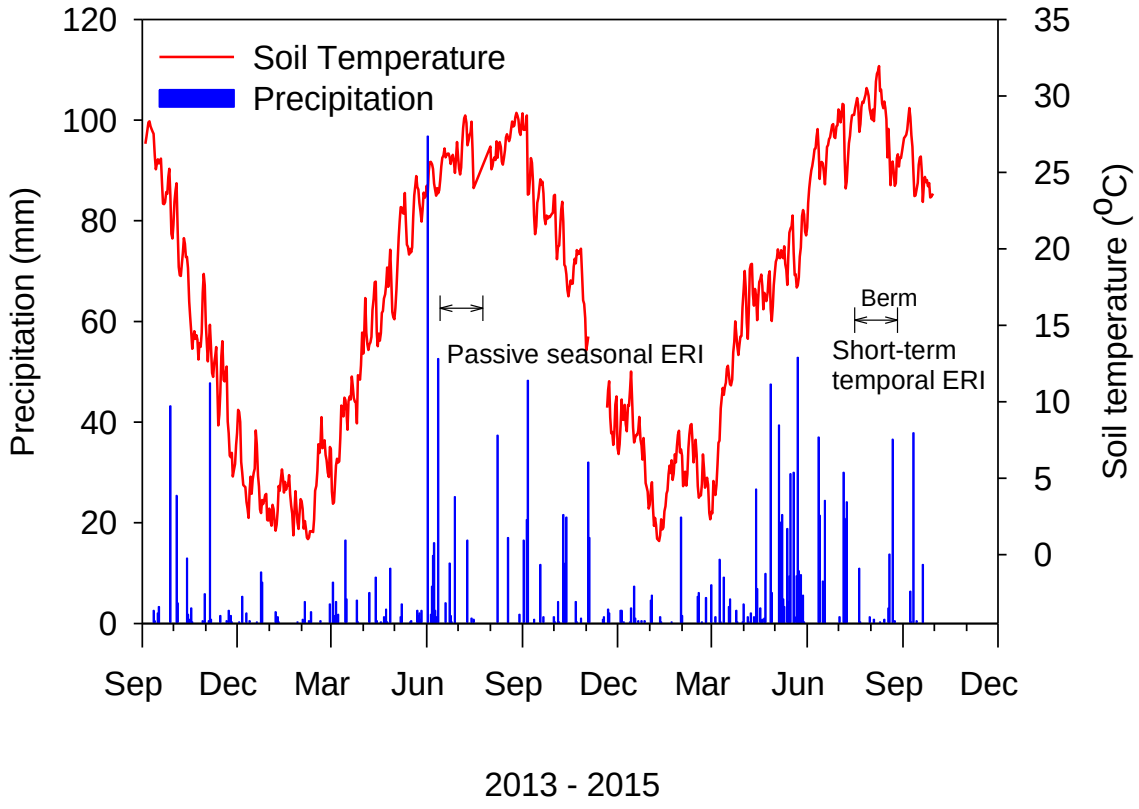

Figure 4.2. Daily precipitation in mm (in blue; TB3 siphoning tipping bucket rain gauge with a 0.254 mm tip; Hydrological Services America, Lake Worth, FL) and soil temperature from 5 cm depth averaged over 5 minutes in degrees Celcius (in red; 107-L temperature probe; Campbell Scientific, Logan UT) recorded from a weather station at CTER site during 9/4/2013 to 9/30/2015.

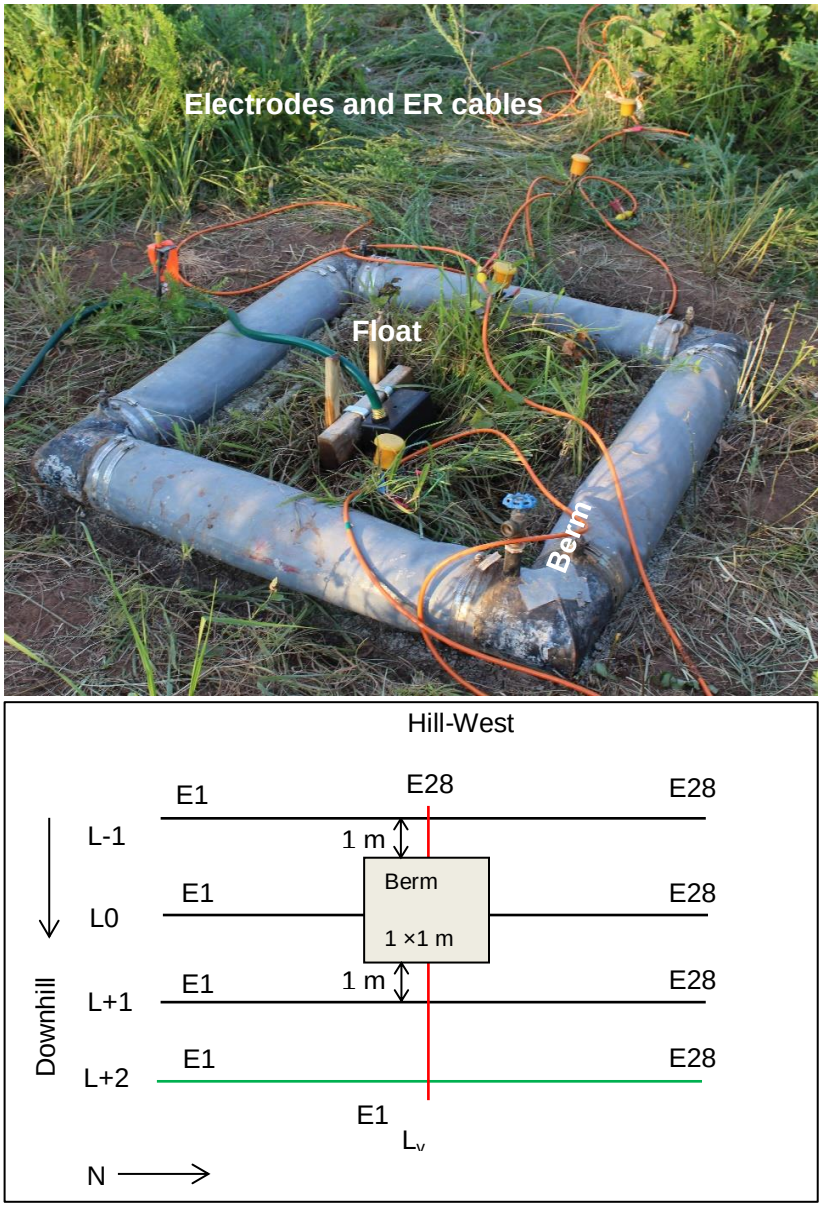

Figure 4.3. Berm infiltration experimental setup displaying the berm partially filled with water, float attached to the garden hose, electrodes with orange rebar caps and electrode cables respectively. L_v and L+2 are the original permanent transects and L0, L+1 and L-1 are the temporary transects. Berm infiltrometer of 1 × 1 m was located at the L0 at the distance of 1 m from L+1 and L-1.

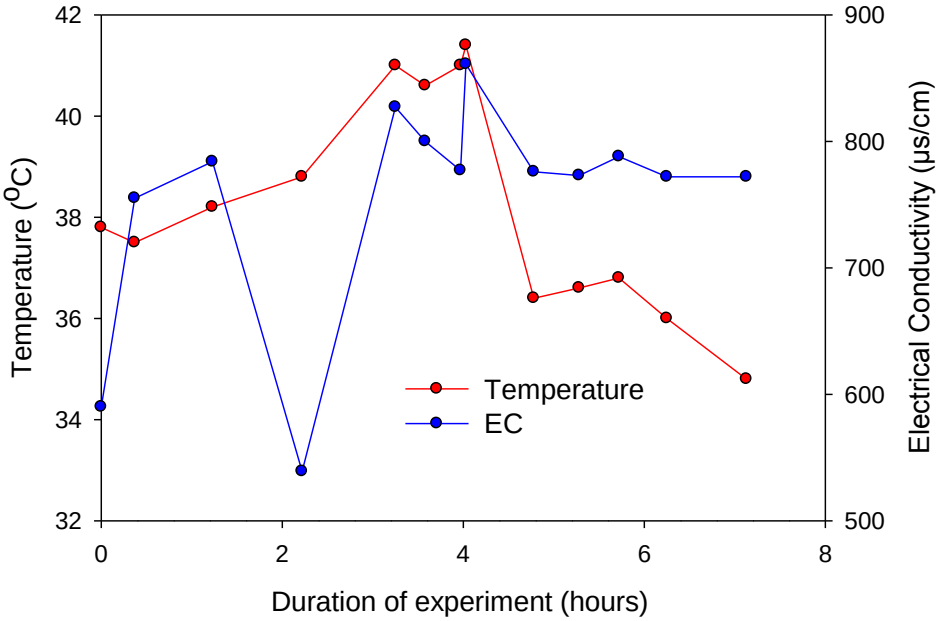

Figure 4.4. Temporal variability in temperature and electrical conductivity during berm infiltration from measurements of fluid inside the berm.

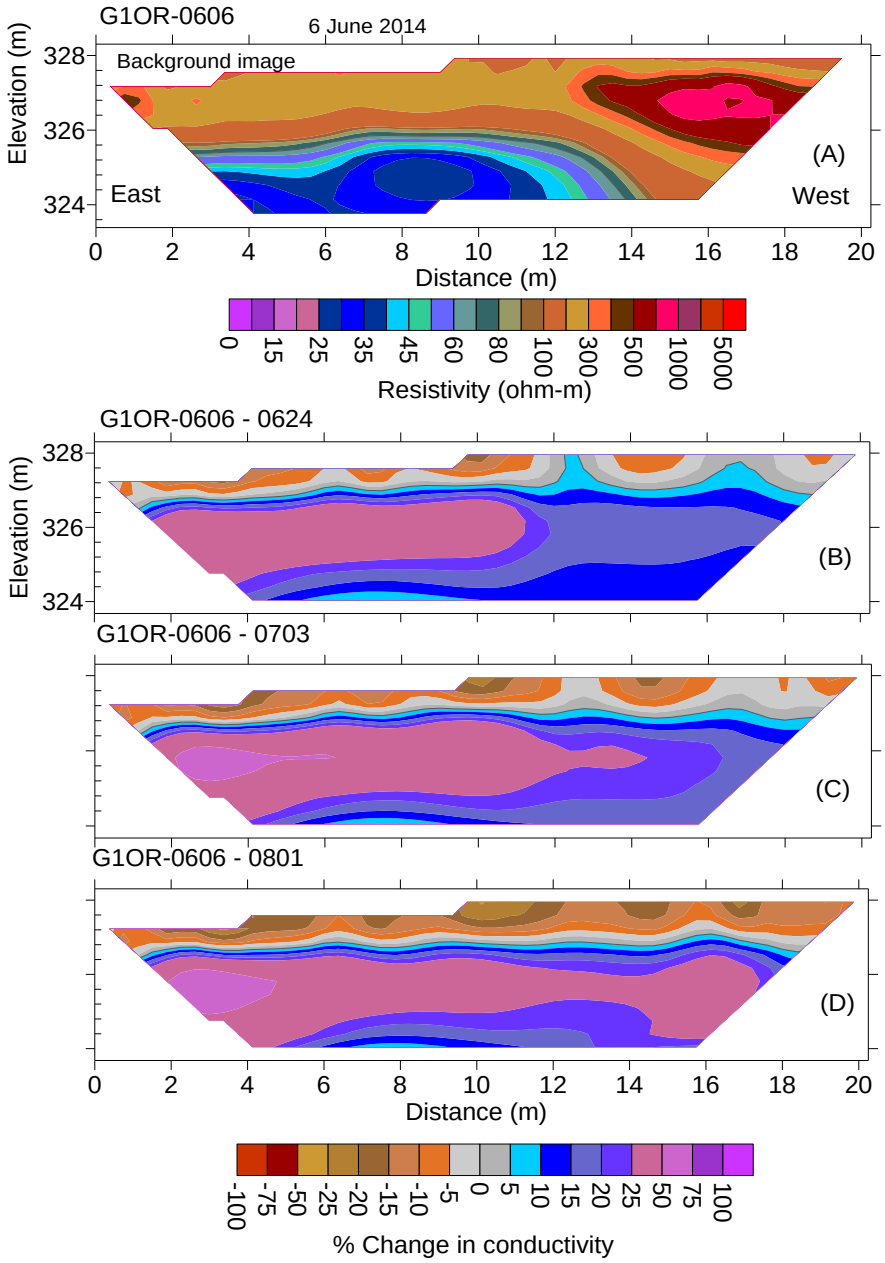

Figure 4.5. Passive seasonal temporal ER images in the grassland catchment. Time lapse images were taken from Line 0 deployed with 28 electrodes. The top image (A) represent background image and subsequent images (B, C and D) are time-lapse pseudosections or transient images showing percent change in conductivity. Transient images show two-layered moisture migration profile and indicate subsurface lateral flow.

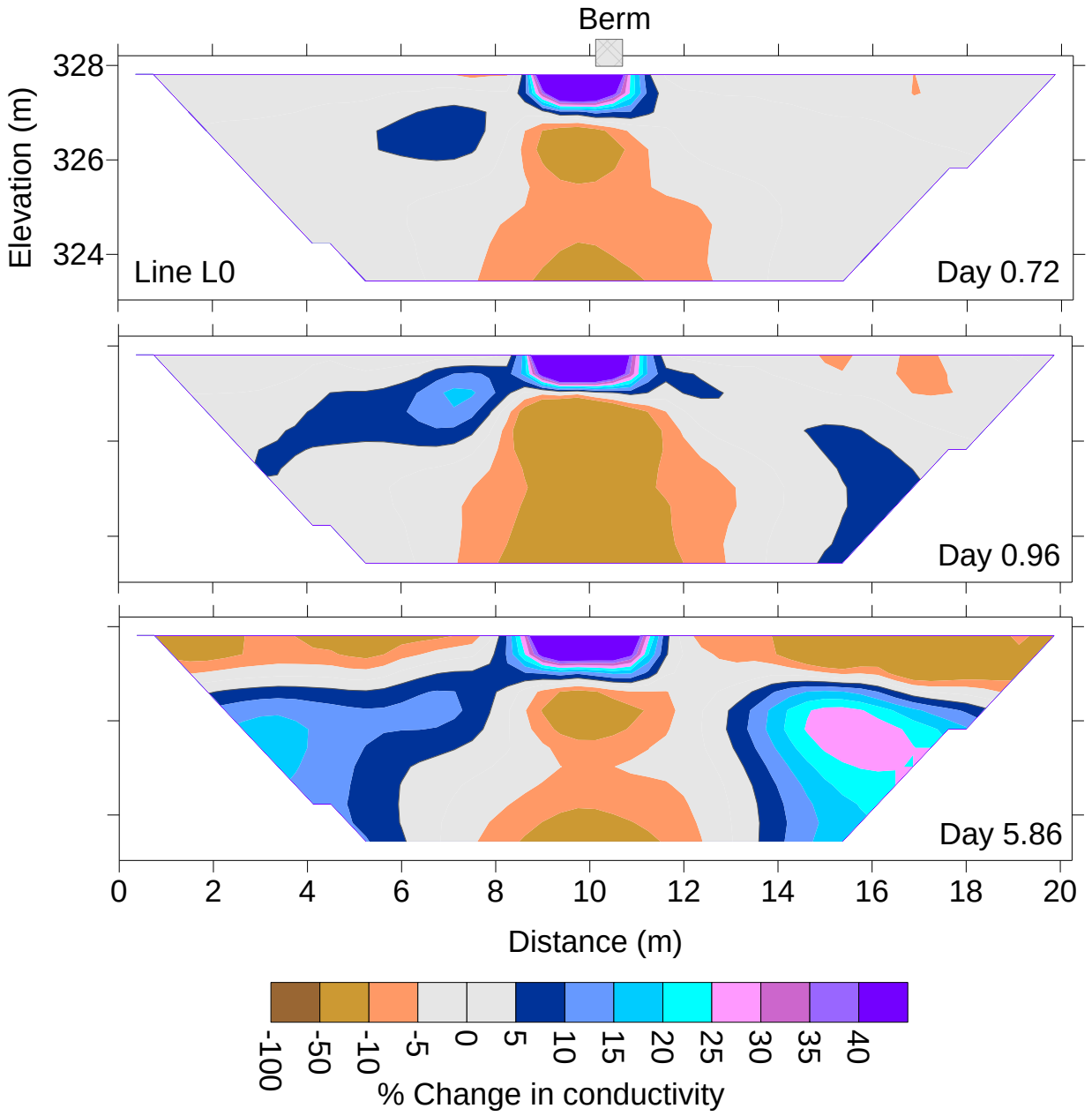
Berm
Elevation (m)
328
326
324
Line L0
Day 0.72
Day 0.96
Day 5.86
0
2
4
6
8
10
12
14
16
18
20
Distance (m)
-100
-50
-10
-5
0
5
10
15
20
25
30
35
40
% Change in conductivity

(A)

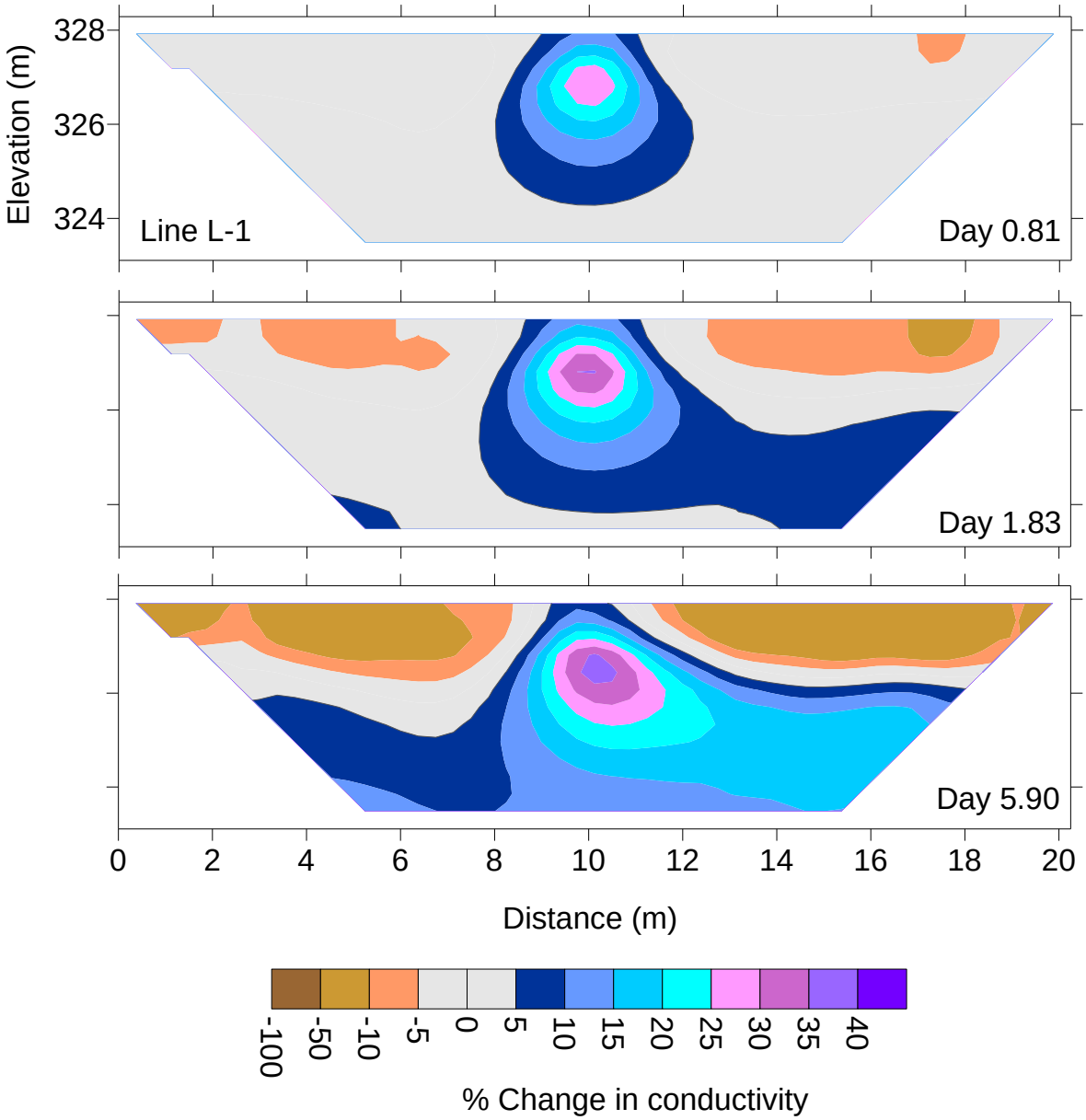
Elevation (m)
328
326
324
Line L-1
Day 0.81
Day 1.83
Day 5.90
0
2
4
6
8
10
12
14
16
18
20
Distance (m)
-100
-50
-10
-5
0
5
10
15
20
25
30
35
40
% Change in conductivity

(B)

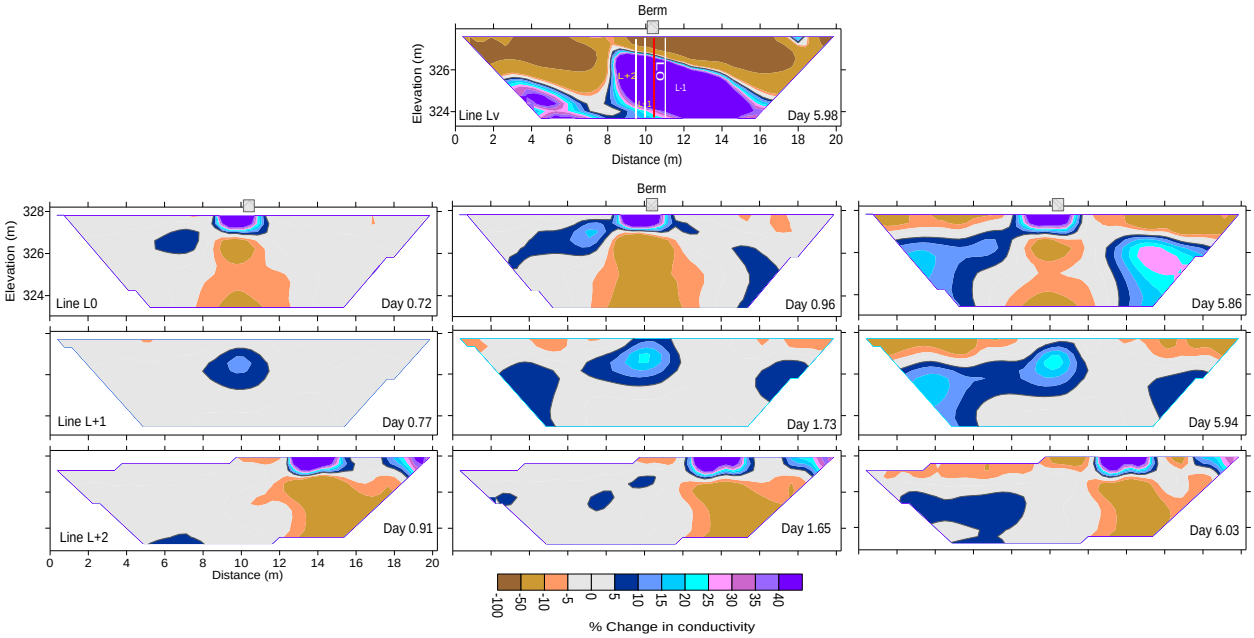

(C)

Figure 4.6. Short-term temporal electrical resistivity images after berm infiltration. L0 transect shows lateral flow of water (A), L-1 transect (B) shows vertical percolation and lateral flow of water, and Lv, L0, L+1 and L+2 transects show temporal change in conductivity after infiltration (C)

CHAPTER V

EASTERN REDCEDAR ENCROACHMENT IMPEDES DOWNWARD WATER FLUX IN TALLGRASS PRAIRIE

ABSTRACT

Vegetation changes alter evapotranspiration which influences the surface and sub-surface flow of water. Natural tracers like chloride and hydrologic flow models are often used to estimate change in deep drainage rates from land use and cover change in arid and semi-arid ecosystems. There is a paucity of information and understanding of the effect of woody plant encroachment on downward movement of water in tallgrass prairies in dry sub-humid regions. This study used both a chloride mass balance method and HYDRUS-1D modeling to estimate and contrasts drainage rates in tallgrass prairies and eastern redcedar (*Juniperus virginiana*) woodlands. Encroachment of eastern redcedar into tallgrass prairies results in an accumulation of chloride in the topsoil layer, suggesting a decrease in the downward flux of water. The estimated deep drainage rate based on the chloride mass balance method was 9.0 mm yr^{-1} in the tallgrass prairie and 0.3 mm yr^{-1} in the eastern redcedar woodland. With site-specific soil and vegetation parameters,

HYDRUS was capable of capturing the change in downward water flux associated with vegetation functional group changes in sub-humid regions. Evergreen eastern redcedar encroachment impeded the downward movement of water and groundwater recharge in this sub-humid region and highlights the importance of controlling eastern redcedar expansion in the southern Great Plains to sustain groundwater resources.

KEY WORDS: Chloride mass balance, HYDRUS-1D, soil hydraulic properties, eastern redcedar, woody plant encroachment, drainage

INTRODUCTION

Rapid landscape transformation from herbaceous dominated grasslands to shrub and tree dominated woodlands in the southern Great Plains of USA has revitalized interest in understanding the plant, soil and water nexus in sub-humid ecosystems. Trees usually improve soil infiltration capacity [*van Dijk and Keenan*, 2007] and facilitate formation of preferential flow pathways and therefore hasten the downward movement of water present in soil [*Alaoui et al.*, 2011]. As a result, forests are critical in reducing surface runoff and postponing flash floods by shifting flow paths from surface to subsurface flows. Analysis of streamflows of multiple rivers in the Edwards Plateau of TX showed a positive correlation between streamflow and rangeland that had recovered from prior over-grazing [*Wilcox and Huang*, 2010]. This general recovery in vegetation was concurrent with a steady increase in woody coverage in last several decades [*Wilcox and Huang*, 2010]. Those two pieces of evidence lead to speculation that conversion of herbaceous vegetation to woody vegetation might enhance local recharge even in a dry sub-humid region where the potential evapotranspiration (PET) was 1.5 to 2 times precipitation [*Safriel*, 2005]. If this is the case, then the hydrological impact of woody encroachment in the tallgrass prairies and related implications for water resources needs to be re-evaluated.

The encroachment of woody plants in grasslands decreases albedo and increases energy trapped in the system due to woody canopy and inter-canopy patch co-existence [*Breshears*, 2006; *Royer et al.*, 2010] and the latent heat partitioning or the ratio of ET to precipitation [*Huxman et al.*, 2005; *Zhang et al.*, 2001]. Conversion of vegetation from

herbaceous to woody vegetation results in a substantial increase in the ET or the ratio of ET to precipitation after woody plant encroachment in dry sub-humid ecosystems [*Dugas et al.*, 1998; *Liu et al.*, 2010]. Based on the water balance equation, an increase in ET will be balanced either by decrease in runoff or deep recharge or both. Although multiple year's observational data from micro-catchments showed substantial decrease in runoff after eastern redcedar encroachment into a tallgrass prairie [*Zou et al.*, 2014], it remains unknown how deep recharge responds to this vegetation change. However, this knowledge is crucial to ensure effective water resource management for tallgrass prairies.

Methods such as chloride mass balance (CMB) [*Adane and Gates*, 2014; *Gaye and Edmunds*, 1996; *Huang et al.*, 2013; *Moore et al.*, 2012; *Scanlon et al.*, 2007; *Wine et al.*, 2015], and hydrologic flow models like HYDRUS-1D [*Ma et al.*, 2010; *Tafteh and Sepaskhah*, 2012] are used to provide valuable information on downward movement of water and drainage rates within a short period of time [*Allison et al.*, 1994]. Based on the CMB method, woody plants and shrubs such as honey mesquite (*Prosopis glandulosa*) were reported to decrease deep percolation of water in semi-arid rangelands of south Texas [*Moore et al.*, 2010]. A combination of the CMB method and HYDRUS-1D illustrated the downward water flux for a mixed grass system [*Wine et al.*, 2015]. However, the groundwater recharge under sub-humid conditions is highly variable and there are no well-established methods to estimate groundwater recharge for a region transitioning from water control to atmospheric control [*Scanlon et al.*, 2005].

The CMB method was originally applied by Eriksson and Khunakasem in 1969 in the saturated zone to estimate recharge on the coastal plain of Israel [*Scanlon et al.*,

2002a] while *Allison and Hughes* [1978] used the method in the unsaturated zone to estimate recharge in the Gambier Plain, Australia. Chloride mass balance method has been used to estimate groundwater recharge throughout the world across arid, semi-arid and sub-humid regions [*Gaye and Edmunds*, 1996; *Huang et al.*, 2013; *Scanlon et al.*, 2007; *Wine et al.*, 2015]. In recent years, chloride mass balance has been applied in the Nebraska Sand Hills [*Adane and Gates*, 2014], semi-arid rangelands in Texas [*Moore et al.*, 2012], the US High Plains and California Central Valley [*Scanlon et al.*, 2012], the semi-arid range in southwest Idaho [*Aishlin and McNamara*, 2011], and a mixed-grass prairie watershed of Oklahoma [*Wine et al.*, 2015] to understand the downward movement of water. Soil chloride accumulates in the near-surface to result in higher concentrations under land use dominated by greater ET such as woodlands. On the contrary, chloride is likely to flush through soil profiles in grasslands with lower ET. The soil chloride distribution may, however, vary with vegetation pattern and/or phenology, water availability, soil types, bulk density, and hydraulic conductivity [*Moore et al.*, 2010; 2012].

Soil chloride based studies are a simple and economical method to provide reliable estimates of deep percolation of water. However, such studies can underestimate the vertical infiltration rate under a system dominated by macropores (e.g. deep desiccation cracks, root tubes, and pipes), and soil chloride use is rather challenging in negatively charged clay-dominated soils. Such soils exhibit anion exclusions that increase chloride concentration in the pore water. This can potentially underestimate the rate of percolation [*Gee et al.*, 2004]. *Tyner et al.* [2000] reported that the chloride mass balance

method can overestimate deep percolation by approximately 20% due to higher velocity of anions compared to water. The chloride mass balance method is rather accurate for and often used in arid and semi-arid regions because of higher Cl^- concentrations; very few studies are conducted in humid and sub-humid regions because climate may restrict the concentration of Cl^- to be measured accurately [*Tyner et al.*, 2000].

HYDRUS is a physically based model coupling water flux with atmospheric demand based on the SPAC concept (Soil, Plant Atmospheric Continuum). HYDRUS-1D is increasingly used to simulate vadose zone soil moisture and recharge in agriculture and forest ecosystems, and more recently HYDRUS-2D and 3D models are being used to simulate subsurface flow and spatio-temporal moisture dynamics at the tree scale [*Fan et al.*, 2015a]. *Wine et al.* [2015] used HYDRUS-1D to understand the sensitivity of deep drainage to soil texture and compaction, climate, water stress, growing season, and rooting depth in the mixed grass prairie of Oklahoma, USA. Soil hydraulic parameters are necessary to model the effect of vegetation transition and root water uptake on the deep drainage of water. Direct methods such as laboratory and in-situ determination of hydraulic properties are challenging, time-consuming, expensive [*Hopmans and Simunek*, 1999b; *Wollschläger et al.*, 2009], and uncertain for large scale [*Ritter et al.*, 2003]. HYDRUS can be effectively be used to predict soil hydraulic properties directly, or estimated by inverse solution by iteratively adjusting and optimizing initial estimates of hydraulic function parameters [*Hopmans and Simunek*, 1999a], to effectively estimate the downward flux of water based on field-scale soil moisture time series [*Wollschläger et al.*, 2009]. HYDRUS is able to simulate changes in downward water flux under woody

plant encroachment in sub-humid regions. Woody plant encroachment into grassland changes soil hydrological properties such as saturated infiltration capacity in sub-humid prairies [*Zou et al.*, 2014] and also the pattern of water flux back to the atmosphere through transpiration [*Caterina et al.*, 2014] and evaporation [*Zou et al.*, 2015], a classic case of modification of SPAC. Use of Richards' equation in combination with the Penman-Monteith equation in HYDRUS can be effective in capturing the downward flux of water in this dry sub-humid region.

This objectives of this study were to: (1) compare and contrast soil chloride concentrations between tallgrass prairie and prairie heavily encroached by eastern redcedar (*Juniperus virigiana*); (2) estimate deep water drainage rates using a steady-state equation; and (3) use measured moisture profiles to estimate deep drainage rate using HYDRUS-1D. We hypothesized the following: (i) more chloride accumulates in the soil and develops strong fluctuation patterns under eastern redcedar woodland. This is because the annual PET (1170 mm) is approximately 1.5 times that of the precipitation (831mm) for our site [*Wine et al.*, 2012]. Eastern redcedar encroachment will reduce albedo and increases energy partitioning towards latent heat, which will lead to increase in ET. *Liu et al.* [2010] reported that annual ET was 10% higher in woodlands than that in adjacent grasslands in central Oklahoma using surface energy balance methods. Similarly, canopy interception of rainfall may reduce effective precipitation, leaving less water in soil to flush chloride. (ii) The deep drainage rate decreases after tallgrass prairie is converted into eastern redcedar woodland. This hypothesis is based on the fact that deep drainage in this region occurs mostly during the spring and early summer rainfall

seasons while warm season grasses are still dormant or not fully developed. Year round plant water uptake by evergreen eastern redcedar and interception of rainfall reduces the frequency of saturated soil water conditions and decreases the deep drainage rate.

MATERIALS AND METHODS

Site description

The study was conducted at the Oklahoma State University Research Range (OSURR). The study area is located 15 km southwest of Stillwater, Payne County, Oklahoma, USA (36^{o} 03'46.73" N, 97^{o}11'03.33" W, and elevation 331 m above sea level). It has continental climate with average annual mean temperature of 15^{o} C and the average annual precipitation of 932 mm (http://www.ncdc.noaa.gov/cdo-web/datasets/). The dominant soil types in the study site include Stephenville-Darnell complex, Grainola-Lucien complex, and Coyle soil series. Stephenville are fine-loamy, siliceous, active, thermic Ultic Haplustalfs; Darnell are loamy, siliceous, thermic, shallow, Udic Ustochrepts; Grainola are fine, mixed, thermic, Vertic Haplustalfs; Lucien are shallow fine sandy loam, mixed, thermic, shallow Typic Haplustolls; and Coyle series are fine-loamy, siliceous, thermic, Udic Argiustolls [*Henley et al.*, 1987; *Soil Survey Staff*, 1999]. The study area is a mosaic of forest, savanna and prairie vegetation types, and forms a transitional zone between the deciduous forest to the east and the prairie to the west.

Site history

Historical aerial images of the study site at OSURR, Marena, Oklahoma show the sequential transformation in land use and land cover at our study site in the past 70 years.

In the 1930s, the site was used for cotton cultivation. Cotton farming resulted in severe soil erosion. As a result, terraces were constructed to prevent soil erosion. The cotton fields were abandoned and reverted back to grasslands in 1950s. However, eastern redcedar (*Juniperus viriginiana*) started to proliferate at the study site in the late 1970s due to fire suppression and grazing. In 1983, prescribed fire with three years return interval was introduced on the western side (tallgrass prairie). However, both tallgrass prairie and eastern redcedar encroached sites were grazed with a moderate stocking rate [*Engle et al.*, 2006].

The dominant herbaceous species in the prairie areas included little bluestem (*Schizachyrium scoparium*), big bluestem (*Andropogon gerardii*), Indiangrass (*Sorghastrum nutans*), switchgrass (*Panicum virgatum*), and tall dropseed (*Sporobolus asper*) [*Limb et al.*, 2010]. Major forbs include western ragweed (*Ambrosia psilostachya)* and broomweed (*Gutierrezia dracunculoides*). In the last few decades, eastern redcedar has rapidly encroached the eastern side of OSURR; covering approximately 75% of the area based on a plot survey in 2011.

Soil water content

A total of 21 soil moisture arrays were installed at the study site in 2009-2010. Nine arrays were distributed in the three tallgrass prairie micro-catchment; 12 arrays in the four eastern redcedar encroached micro-catchments [*Zou et al.*, 2014]. Each array was equipped with a Decagon EM50 data logger and installed with ECH_2O EC-5 soil water content probes (Decagon, Pullman, WA, USA) at four soil layers- H_1: 0 – 100 mm (at 5 cm), H_2:100 – 300 mm (at 20 cm), H_3: 300 – 600 mm (at 45 cm) and H_4: 600 -1000 mm

(at 80 cm) to measure volumetric water content of the soil (Decagon, Pullman, WA, USA) at 15-min intervals.

Chloride mass balance and soil chloride measurements

Chloride is assumed to be a conservative anion in the CMB method. That means it is assumed to be nonreactive in nature and neither repelled nor absorbed by soil particles and sediments. It is also assumed not to be taken up by plants. The CMB method is based upon the following additional assumptions [*Gaye and Edmunds*, 1996; *Sibanda et al.*, 2009]. (a) Net change in storage of Cl^- in the unsaturated zone is zero. (b) Cl^- mass flux over time is constant. (c) There is no unaccounted source of Cl^- input such as weathering and dissolution of minerals. (d) The flux of Cl^- due to wet and dry deposition at the surface is equivalent to the flux beneath the root zone.

The dominating soil types in the prairie include Stephenville-Darnell complex, Coyle loam, Harrah-Pulaski complex and Zaneis-Huska complex. The dominating soil types in the eastern redcedar woodland include Coyle-Zaneis complex, Grainola-Lucien complex, Stephenville fine sandy loam, and Coyle-Lucien complex. The major soil texture was fine sandy loam across both vegetation cover types. Mean soil bulk density for the top 30 cm was 1.19 g cm^{-3} and 1.25 g cm^{-3} in the prairie and the eastern redcedar woodland, respectively [*Zou et al.*, 2014]. Soil samples were collected from the prairie and the eastern redcedar woodland sites (Fig. 5.1). Two tallgrass prairie micro-catchments and two eastern redcedar encroached micro-catchments were chosen and three locations were selected in each micro-catchment. At each sampling point, herbaceous vegetation was clipped and litter layer was removed to expose mineral soil.

Soil was cored using hand auger up to a depth of 2.75 m and the soil core was sampled in sections of 25-cm increments to obtain a total of 91 samples. About 100 g of soil sample were collected from each section and stored in plastic bags, labeled, brought to the laboratory and refrigerated at 2^{o} C until processing.

Soil samples were initially weighed and a subsample of about 50 g from each section was oven dried for 24 hours at 105^{0}C to estimate gravimetric water content. The oven dried soil sample was sieved through a 2 mm sieve to remove rocks, gravels or roots. 25 mL of 0.01 M CaPO4 was added to 10 g of soil and shaken for 0.5 hour at 200 rpm in a shaker followed by filtration through Whatman No. 2 filter paper. The Cl^- anion in the soil was determined by mercury thiocynate method using QuikChem 8500 Flow Injection Analysis System (Lachat Instruments, Loveland, CO, USA). The Cl^- content in the pore water was estimated by dividing soil Cl^- by gravimetric water [*Kim and Jackson*, 2012]. Deep drainage rate was estimated by using a steady-state equation which assumes that Cl^- deposited by rain is removed by drainage from the unsaturated zone and can be used as a surrogate for deep drainage.

$$P \times Cl_p = D \times Cl_s \qquad [1]$$

where P is the average annual precipitation (mm yr^{-1}), Cl_p is the average Cl input from all sources (mg L^{-1}), Cl_s is the average Cl^- concentration of pore water (mg L^{-1}), and D is the average annual deep drainage rate (mm yr^{-1}).

Based on National Atmospheric Deposition Program (NADP) (http://nadp.sws.uiuc.edu/), the closest site is Kessler Farm Field Laboratory,

approximately 161 km south of our sites. The mean Cl^- concentration in precipitation during 1983 -2014 from Kessler Farm Field Laboratory, OK was 0.19 mg L^{-1} (Fig. 2). In this study, the approach used for Cl_p was to double mean Cl^- concentration in precipitation to account for dry deposition [*Scanlon et al.*, 2012; *Wine et al.*, 2015]. Dry fallout is not measured separately and there are no historical data. As a result, there are uncertainties in dry deposition of Cl^- from eolian deposition: windblown soil, dust and aerosols [*Ping et al.*, 2014; *Scanlon et al.*, 2007]. Therefore, for this study, we assumed that the rate of dry deposition of Cl^- is equivalent to the wet deposition.

HYDRUS-1D

Hydrus-1D is a finite element model that numerically solves Richards' equation to simulate water movement in variably saturated soils. The one dimensional uniform water flow in a partially saturated porous media is given by equation [2], where h is soil water pressure head [L], Θ is the volumetric water content [$L^3\ L^{-3}$], t is time [T], x is the vertical coordinate [L], K is the unsaturated hydraulic conductivity [$L\ T^{-1}$], α is the angle between the flow direction and the vertical axis and S is a sink term [$L^3\ L^{-3}\ T^{-1}$].

$$\frac{\partial \theta}{\partial t} = \frac{\partial}{\partial x}\left[K\left(\frac{\partial h}{\partial x} + \cos\alpha\right)\right] - S \qquad [2]$$

HYDRUS-1D simulations were conducted for a two-layered soil system consisting of a sandy loam up to the depth of 75 cm and sandstone extending from 75 cm to the depth of 275 cm based on field observation. Time variable boundary conditions and meteorological data were selected for precipitation input and Penman-Monteith equation for 1324 days. The number of days was selected based on climatic data obtained

from a weather station (WS15) at the Oklahoma State University Range Research Station. An observation node was kept at 80 cm since a soil moisture sensor was instrumented in this depth. Root depth was set to 100 cm for both grass and eastern redcedar. The rooting depth was based on root distribution of grass and shrubs across all biomes as reported by *Jackson et al.* [1996]. Daily volumetric soil moisture data collected for each vegetation from nine soil moisture arrays in grassland and twelve arrays in the juniper encroached catchment since 4th January 2011 was used during forward modelling. HYDRUS uses van Genuchten-Mualem hydraulic model and/or single porosity model to obtain parameters for soil water retention with an air entry pressure/suction value of -2 cm:

$$\theta(h) = \begin{cases} \theta_r + \dfrac{\theta_s - \theta_r}{[1 + |\alpha h|^n]^m} & h < 0 \\ \theta_s & h \geq 0 \end{cases} \qquad [3]$$

$$K(h) = K_s S_e^l \left[\left(1 - s_e^{1/m}\right)^m\right]^2 \qquad [4]$$

$$m = 1 - {}^1/_n, n > 1 \qquad [5]$$

where S_e is the effective saturation [L^3 L^{-3}], Θ_s is the saturated water content [L^3 L^{-3}], Θ_r is the residual water content [L^3 L^{-3}], K_s is the saturated hydraulic conductivity [L T^{-1}], α is the inverse of air-entry value or bubbling pressure [L^{-1}], n is the pore size distribution parameter [-], and l is the pore connectivity parameter [-], with value of 0.5 for most of the soils. HYDRUS uses FAO Penman-Monteith equation to estimate ET [mm day^{-1}] using the specific heat of air (c_p), density of air (ρ_a), surface temperature, air

temperature, atmospheric resistance to water vapor transport (r_a), psychrometric constant (γ), and surface resistance to water vapor transport (r_s) assuming vegetated canopy and negligible flux from soil surface.

$$\lambda ET = \frac{\Delta(R_n - G) + \rho_a c_p \frac{(e_s - e_a)}{r_a}}{\Delta + \gamma(1 + \frac{r_s}{r_a})} \qquad [6]$$

where, R_n is net radiation, G is soil heat flux, $e_s - e_a$ is vapor pressure deficit of the air and Δ is the slope of saturation vapor pressure curve and temperature relation.

Boundary conditions included an atmospheric boundary condition with surface runoff as the upper boundary condition and the lower boundary defined as free drainage. The upper boundary was chosen such that precipitation rate in excess of hydraulic conductivity is unlikely to increase pressure head. Similarly, HYDRUS uses Feddes [1977] and *S* shaped function [van Genuchten (1985)] as root water uptake models. Time variable boundary conditions include precipitation in cm/day and hCritA. The latter term refers to an absolute value of the minimum pressure head allowed for the soil surface. The hCritA was set to -100, 000 cm. This low value prevents the numeric solution from being unstable. An example of such situation could be sandy soil where a small change in water content results in large change in pressure head. If the pressure head on soil surface drops below -100, 000 cm, evaporation will fall below the potential evaporation rate. Moreover, this criterion controls the flux across the boundary and should be lower than the pressure head below which water uptake by plant terminates.

Soil hydraulic properties may have different maximum and minimum values as indicated by *Ries et al.* [2015]. The parameters values for layer 1 were default values obtained for two-layered soil system in this study (Table 5.1). The hydraulic conductivity of sandstone was similar to the conductivity of sandstone strata in Garber-Willington formation. The hydraulic parameters for sandstone were obtained from Oklahoma Water Resource Board report [https://www.owrb.ok.gov/studies/reports/gwvulnerability/] and *Farzamian et al. [*2015]. Root water uptake parameters (after Feddes et al. 1978) were obtained from *Lv et al.* [2014] for eastern redcedar and from *Wine et al.* [2015] for tallgrass, and are shown in Table 5.2. The pressure head below which root extract water at maximum rate were increased from -800 cm (default value for pasture) to -600 for tallgrass [*Wine et al.*, 2015] and the pressure head was maintained at -12, 800cm for eastern redcedar [*Lv et al.*, 2014]. The pressure head at which water uptake ceases in eastern redcedar was maintained at -21, 500 cm. Vegetation parameters such as albedo and leaf area index (LAI) were obtained from *Ge and Zou* [2013]. The albedo for tallgrass prairie and eastern redcedar were 0.26 and 0.18, respectively, and LAI were 2.0 and 5.0, respectively.

Statistical analysis

The experiment was laid out in completely randomized block design (CRBD). Two micro-catchments for each vegetation cover types were considered as blocks. Three sampling points in each micro-catchment were replicates for each block and the sample size (n) = 3. Two ways analysis of variance (ANOVA) was carried out to determine significant differences in Cl^- concentrations and gravimetric moisture contents across soil

depth and vegetation, as well as their interactions at $\alpha = 0.05$ level. All analyses were conducted using the Proc ANOVA procedure (SAS v9.4; SAS Inc., Cary, NC, USA). Tukey's studentized posthoc (HSD) test was used to determine differences in Cl^- and moisture content across depths.

RESULTS

Soil chloride concentration and drainage rates

Mean soil Cl^- content varied between 5 to 162 mg L^{-1} in the prairie and 88 to 612 mg L^{-1} in eastern redcedar encroached woodland (Fig. 5.4). Mean Cl^- concentration was significantly higher in eastern redcedar woodland than that in the prairie ($p = 0.001$). Gravimetric water content was significantly affected by vegetation cover type ($p = 0.0006$), soil depth ($p < 0.0001$) and the interaction between cover type and depth ($p = 0.0037$). Gravimetric water content was significantly higher in the prairie than in the woodland ($p = 0.0006$). Gravimetric water content in soil sampled at 25 cm depth in the prairie was significantly higher than at other depths except at 50 and 225 cm ($p < 0.05$). The maximum possible drainage rate based on the lower limit for Cl^- detection was 33 mm yr^{-1}. The estimated drainage rate below 75 cm depth was 9 mm yr^{-1} in the prairie and 0.3 mm yr^{-1} for eastern redcedar woodland.

Forward simulation in HYDRUS-1D and water flux

Downward flux of water at the HYDRUS observation node located at 80 cm depth occurred at the beginning of simulation, at day 400, day 900, and day 1300 since

simulation at 4th January 2011 for tall grass prairie and at the beginning of simulation for eastern redcedar, and was in general higher in the tallgrass prairie (Fig. 5.5).

The simulated downward fluxes of water (percolation) below 275 cm were similar in pattern for the prairie and eastern redcedar. Free drainage of water below 275 cm, a lower boundary condition, was higher in the prairie at the beginning of the simulation.

DISCUSSION

In arid and semi-arid regions, the vertical fluctuation patterns in Cl^- concentration is well understood and are important for estimating site-specific drainage rates [*Gates et al.*, 2008; *Moore et al.*, 2010; *Wine et al.*, 2015]. Our Cl^- concentration data showed that encroachment of eastern redcedar, and therefore conversion of tallgrass prairie to woodland in dry sub-humid regions, resulted in an increase of Cl^- in the soil. Our concentrations were within the range of values reported for mixed prairie in Oklahoma [*Wine et al.*, 2015] and natural systems in Texas High Plains [*Scanlon et al.*, 2010]. The Cl^- concentration below 80 cm was fairly stable (5 mg L^{-1} in tallgrass prairie and 110 mg L^{-1} in eastern redcedar woodland). A sandstone substrate exists roughly between 60 to 100 cm for this study site and impedance of sandstone to root growth may be associated with the stable Cl^- concentrations. Once water percolates into the sandstone layer with limited root access, it will be likely to contribute to the deep recharge and this difference may reflect the difference of deep recharge. Increase of soil Cl^- concentration indicates reduced percolation and groundwater recharge potential after eastern redcedar encroached into tallgrass prairie. Daily water use by eastern redcedar woodland is substantially high and may range from 1 to 66 liters depending on tree size [*Caterina et*

al., 2014]. Higher plant water use and canopy interception of rainfall [Zou et al., 2015] reduce water availability to flush soil chloride through soil profile. *Zou et al.* [2014] reported relatively lower soil water content in eastern redcedar woodland, especially in spring and early summer, compared to tallgrass prairie catchment during 2009 - 2011.

The drainage rate of 0.3 mm yr^{-1} estimated for eastern redcedar woodland in this study is lower than drainage rate in a recent study for Council Creek watershed, Stillwater, OK [*Wine et al.*, 2015]. This difference could be due to the differences in location and scale. The drainage rate of *Wine et al.* [2015] was a mean value for a watershed with partial tree cover (less than 15%) and also included a riparian region. However, we sampled the upland micro-catchments only in this study. Importantly, eastern redcedar covered approximately 80% of these micro-catchments, five times higher than tree cover in *Wine et al.* [2015].

Among seven different numerical water balance models based on Richards' equation, HYDRUS-1D performed better in simulation of deep drainage under dry climate of Idhao [*Scanlon et al.*, 2002c]. To reduce uncertainty in simulated drainage in a sub-humid climate, we included site specific information such as climatic time series and soil moisture to constrain the model [*Wollschläger et al.*, 2009]. The strength of our HYDRUS simulation is to account for heterogeneity in the hydraulic properties and we are confident of our simulated results. Our results indicated that downward flux of water was reduced after eastern redcedar encroachment into tallgrass prairie. At first glance, this is in contrast to our general belief that trees improve infiltration capacity and facilitate deep recharge. *Scanlon et al.* [2005] showed groundwater recharge rates under

different land use and suggested that irrigated agriculture exhibits moderate to higher recharge whereas non-irrigated lands and arid and semi-arid rangelands have moderate and low recharge, respectively. This conclusion was further expanded in a global synthesis of groundwater recharge in arid and semi-arid regions indicating highest recharge rate under no vegetation followed by cropland, grassland and woodland [*Kim and Jackson*, 2012]. For rangeland, deep drainage could be affected by the interaction of plant phenology and rainfall regime as chloride profiles respond to seasonal precipitation [*Huang et al.*, 2013]. In our system, our rainfall concentrates between April and May when warm season grasses are not usually fully grown and saturated soil conditions often occur in grassland, while depletion of soil moisture at multiple depth were evident under eastern redcedar woodland [*Zou et al.*, 2014]. This evidence supports the results of reduced downward water flux and deep recharge potential from this project.

CONCLUSION

Our results show that encroachment of eastern redcedar into tallgrass prairie reduces the downward flux of water. Higher chloride concentrations in the soil profile accounts for a substantial decrease in deep drainage rate after the tallgrass prairie is converted into eastern redcedar woodland. With site-specific soil and vegetation parameters, HYDRUS is able to capture change in downward water flux associated with vegetation functional group change in the tallgrass prairie. In a dry sub-humid region, afforestation, especially evergreen tree species in herbaceous dominated rangeland, will alter hydrologic processes and have impact on downward water flux and therefore runoff and groundwater recharge. To sustain the provisioning service of grassland, groundwater

recharge, we should prevent large-scale eastern redcedar conversion of the rangeland in the southern Great Plains. Improved understanding of vegetation change on deep drainage in different soil types, geologic substrates and under different climate change scenarios are necessary to assist our land based mitigation and adaptation strategy for sustaining ecosystem function and services and to ensure effective water resource management planning.

ACKNOWLEDGEMENTS

The study was supported by USGS OWRRI grants and USDA NIFA award (2014-67010-216530). The data analysis and paper writing were partially supported with funding from NSF EPSCoR (NSF-1301789) and NSF Dynamics of Coupled Natural and Human Systems (CNH) program (DEB-1413900). The authors extend their appreciation to Briana Sallee from Plant and Soil Sciences, Oklahoma State University, for her technical assistance with HYDRUS-1D. We thank Dr. Daihua Qi for assisting in the soil sampling for chloride study.

REFERENCES

Adane, Z., and J. Gates (2014), Determining the impacts of experimental forest plantation on groundwater recharge in the Nebraska Sand Hills (USA) using chloride and sulfate, *HydJ*, *23*(1), 81-94.

Aishlin, P., and J. P. McNamara (2011), Bedrock infiltration and mountain block recharge accounting using chloride mass balance, *HyPr*, *25*(12), 1934-1948.

Alaoui, A., U. Caduff, H. H. Gerke, and R. Weingartner (2011), A Preferential Flow Effects on Infiltration and Runoff in Grassland and Forest Soils, *Vadose Zone J.*, *10*(1), 367-377.

Allison, G., and M. Hughes (1978), The use of environmental chloride and tritium to estimate total recharge to an unconfined aquifer, *Soil Research*, *16*(2), 181-195.

Allison, G., G. Gee, and S. Tyler (1994), Vadose-zone techniques for estimating groundwater recharge in arid and semi-arid regions, *Soil Sci. Soc. Am. J.*, *58*(1), 6-14.

Breshears, D. D. (2006), The grassland-forest continuum: trends in ecosystem properties for woody plant mosaics?, *Front. Ecol. Environ.*, *4*(2), 96-104.

Caterina, G. L., R. E. Will, D. J. Turton, D. S. Wilson, and C. B. Zou (2014), Water use of Juniperus virginiana trees encroached into mesic prairies in Oklahoma, USA, *Ecohydrology*, *7*, 1124-1134.

Dugas, W., R. Hicks, and P. Wright (1998), Effect of removal of Juniperus ashei on evapotranspiration and runoff in the Seco Creek watershed, *Water Resources Research*, *34*(6), 1499-1506.

Engle, D. M., T. N. Bodine, and J. Stritzke (2006), Woody plant community in the cross timbers over two decades of brush treatments, *Rangeland Ecol. Manage.*, *59*(2), 153-162.

Fan, J., T. Baumgartl, A. Scheuermann, and D. A. Lockington (2015), Modeling Effects of Canopy and Roots on Soil Moisture and Deep Drainage, *Vadose Zone Journal*, *14*(2).

Farzamian, M., F. A. M. Santos, and M. A. Khalil (2015), Estimation of unsaturated hydraulic parameters in sandstone using electrical resistivity tomography under a water injection test, *Journal of Applied Geophysics*, *121*, 71-83.

Gates, J. B., W. Edmunds, J. Ma, and B. R. Scanlon (2008), Estimating groundwater recharge in a cold desert environment in northern China using chloride, *HydJ*, *16*(5), 893-910.

Gaye, C., and W. Edmunds (1996), Groundwater recharge estimation using chloride, stable isotopes and tritium profiles in the sands of northwestern Senegal, *Environ. Geol.*, *27*(3), 246-251.

Ge, J., and C. Zou (2013), Impacts of woody plant encroachment on regional climate in the southern Great Plains of the United States, *Journal of Geophysical Research: Atmospheres*, *118*(16), 9093-9104.

Gee, G., Z. Zhang, S. Tyler, W. Albright, and M. Singleton (2004), Chloride-mass-balance for predicting increased recharge after land-use change, edited, Lawrence Berkeley National Laboratory, Berkeley, California.

Henley, J., R. Gelnar, and R. E. Mayhugh (1987), *Soil survey of Payne County, Oklahoma*, US Government Printing Office.

Hopmans, J., and J. Simunek (1999a), Review of inverse estimation of soil hydraulic properties, *Proceedings of the International Workshop on Characterization and Measurement of the Hydraulic Properties of Unsaturated Porous Media*, 643-659.

Hopmans, J., and J. Simunek (1999b), Review of inverse estimation of soil hydraulic properties, paper presented at Proceedings of the International Workshop on Characterization and Measurement of the Hydraulic Properties of Unsaturated Porous Media.

Huang, T., Z. Pang, and W. M. Edmunds (2013), Soil profile evolution following land-use change: implications for groundwater quantity and quality, *HyPr*, *27*(8), 1238-1252.

Huxman, T. E., B. P. Wilcox, D. D. Breshears, R. L. Scott, K. A. Snyder, E. E. Small, K. Hultine, W. T. Pockman, and R. B. Jackson (2005), Ecohydrological implications of woody plant encroachment, *Ecology*, *86*(2), 308-319.

Jackson, R., J. Canadell, J. R. Ehleringer, H. Mooney, O. Sala, and E. Schulze (1996), A global analysis of root distributions for terrestrial biomes, *Oecologia*, *108*(3), 389-411.

Kim, J. H., and R. B. Jackson (2012), A global analysis of groundwater recharge for vegetation, climate, and soils, *Vadose Zone Journal*, *11*(1), 0-0.

Limb, R. F., D. M. Engle, A. L. Alford, and E. C. Hellgren (2010), Tallgrass prairie plant community dynamics along a canopy cover gradient of eastern redcedar (Juniperus virginiana L.), *Rangeland Ecol. Manage.*, *63*(6), 638-644.

Liu, W., Y. Hong, S. I. Khan, M. Huang, B. Vieux, S. Caliskan, and T. Grout (2010), Actual evapotranspiration estimation for different land use and land cover in urban regions using Landsat 5 data, *Journal of Applied Remote Sensing*, *4*(1), 041873-041873-041814.

Lv, L., T. E. Franz, D. A. Robinson, and S. B. Jones (2014), Measured and modeled soil moisture compared with cosmic-ray neutron probe estimates in a mixed forest, *Vadose Zone Journal*, *13*(12).

Ma, Y., S. Feng, D. Su, G. Gao, and Z. Huo (2010), Modeling water infiltration in a large layered soil column with a modified Green–Ampt model and HYDRUS-1D, *Comput. Electron. Agric.*, *71*, S40-S47.

Moore, G. W., D. A. Barre, and M. K. Owens (2010), Changes in soil chloride following shrub removal and subsequent regrowth, *Geoderma*, *158*(3), 148-155.

Moore, G. W., D. A. Barre, and M. K. Owens (2012), Does Shrub Removal Increase Groundwater Recharge in Southwestern Texas Semi-arid Rangelands?, *Rangeland Ecol. Manage.*, *65*(1), 1-10.

Ping, J., C. Nichol, and X. Wei (2014), Quantification of groundwater recharge using the chloride mass balance method in a semi-arid mountain terrain, South Interior British Columbia, Canada, *J. Chem. Pharm. Res.*, *6*(1),383-388.

Ries, F., J. Lange, S. Schmidt, H. Puhlmann, and M. Sauter (2015), Recharge estimation and soil moisture dynamics in a Mediterranean, semi-arid karst region, *HESS*, *19*(3), 1439-1456.

Ritter, A., F. Hupet, R. Muñoz-Carpena, S. Lambot, and M. Vanclooster (2003), Using inverse methods for estimating soil hydraulic properties from field data as an alternative to direct methods, *Agric. Water Manage.*, *59*(2), 77-96.

Royer, P. D., D. D. Breshears, C. B. Zou, N. S. Cobb, and S. A. Kurc (2010), Ecohydrological energy inputs in semi-arid coniferous gradients: Responses to management-and drought-induced tree reductions, *For. Ecol. Manage.*, *260*(10), 1646-1655.

Safriel, U., Adeel, Z., Niemeijer, D., Puigdefabregas J., White R., (2005), Dryland Systems, in *Ecosystems and Human Well-Being: Current State and Trends. Millennium Ecosystem Assessment*, edited by S. R. Hassan R., and Ash N.,, Island Press, Washington.

Scanlon, B., R. Reedy, J. Gates, and P. Gowda (2010), Impact of agroecosystems on groundwater resources in the Central High Plains, USA, *Agric., Ecosyst. Environ.*, *139*(4), 700-713.

Scanlon, B. R., R. W. Healy, and P. G. Cook (2002a), Choosing appropriate techniques for quantifying groundwater recharge, *HydJ*, *10*(1), 18-39.

Scanlon, B. R., A. R. Dutton, and M. A. Sophocleous (2002b), *Groundwater recharge in Texas*, Bureau of Economic Geology, University of Texas at Austin.

Scanlon, B. R., R. C. Reedy, and J. A. Tachovsky (2007), Semi-arid unsaturated zone chloride profiles: Archives of past land use change impacts on water resources in the southern High Plains, United States, *Water Resources Research*, *43*(6), W06423.

Scanlon, B. R., R. C. Reedy, D. A. Stonestrom, D. E. Prudic, and K. F. Dennehy (2005), Impact of land use and land cover change on groundwater recharge and quality in the southwestern US, *Global Change Biol.*, *11*(10), 1577-1593.

Scanlon, B. R., M. Christman, R. C. Reedy, I. Porro, J. Simunek, and G. N. Flerchinger (2002c), Intercode comparisons for simulating water balance of surficial sediments in semi-arid regions, *Water Resources Research*, *38*(12).

Scanlon, B. R., C. C. Faunt, L. Longuevergne, R. C. Reedy, W. M. Alley, V. L. McGuire, and P. B. McMahon (2012), Groundwater depletion and sustainability of irrigation in the US High Plains and Central Valley, *Proceedings of the national academy of sciences*, *109*(24), 9320-9325.

Seyfried, M. S., and B. P. Wilcox (2006), Soil water storage and rooting depth: key factors controlling recharge on rangelands, *HyPr*, *20*(15), 3261-3275.

Sibanda, T., J. C. Nonner, and S. Uhlenbrook (2009), Comparison of groundwater recharge estimation methods for the semi-arid Nyamandhlovu area, Zimbabwe, *HydJ*, *17*(6), 1427-1441.

Soil Survey Staff. (1999), *Soil taxonomy: a basic system of soil classification for making and interpreting soil surveys*, United States Department of Agriculture.

Tafteh, A., and A. R. Sepaskhah (2012), Application of HYDRUS-1D model for simulating water and nitrate leaching from continuous and alternate furrow irrigated rapeseed and maize fields, *Agric. Water Manage.*, *113*, 19-29.

Tyner, J., G. Brown, J. Vogel, and J. Garbrecht (2000), Chloride mass balance to determine water fluxes beneath KCl-fertilized crops, *Trans. ASAE*, *43*(6), 1553-1560.

van Dijk, A. I., and R. J. Keenan (2007), Planted forests and water in perspective, *For. Ecol. Manage.*, *251*(1), 1-9.

Wilcox, B. P., and T. L. Thurow (2006), Emerging issues in rangeland ecohydrology: vegetation change and the water cycle, *Rangeland Ecol. Manage.*, *59*(2), 220-224.

Wilcox, B. P., and Y. Huang (2010), Woody plant encroachment paradox: Rivers rebound as degraded grasslands convert to woodlands, *Geophys. Res. Lett.*, *37*(7).

Wine, M. L., T. E. Ochsner, A. Sutradhar, and R. Pepin (2012), Effects of eastern redcedar encroachment on soil hydraulic properties along Oklahoma's grassland-forest ecotone, *HyPr*, *26*(11), 1720-1728.

Wine, M. L., J. M. Hendrickx, D. Cadol, C. B. Zou, and T. E. Ochsner (2015), Deep drainage sensitivity to climate, edaphic factors, and woody encroachment, Oklahoma, USA, *HyPr*.

Wollschläger, U., T. Pfaff, and K. Roth (2009), Field-scale apparent hydraulic parameterisation obtained from TDR time series and inverse modelling, *HESS*, *13*(10), 1953-1966.

Zhang, L., W. Dawes, and G. Walker (2001), Response of mean annual evapotranspiration to vegetation changes at catchment scale, *Water Resources Research*, *37*(3), 701-708.

Zou, C. B., D. J. Turton, R. E. Will, D. M. Engle, and S. D. Fuhlendorf (2014), Alteration of hydrological processes and streamflow with juniper (Juniperus virginiana) encroachment in a mesic grassland catchment, *Hydrol. Process.*, *28*, 6173-6182.

Zou, C. B., G. L. Caterina, R. E. Will, E. Stebler, and D. Turton (2015), Canopy Interception for a Tallgrass Prairie under Juniper Encroachment, *PLoS ONE*, *10*(11), e0141422.

Table 5.1. Soil hydraulic properties for a two-layered soil system. The values for layer 1 and 2 are default water flow parameters in HYDRUS-1D

Soil layer	*Estimates*	Θ_r ($cm^3\ cm^{-3}$)	Θ_s ($cm^3\ cm^{-3}$)	A (cm^{-1})	n	K_s ($cm\ day^{-1}$)	L (-)
Layer 1/sandy loam		0.060	0.40	0.07	1.80	106.10	0.5
Layer 2/sandstone		0.024	0.37	0.02	2.10	137.16	0.5
[*Ries et al.*, 2015]	Min value	0	0.3	0.0001	1.01	5	-2
	Max value	0.3	0.6	0.1	3	10,000	2

Table 5.2. Root water uptake parameters used in the simulation based on Feddes et al. (1978). These parameters denote pressure heads below which roots extract water (P0), extract water at maximum possible rate (Popt), water extraction at maximum rate is hindered (P2) and water uptake terminates (P3), respectively.

Vegetation	P0 (cm)	Popt (cm)	P2 (cm)	P3 (cm)	Reference
Tallgrass prairie	-10	-25	-600	-8000	*Wine et al.* [2015]
Eastern redcedar	0	0	-12800	-21500	*Lv et al.* [2014]

Fig. 5.1. Tallgrass prairie (left panel) and eastern redcedar encroached catchment (right panel)

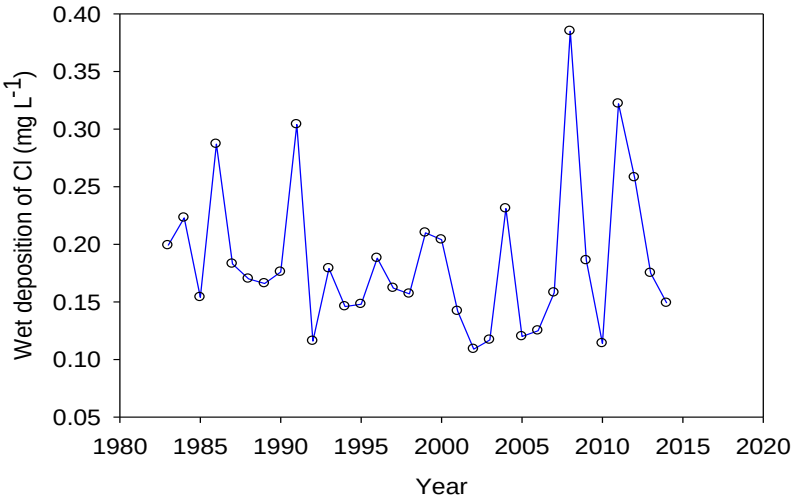

Fig. 5.2. Wet deposition of chloride as weighted mean concentration in precipitation recorded at Kessler Farm Field Laboratory, OK during 1983 -2014.

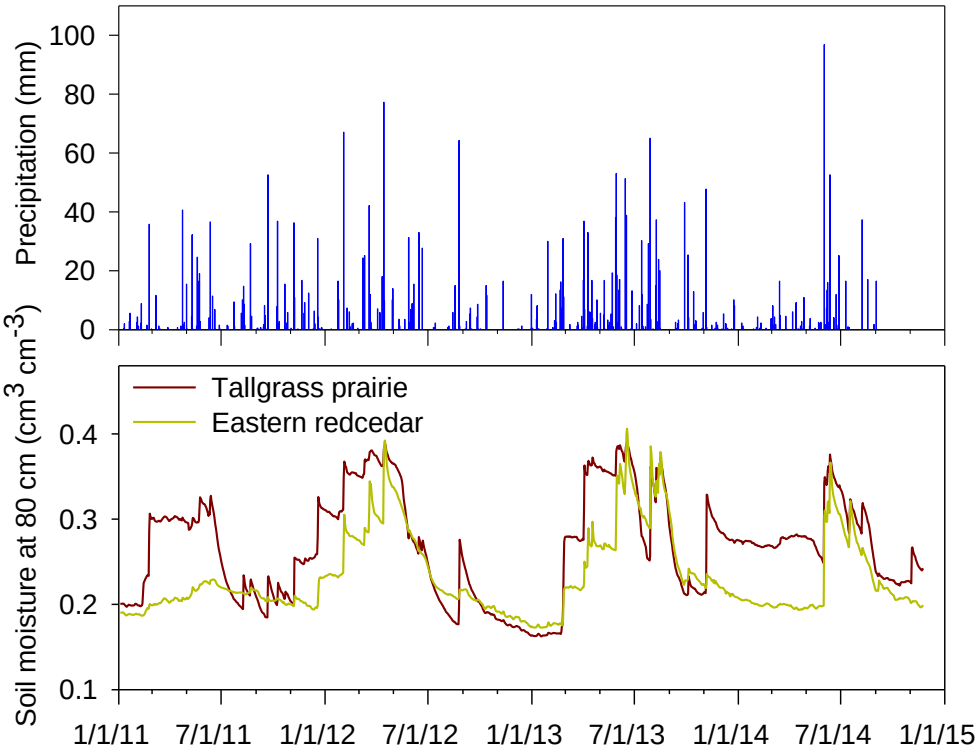

Fig. 5.3. Daily values of precipitation recorded at a weather station (WS15) at the Oklahoma State University Range Research Station and volumetric soil moisture content at 80 cm soil depth in the tallgrass prairie and eastern redcedar encroached catchments. The daily volumetric water content in tallgrass prairie and eastern redcedar encroached catchment was a mean value from 9 locations (n=9), and 12 locations (n=12) respectively.

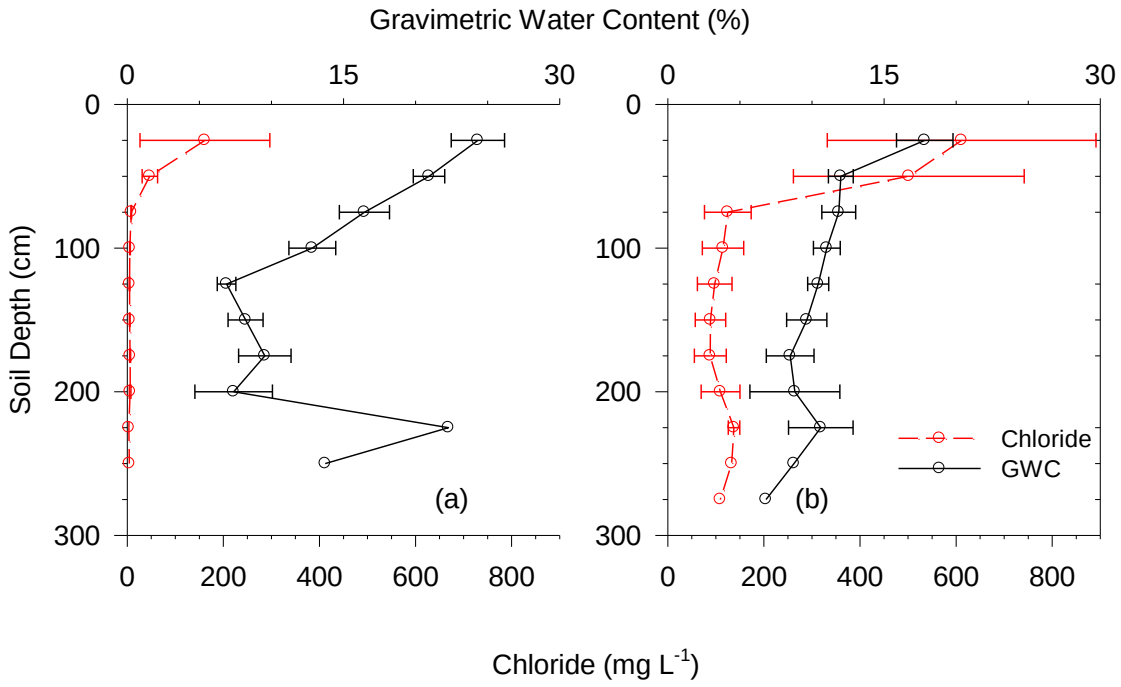

Fig. 5.4. Distribution of soil chloride (mg L-1) and gravimetric water content (%) across different soil depth in tallgrass prairie (a) and eastern redcedar encroached catchments (b). Values are mean ± SE

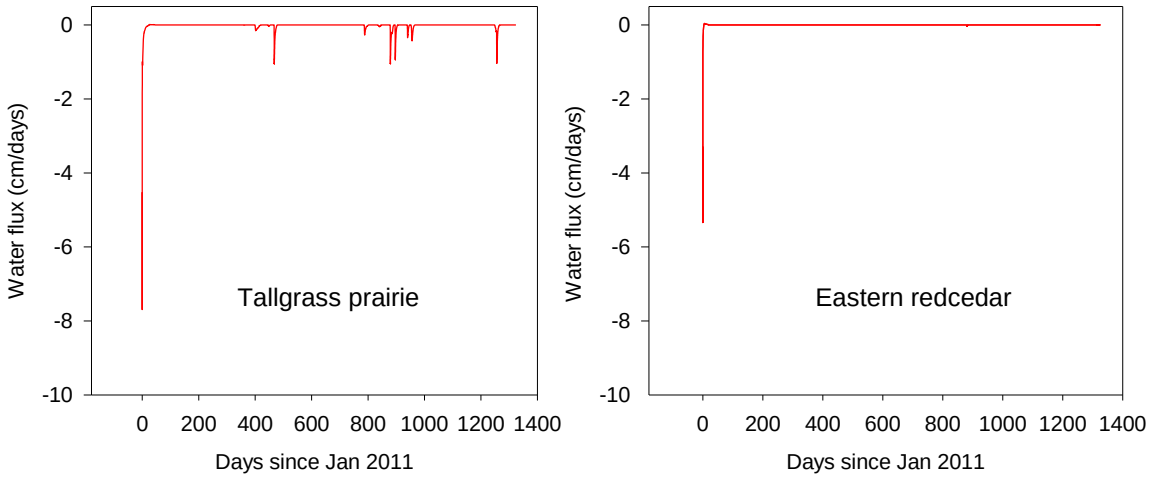

Fig. 5.5. Observation node water fluxes in the tallgrass prairie and eastern redcedar. Note that –ve sign indicates downward flux

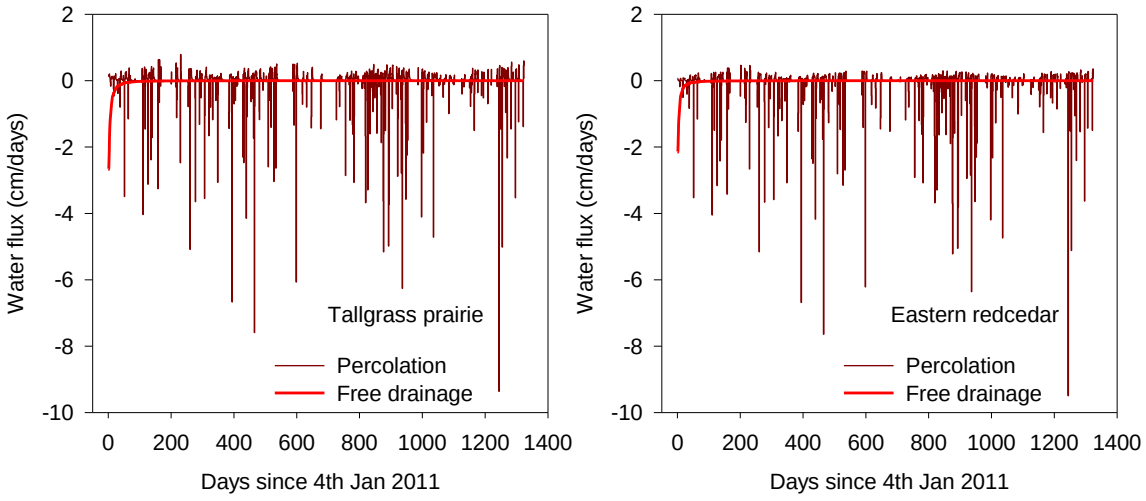

Fig. 5.6. Percolation, and free drainage below 275 cm depth in tall grass prairie and eastern redcedar. Note that –ve sign indicates downward flux

SUMMARY AND CONCLUSIONS

The objectives of this dissertation were to (a) quantify rainfall interception by eastern redcedar litter under controlled and field conditions using a leaf wetness sensor, (b) evaluate how grassland, eastern redcedar woodland, and oak forest control downward water movement through the vadose zone using electrical resistivity imaging (ERI), (c) demonstrate subsurface lateral flow using temporal ERI and berm infiltrometer, and (d) quantify and contrast drainage rates in dry sub-humid grassland and eastern redcedar woodland using chloride mass balance (CMB). Conventional gravimetric and sensor based approaches have limited application in understanding soil moisture at deeper depths. Our results demonstrate that hydrogeophysical techniques can potentially improve our understanding of vadose zone moisture and deep drainage under different vegetation cover type. On the whole, the following conclusions were drawn from this study:

i. A commercially available leaf wetness sensor (LWS, Decagon Devices Inc, Utah, USA) can be used to monitor the gravimetric water content of redcedar (*Juniperus virginiana*) litter and estimate litter interception *in situ*. A linear correlation between leaf wetness sensor counts and measured gravimetric litter water content of redcedar was observed under laboratory and field conditions.

ii. Redcedar litter interception accounted for about 10% of gross rainfall, constituting a substantial component of water budget in sub-humid environments.

iii. Redcedar encroachment in grassland was associated with increased spatial-temporal variability in root zone conductivity.

iv. Two-layered moisture migration profiles existed in grassland, redcedar woodland and oak forest. The relationship between inverted electrical resistivity and volumetric soil water content followed a power trend, and the relationship was used to develop moisture maps. At higher electrical resistivity, the volumetric water content was lower and vice versa. Electrical resistivity imaging was therefore applicable to detect deep moisture dynamics.

v. Vegetation transition such as woody plant encroachment in grassland was likely to reduce deep moisture. Volumetric moisture content was higher in deep soil layers in grassland.

vi. Woody plants can decrease the water table in a perched aquifer by a significant amount. Groundwater monitoring wells indicated higher water level under grassland than under grassland heavily encroached by redcedar.

vii. Passive seasonal temporal ERI showed subsurface lateral flow of water in grassland. This was confirmed and approved by short-term temporal ERI that tracked the movement of simulated water from a berm infiltrometer.

viii. Short-term temporal electrical resistivity imaging plays an important role to infer subsurface flow in the unsaturated zone and to act as ground truth for passive ERI.

ix. Mean Cl^- was higher under redcedar woodland than under grassland, which indicates reduced percolation and groundwater recharge potential associated with woody plant encroachment.

Future studies should investigate the feasibility of using leaf wetness sensors in litter of different types and shapes, and scrutinize the sensitivity of sensor to below canopy temperature, wind, and solar radiation variations. Vegetation controls spatial and temporal difference in vadose zone moisture, but some of differences may be due to specific soil types, and lithology that was under the specific transects. Future study should monitor subsurface physical properties, and evaluate hydraulic properties of unconsolidated materials. Similarly, it would be interesting to observe how simulated water from a berm infiltrometer moves under redcedar encroachment. A redcedar encroached site is likely to have preferential connection through macropores formed from dead root channels, cracks and animal burrows, but sub-surface water could be limited, which restricts water supply to the macropores. Overall, this study illustrated that the information on forest floor interception, deep water dynamics, subsurface flowpaths, and downward movement of water can be used for broader understanding of interrelations between soil, vegetation and subsurface hydrology for water resource management.

.

APPENDICES

Spacing and spatial resolution: Preliminary evaluation

A set of preliminary ERI surveys were conducted in February 2014 in a juniper-encroached site to identify appropriate spacing of electrodes and transect length for producing images necessary to detect deep drainage of water for our study site. Spacing between electrodes affected the resolution of subsurface electrical resistivity images. The depth of image was 1/5 of the array length and resolution is half of the electrode spacing. Thus, the 0.5 m spacing of electrodes produced more information likely associated with soil moisture patterns. On the contrary, wider spacing's of electrodes produced images with a greater imaging depth but broader details in subsurface resistivity variation. Soil horizons below 3.0 m were highly resistive with electrical resistivity ranging from 150 to 300 Ω-m, coincident with sandstone deposits running up to 8 m depth (Fig. A1; 2 m spacing, left part and light colored). The assessment of electrode alignment and length necessary for time-lapse ERI via test imaging showed an electrically resistive zone underneath the juniper tree. This was largely distinct under closer electrode spacing (Fig. A1, 0.5 m spacing) due to greater spatial resolution.

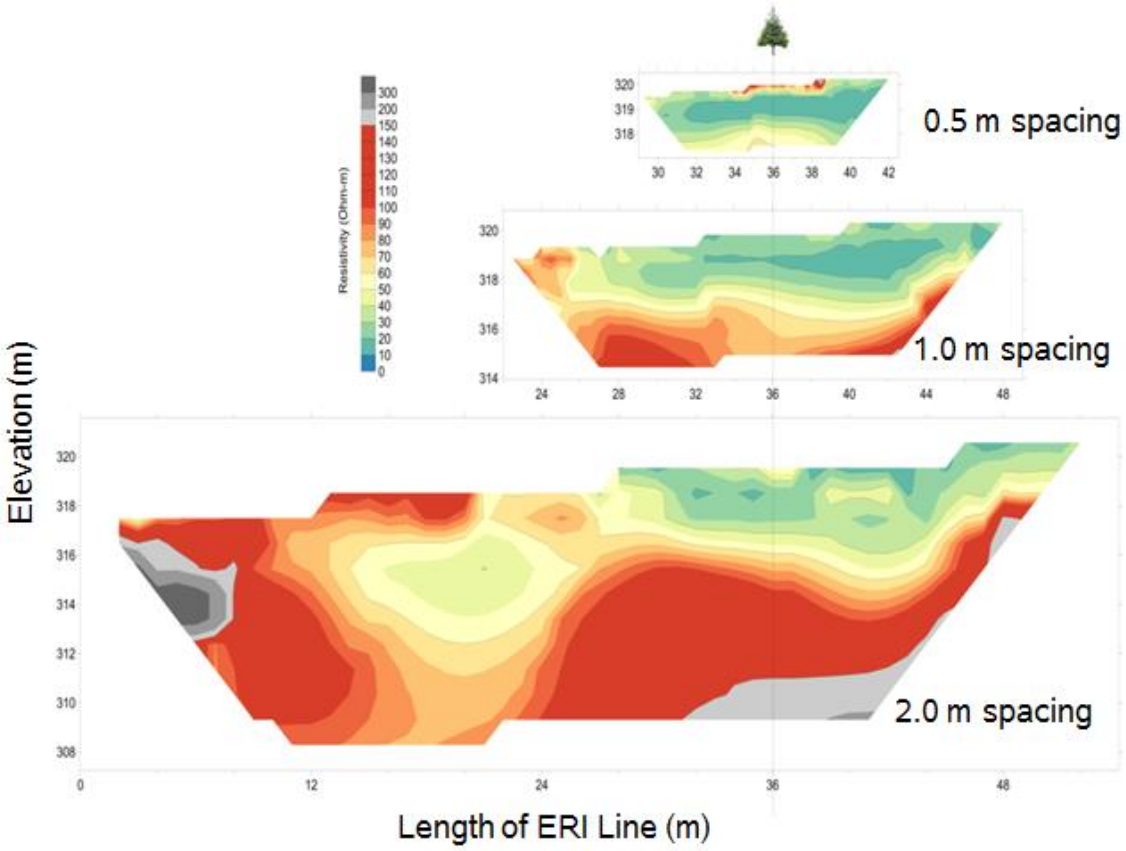

Fig. A1. Comparison of electrical resistivity image at 0.5 m, 1.0 m and 2.0 m inter-electrode spacing in a randomly chosen juniper-encroached catchment (15th Feb, 2014).

Relationship between % change in conductivity and resistivity, and moisture

Change in volumetric moisture content across all vegetation cover types (prairie, juniper-encroached, juniper woodland and oak forest) strongly correlates with change in inverted conductivity and resistivity. This relationship developed from transient data can better describe soil layering effects.

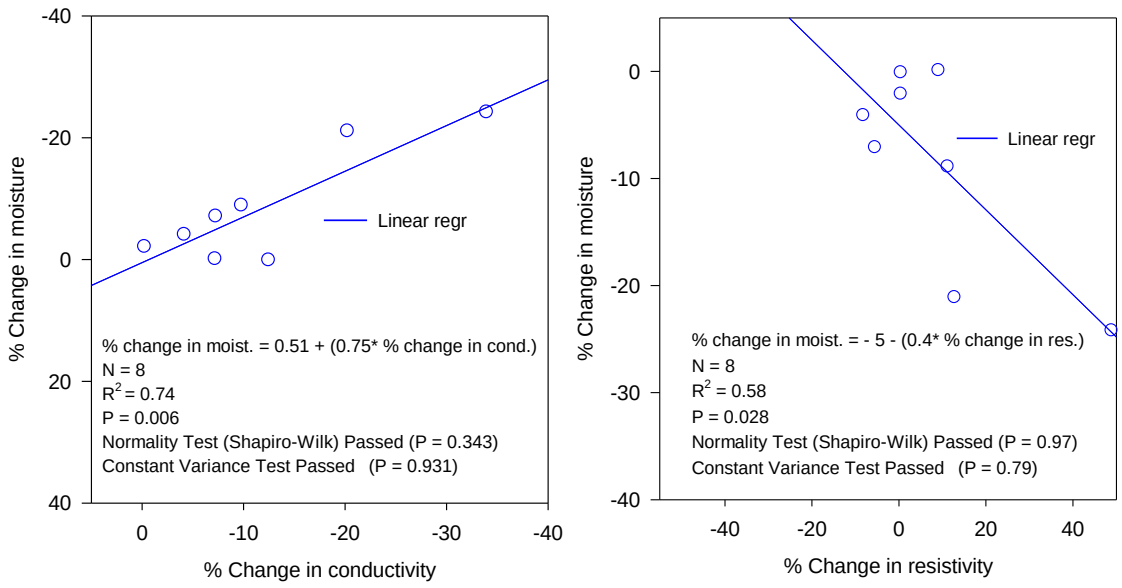

Fig. A2. The linear relation between change in conductivity and change in resistivity after inversion with the change in volumetric moisture content across all vegetation cover types

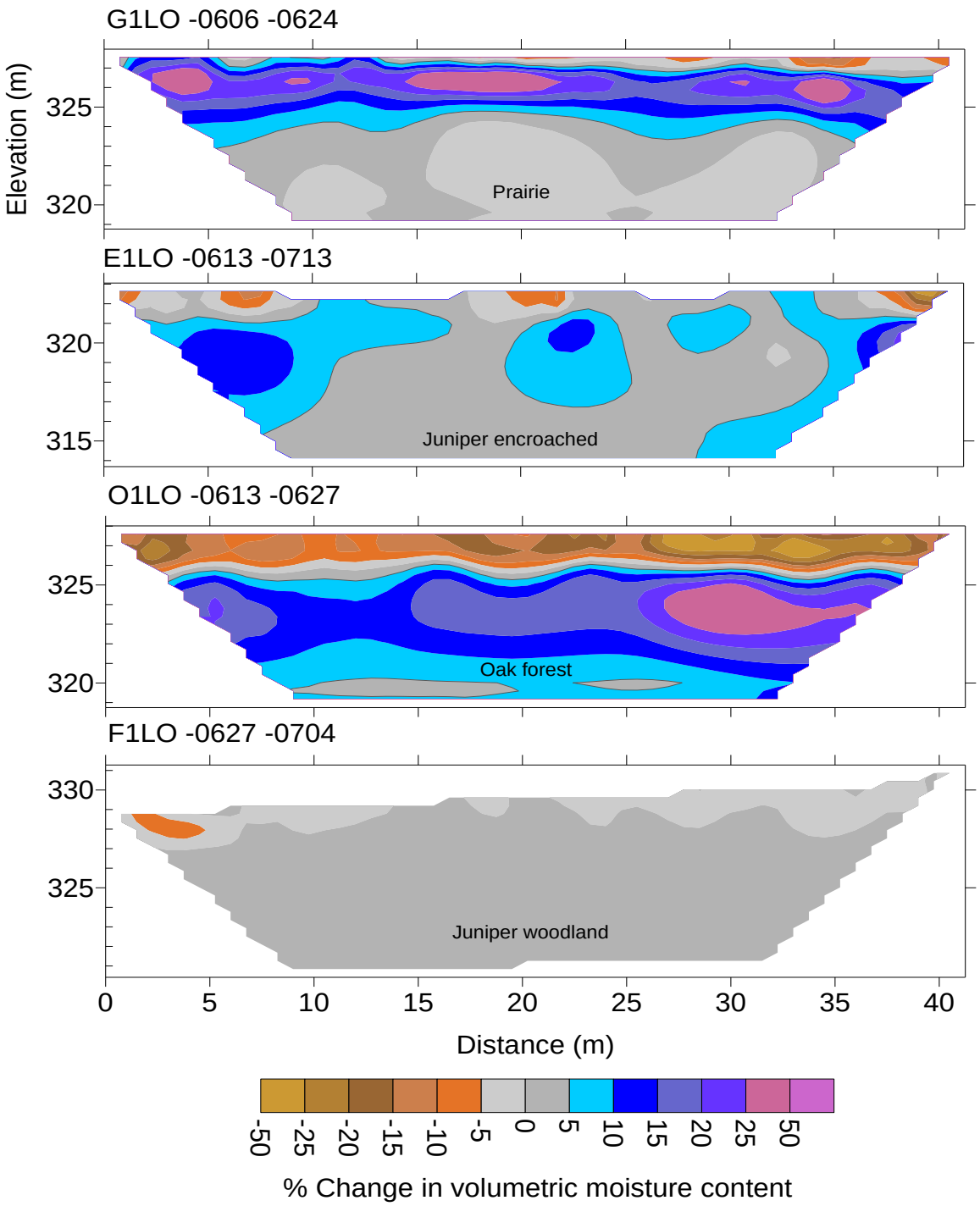

Fig. A2.1. Time-lapse pseudosections showing % change in volumetric moisture content in prairie, juniper-encroached, oak forest and juniper woodland. Percent change in conductivity was converted to % change in volumetric moisture content using linear relation in Fig. A2

VITA

Bharat Sharma Acharya

Candidate for the Degree of

Doctor of Philosophy

Thesis: HYDROGEOPHYSICAL EVALUATION OF VEGETATION INFLUENCE ON ECOHYDROLOGICAL PROCESSES

Major Field: Natural Resource Ecology and Management

Biographical:

Education:

Completed the requirements for the Doctor of Philosophy in Natural Resource Ecology and Management at Oklahoma State University, Stillwater, Oklahoma in May, 2016.

Completed the requirements for the Master of Science in Agro-environmental Management at Aarhus University, Aarhus, Denmark in 2011.

Completed the requirements for the Bachelor of Science in Agriculture at Tribuvan University, Nepal in 2008.

Experience:

- Graduate Research Assistant (2012 - 2016), Department of Natural Resource Ecology and Management, Oklahoma State University, Stillwater, OK
- Technical Assistant (2009), Research Center Folum, Aarhus University, Denmark

Professional Memberships:

- American Geophysical Union (AGU) (2015 - 2016)
- Oklahoma Clean Lakes and Watersheds Association (2014 - 2016)